NATIONAL CENTER FOR EARTHQUAKE
ENGINEERING RESEARCH
State University of New York at Buffalo

CENTRIFUGAL MODELING OF DYNAMIC SOIL-STRUCTURE INTERACTION

by

K. Weissman and J. H. Prevost
Department of Civil Engineering and Operations Research
School of Engineering and Applied Science
Princeton University
Princeton, New Jersey 08544

Technical Report NCEER-89-0040

May 10, 1989

This research was conducted at Princeton University and was partially supported by the National Science Foundation under Grant No. ECE 86-07591.

NOTICE

This report was prepared by Princeton University as a result of research sponsored by the National Center for Earthquake Engineering Research (NCEER). Neither NCEER, associates of NCEER, its sponsors, Princeton University, nor any person acting on their behalf:

a. makes any warranty, express or implied, with respect to the use of any information, apparatus, method, or process disclosed in this report or that such use may not infringe upon privately owned rights; or

b. assumes any liabilities of whatsoever kind with respect to the use of, or the damage resulting from the use of, any information, apparatus, method or process disclosed in this report.

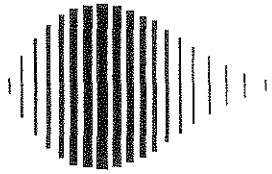

CENTRIFUGAL MODELING OF DYNAMIC SOIL-STRUCTURE INTERACTION

by

Karen Weissman[1]

Superivsed by Jean H. Prevost[2]

May 10, 1989

Technical Report NCEER-89-0040

NCEER Contract Number 86-2032 and 87-1312

NSF Master Contract Number ECE 86-07591

1 Graduate Student, Department of Civil Engineering and Operations Research, Princeton University
2 Professor, Department of Civil Engineering and Operations Research, Princeton University

NATIONAL CENTER FOR EARTHQUAKE ENGINEERING RESEARCH
State University of New York at Buffalo
Red Jacket Quadrangle, Buffalo, NY 14261

PREFACE

The National Center for Earthquake Engineering Research (NCEER) is devoted to the expansion and dissemination of knowledge about earthquakes, the improvement of earthquake-resistant design, and the implementation of seismic hazard mitigation procedures to minimize loss of lives and property. The emphasis is on structures and lifelines that are found in zones of moderate to high seismicity throughout the United States.

NCEER's research is being carried out in an integrated and coordinated manner following a structured program. The current research program comprises four main areas:

- Existing and New Structures
- Secondary and Protective Systems
- Lifeline Systems
- Disaster Research and Planning

This technical report pertains to Program 1, Existing and New Structures, and more specifically to geotechnical studies.

The long term goal of research in Existing and New Structures is to develop seismic hazard mitigation procedures through rational probabilistic risk assessment for damage or collapse of structures, mainly existing buildings, in regions of moderate to high seismicity. The work relies on improved definitions of seismicity and site response, experimental and analytical evaluations of systems response, and more accurate assessment of risk factors. This technology will be incorporated in expert systems tools and improved code formats for existing and new structures. Methods of retrofit will also be developed. When this work is completed, it should be possible to characterize and quantify societal impact of seismic risk in various geographical regions and large municipalities. Toward this goal, the program has been divided into five components, as shown in the figure below:

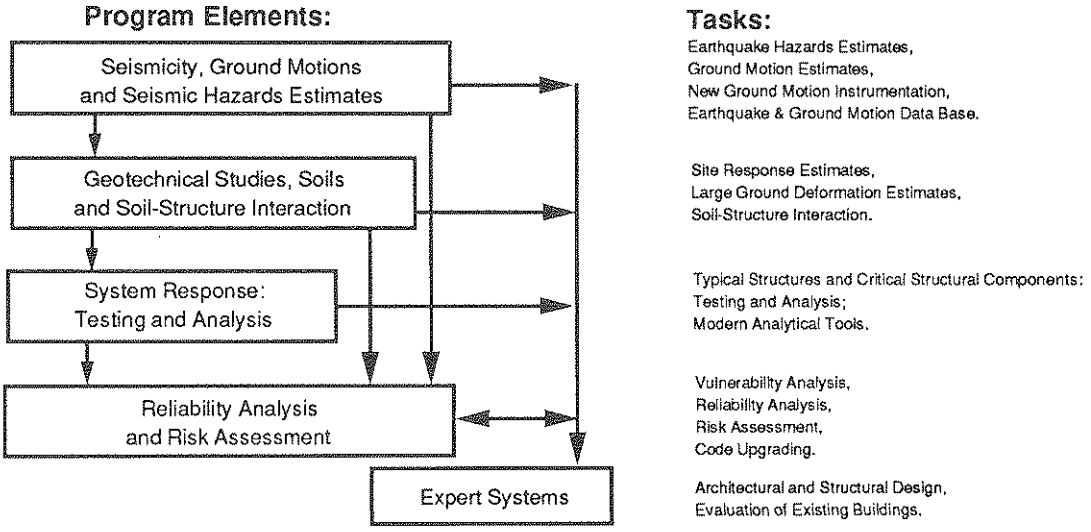

Geotechnical studies constitute one of the important areas of research in Existing and New Structures. Current research activities include the following:

1. Development of linear and nonlinear site response estimates.
2. Development of liquefaction and large ground deformation estimates.
3. Investigation of soil-structure interaction phenomena.
4. Development of computational methods.
5. Incorporation of local soil effects and soil-structure interaction into existing codes.

The ultimate goal of projects concerned with geotechnical studies is to develop methods of engineering estimation of large soil deformations, soil-structure interaction, and site response.

A parametric experimental study of seismic soil-structure interaction is performed in the "centrifuge." System identification techniques are employed to deduce stiffness and damping factors of the soil-structure system. The results are compared with closed-form solutions from the literature.

ABSTRACT

This report documents research performed at Princeton University which was supported in part by NSF grant No. CEE-8320115 (under the management of C. Astill) and NSF grant No. ECE-86-07591 via sub-contract Nos. SUNYRF-NCEER-86-2032.A3 and SUNYRF-NCEER-87-1312 with the National Center for Earthquake Engineering Research. The report is based on the doctoral dissertation by Karen Weissman submitted in June, 1989 to the Department of Civil Engineering and Operations Research at Princeton University in partial fulfillment of the requirements for the Ph.D. degree. The report is presented as a companion to Technical Report NCEER-88-0013 (May 24, 1988) entitled *A Study of Radiation Damping and Soil-Structure Interaction Effects in the Centrifuge* by K. Weissman and J.H. Prevost.

In this report a centrifuge model is presented that is capable of realistically representing soil-structure systems subjected to earthquake-like excitation. The model is validated by first characterizing the model system, second performing an in depth experimental study of radiation damping and soil-structure interaction effects, and third performing a numerical analysis of the experimental results. The model system is characterized by performing free field experiments, scattered field experiments, and a preliminary soil-structure interaction experiment. The free field experiments examine the behavior of a horizontal soil layer during a simulated earthquake. These experiments show that the simulated earthquake, which is generated by the hammer-exciter plate method, is similar in amplitude and frequency content to a real earthquake. The experiments also demonstrate that a confined soil sample can satisfactorily model a horizontal soil stratum of infinite lateral extent when the containment walls are lined with an absorptive material to attenuate wave reflections that would otherwise occur. The scattered field experiments focus on the effects of footing geometry on the input acceleration in a soil-structure system. The preliminary soil-structure interaction experiment investigates the response of a rigid circular footing to a simulated earthquake.

Next, an experimental study of radiation damping and soil-structure interaction effects is performed which shows that the centrifuge system is capable of modeling soil-structure interaction phenomena such as radiation damping. The experiments are designed to create a data pool which demonstrates the influence of (1) the natural frequencies of the structure, (2) the foundation embedment, and (3) the foundation shape on radiation damping and soil-structure interaction effects for a structure on a layer of soil over bedrock during an earthquake. The experimental results are shown to be consistent with established theories.

Finally, the experimental results are used to compute the damping and stiffness values of a two degree of freedom piecewise linear numerical model of the soil-structure systems. The parameter values are extracted from the experimental results by methods of system identification. These parameter values are then compared to those computed by classical text book formulas. This analysis shows that the behavior of the centrifuge system can be modeled by established analytical procedures.

The research in this report results in establishing the centrifuge model as a useful and realistic tool for the validation and future development of soil-structure interaction theory.

TABLE OF CONTENTS

LIST OF FIGURES

LIST OF TABLES

CHAPTER 1

INTRODUCTION AND ORGANIZATION OF TEXT

The interest in soil-structure interaction is rapidly growing in the field of earthquake engineering. With this growing interest comes an increased need for adequate physical data to substantiate newly developed analytical theories. It is shown in this report that the centrifuge can be used to provide a controlled experimental environment in which such physical data can be generated. A centrifuge model is presented which is capable of realistically representing soil-structure systems subjected to earthquake-like excitation.

An overview of dynamic centrifuge modeling and earthquake simulation is given in Chapter 2. Some of the problems that frequently occur in dynamic modeling and which motivate the development of the proposed model are discussed. The problems addressed include attenuating wave reflections at the boundary walls of the model soil deposit and cost effectiveness of the earthquake simulation device. In Chapter 3 the centrifuge facility at Princeton University and the development of the testing procedure are described.

Once the testing procedure is fully developed, the model is validated by first characterizing the model system, second performing an in depth experimental study of radiation damping and soil-structure interaction effects, and third carrying out a numerical analysis of the experimental results. The characterization of the model system is presented in Chapter 4. The goal is to learn as much about the experimental system as possible in order to (1) verify that the simulated earthquake (which is generated by the hammer-exciter plate technique) and its propagational characteristics in the model soil deposit are representative of a real system, and (2) insure that the experimental data obtained from the model is properly interpreted. This goal is achieved by performing free field experiments, scattered field experiments, and a preliminary soil-structure interaction experiment. The free field experiments examine the behavior of a horizontal soil layer during a

simulated earthquake. The scattered field experiments focus on the effects of footing geometry on the input acceleration in a soil-structure system. The preliminary soil-structure interaction experiment investigates the response of a rigid circular footing to a simulated earthquake and is a precursor to the more complex soil-structure interaction experiments to be performed in Chapter 5.

The second task in validating the model system is the study of radiation damping and soil-structure interaction effects performed in the centrifuge. This study is described in Chapter 5. The purpose of this chapter is to show that the centrifuge system is capable of modeling soil-structure interaction phenomena such as radiation damping. The experiments are designed to create a data pool which demonstrates the influence of (1) the natural frequencies of the structure, (2) the foundation embedment, and (3) the foundation shape on radiation damping and soil-structure interaction effects for a structure on a layer of soil over bedrock during an earthquake. The experimental results are shown to be consistent with established theories.

In Chapter 6 the experimental results are used to compute the damping and stiffness values of a two degree of freedom piecewise linear model of the soil-structure system. The parameter values are extracted from the experimental results by methods of system identification. These parameter values are then compared to those computed by classical text book formulas to show that the behavior of the centrifuge system can be modeled by established analytical procedures.

Finally, in Chapter 7 general conclusions are drawn and suggestions are made for future research.

CHAPTER 2

OVERVIEW OF DYNAMIC CENTRIFUGE MODELING AND EARTHQUAKE SIMULATION

In studying soil-structure interaction during earthquakes perhaps the most difficult problem facing the engineer is the lack of control over the source of excitation. Such difficulty precipitates the development of simulated earthquakes on model systems in a controlled laboratory environment. One such simulation employs centrifugal modeling to create an accurately proportioned model system. The basic principle behind the centrifugal modeling technique [see e.g. 2.2, 2.3, 2.4, 2.5] is that when a soil sample is accelerated to n times the earth's gravitational acceleration, it is essentially a $1/n^{th}$ scale model of a prototype system. Under this increased gravity load, the $1/n^{th}$ scale model has the same stresses as its prototype at homologous points. The centrifuge allows small scale soil models, which are inexpensive and easily constructed, to be tested without the problems that normally occur in trying to scale stresses in small soil deposits at 1 g [2.5]. Certain quantities like length and time scale linearly, and all scaling relations are consistent with dimensional analysis. A full list of scaling properties is given in Table 2.1. These scaling relationships have been verified experimentally by comparing the dynamic behavior of models and their prototype [e.g. 2.14, 2.17, 2.19] or by comparing the output from model and model-of-model systems [e.g. 2.8]. In the latter case, a model at n g is compared to a $1/m^{th}$ model-of-the-model at mn g, where m and n are different scale factors.

In a centrifuge, the soil system is contained in a bucket that is attached to the centrifuge arm by a hinged support. When the centrifuge is "in flight," the bucket rotates 90 degrees so that the centrifugal acceleration is acting perpendicular to the soil model. To simulate an earthquake, dynamic excitation must be applied to the spinning model. The excitation can be external, by shaking the entire bucket, or internal, by applying a disturbance directly inside the soil deposit.

In the centrifuge experiments reported in the literature [2.9, 2.10, 2.13, 2.15], external excitation has been used almost exclusively. Examples of external shakers are the piezoelectric shaker used by Arulanandan *et.al.* [2.9], the toggle and spring mechanism used at Caltech [2.10], the Cambridge University Bumpy Road technique [2.15], and the Morris spring-mass resonant shaker [2.13]. One drawback common to all these external methods is that the shaker must provide enough force to accelerate both the mass of the bucket and the mass of the soil model inside it. A possible method of internal excitation was provided by Zelikson *et.al.* [2.18] in which explosives were used to produce an earthquake-like signal in the centrifuge bucket.

At Princeton University a hammer-exciter plate device is used to provide internal excitation. The hammer-exciter plate method has several advantages over other internal and external methods of excitation. Unlike the devices used in the external methods, the exciter plate does not shake the entire payload of the bucket and is, therefore, a small and relatively inexpensive apparatus. In addition, the hammer-exciter plate method is capable of repeating a particular earthquake as many times as necessary per flight. Although the hammer-exciter plate technique is only capable of generating one type of earthquake, it is shown in Chapter 4 of this report that this particular earthquake is realistic and the disadvantage of only studying one type of earthquake is far outweighed by the economy and the simplicity of the device. All tests reported in this thesis are performed in the Princeton University Geotechnical Centrifuge and use this method of excitation. The early developments of the technique are documented in Reference 2.12 and recent modifications are explained in Chapter 3 of this thesis.

An important consideration in dynamic modeling is the presence of an artificial boundary on the soil system due to the containment walls. Coe [2.1] and Coe, Prevost and Scanlan [2.12] have demonstrated the existence of standing waves due to wave reflection at the centrifuge bucket walls during dynamic excitation. Several studies have been done in the past which com-

pared dynamic soil and soil-structure properties exhibited in the centrifuge model to those predicted by classical theories. Topics that have been investigated in these studies include dynamic response of earth embankments [2.7], dynamic lateral earth pressures on retaining walls [2.10, 2.16, 2.20], dynamic response of piles [2.11], dynamic response of surface footings [2.11], and rocking motions of tall, slender towers [2.6]. In most of these investigations, however, [2.6, 2.7, 2,10, 2.16, 2.20], nothing was done to attenuate wave reflections in the experimental system. In an attempt to address this issue, Whitman *et.al.* [2.21] have developed a stacked ring apparatus to simulate a soil column within a stratum. The rings surround the column of soil and are fairly stiff in the vertical direction but are free to move laterally with the soil at high accelerations. However, it is questionable that such a setup could be tuned to absorb the wide range of wave frequencies present in a soil-structure experiment that will otherwise be reflected back into the system. Coe [2.1] has shown that by lining the bucket walls with an appropriate absorptive material, wave reflections can be averted. In accordance with Coe's findings, a clay-like material called Duxseal is used as a lining in all the experiments reported herein.

The literature indicates that few dynamic soil and soil-structure interaction experiments have been performed in the centrifuge with adequate consideration given to the problem of wave reflection. Hence, most previous experiments have not employed very realistic models. The goal of this report is to present a centrufuge model that is capable of realistically representing soil-structure systems subjected to earthquake-like excitation.

TABLE 2.1

SCALING RELATIONS

Quantity	Full Scale Prototype	Centrifugal Model at n g's
Linear Dimension, Displacement	1	$1/n$
Area	1	$1/n^2$
Volume	1	$1/n^3$
Stress	1	1
Strain	1	1
Force	1	$1/n^2$
Mass	1	$1/n^3$
Acceleration	1	n
Energy	1	$1/n^3$
Density	1	1
Energy density	1	1
Velocity	1	1
Time		
In Dynamic Terms	1	$1/n$
In Diffusion Cases	1	$1/n^2$
In Viscous Flow Cases	1	1
Frequency in Dynamic Problems	1	n

References for Chapter 2

2.1 Coe, Carlos, "On the Feasibility of Performing Dynamic Soil Tests in a Centrifuge," Ph.D. Thesis, Princeton University, Princeton, N.J., 1985.

2.2 Bucky, P.B., *Use of Models for the Study of Mining Problems*, AIMME Tech. Publ. No. 425, 1931.

2.3 Hoek, E., "The Design of a Centrifuge for the Simulation of Graviational Force Fields in Mine Models," *J. of the South African Inst. of Mining and Metallurgy*, 1965, 65 (9), 455.

2.4 Pokrovsky, G.I. and Fyodorov, I.S., *Centrifugal Model Testing in the Constructuion Industry*, Vols. I and II, draft translation by UK Building Research Establishment, 1975.

2.5 Roscoe, K.H., "Soil and Model Tests", *J. Strain Analysis*, 1968, 3, 57.

2.6 Morris, Derek V., "Dynamic Soil-Strucutre Interaction Modelled Experimentally on a Geotechnical Centrifuge," *Canadian Geotechnical Journal*, 1981, Vol. 18, pp 40-51.

2.7 Finn, W.D.L., Ledbetter, R.H., Beratan, L.L., "Seismic Soil-Structure interaction: Analysis and Centrifuge Model Studies," *Nuclear Engineering and Design*, 1986, Vol. 94, pp 53-66, North Holland, Amsterdam.

2.8 Lambe, Philip C., Whitman, Robert V., "Scaling for Earthquake Shaking Tests on a Centrifuge," Proceedings of the Conference on Soil Dynamics and Earthquake Engineering, 13-25 July, 1982, Southampton, U.K., Vol. 1, pp 367-378.

2.9 Arulanandan, K., Canclini, J., Anandarajah, A., "Simulation of Earthquake Motions in the Centrifuge," *Journal of the Geotechnical Division*, ASCE, Vol. 108, No. GT5, May, 1982.

2.10 Ortiz, L.A, Scott, R.F., Lee, J., "Dynamic Centrifuge Testing of a Cantilever Retaining Wall," *Earthquake Engineering and Structural Dynamics*, 1983, Vol. 11 pp 251-268.

2.11 Prevost, J.H., Scanlan, R.H., "Dynamic Soil-Structure Interaction: Centrifuge Modeling," *Soil Dynamics and Earthquake Engineering*, 1983, Vol. 2 No. 4, pp 212-221.

2.12 Coe, C.J., Prevost, J.H., Scanlan, R.H., "Dynamic Stress Wave Reflections/Attenuation: Earthquake Simulation in Centrifuge soil models," *Earthquake Engineering and Structural Dynamics*, 1985, Vol. 13, pp 109-128.

2.13 Morris, D.V., "The Centrifugal Modelling of Dynamic Soil-Stucture Intereaction and Earthquake Behaviour," *Ph.D. Thesis*, Cambridge University, England, 1979.

2.14 Schmidt, R.M., "Centrifuge Simulation of the JOHNIE BOY 500 ton Cratering Event," *Proceedings of the 9th Lunar Planet Sci. Conf.*, pp 3877-3889.

2.15 Kutter, Bruce L., "Deformation of Centrifuge Models of Clay Embankments Due to 'Bumpy Road' Earthquakes," *Proceedings of the Conference on Soil Dynamics and Earthquake Engineering*, 13-25 July, 1982, Southampton, U.K., Vol. 1, pp 331-349.

2.16 Bolton, M.D., Steedman, R.S., "Centrifuge Testing of Microconcrete Retaining Walls Subjected to Base Shaking," *Proceedings of the Conference on Soil Dynamics and Earthquake Engineering*, 13-25 July, 1982, Southampton, U.K., Vol. 1, pp 311-329.

2.17 Scott, R.F., Ting, J.M., Lee, J., "Comparison of Centrifuge and Full Scale Dynamic Pile Tests," *Proceedings of the Conference on Soil Dynamics and Earthquake Engineering*, 13-25 July, 1982, Southampton, U.K., Vol. 1, pp 299-309.

2.18 Zelikson, A., Leguay, P., Pascal, C., "Centrifuge Modal Comparison of Pile and Raft Foundations Subject to Earthquakes," *Proceedings of the Conference on Soil Dynamics and Earthquake Engineering*, 13-25 July, 1982, Southampton, U.K., Vol. 1, pp 283-297.

2.19 Trott, J.J., Taylor, R.N., Symons, I.F., "Tests to Validate Centrifuge Modelling of Flexible Pipes," *Proceedings of a Symposium on the Application of Centrifuge Modelling to Geotechnical Design*, April 16-18, 1984, Manchester, U.K., pp 223-251.

2.20 Bolton, M.D., Steedman, R.S., "The Behaviour of Fixed Cantilever Walls Subjected to Lateral Shaking," *Proceedings of a Symposium on the Application of Centrifuge Modelling to Geotechnical Design*, April 16-18, 1984, Manchester, U.K., pp 301-313.

2.21 Lambe, Philip C., Whitman, Robert V., Kutter, Bruce L., "Initial Results from a Stacked Ring Apparatus for Simulation of a Soil Profile," *Proceedings of the International Conference on Recent Advances in Geotechnical Earthquake Engineering and Soil Dynamics*, April 26 - May 3, 1981, Rolla, Missouri, Vol.III, pp 1105-1110.

CHAPTER 3

THE CENTRIFUGE FACILITY AND DEVELOPMENT OF THE TESTING PROCEDURE

3.1 Physical Setup

The centrifuge used for all the experiments described in this study is manufactured by Genisco. Inside a containing wall is a rotating arm that is 6 feet 8 inches (2.03 meters) in diameter and has a maximum payload capacity of 10 g-tons. At the end of each arm is a rectangular bucket attached by a hinged support. One bucket contains the model system and the other is used as a counter weight. When the centrifuge is spinning, the buckets rotate 90° from their position at rest. The centrifugal acceleration is, therefore, acting perpendicular to the model system (Fig. 3.1).

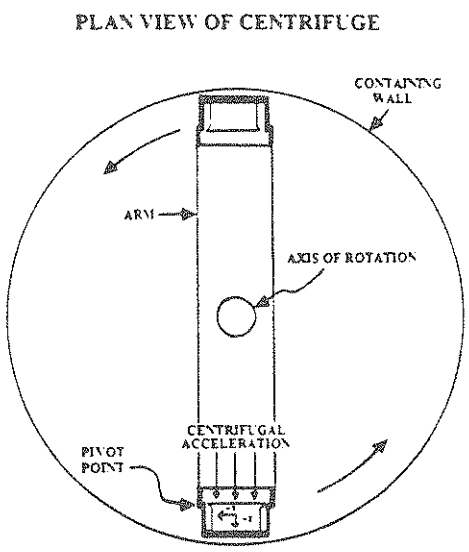

FIGURE 3.1

The earthquake is simulated within the spinning model by the hammer-exciter plate method which was originally developed by Coe, Prevost and Scanlan [3.1]. Figure 3.2 shows a cross section of the centrifuge bucket. Beneath the soil, at the bottom of the bucket, is the exciter plate. The plate is 5.5 square inches in plan and 0.5 inches thick. The plate is supported on the right side by two steel rods which run through teflon bearings inside aluminum tubes. The tubes go through the side of the bucket enabling the steel rods to connect to the 1/4 inch by 12 inch by 1 inch steel striker bar. The striker bar is hit by a pneumatically driven lever. The vibration of the plate induced by the blow of this pneumatic "hammer" sends vertically propagating shear waves up through the soil; these are the simulated seismic waves.

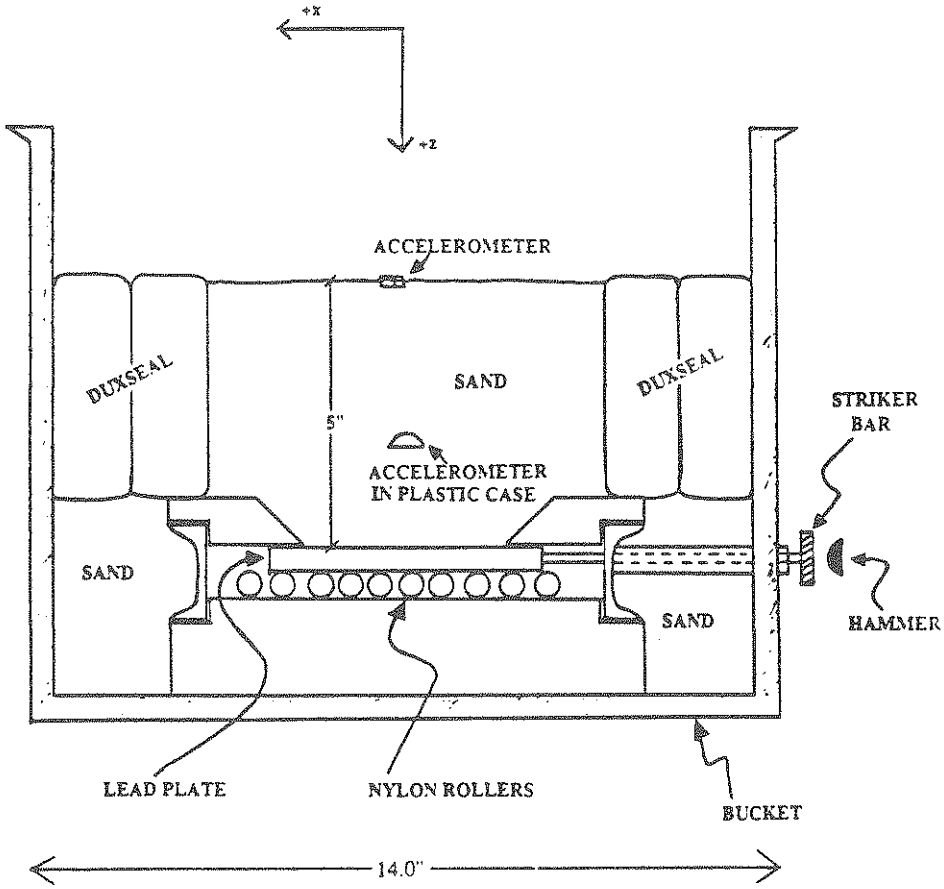

FIGURE 3.2
Cross Section of Centrifuge Bucket

Both the driving force of the hammer and the material composition of the plate affect the amplitude and frequency content of the simulated earthquake. Harder hammer blows induce larger peak accelerations and higher frequencies of vibration. To simulate an earthquake it is desirable to have large amplitudes and lower frequencies. Therefore, it is important to use an exciter plate with a low fundamental frequency so that hard hammer blows will not induce vibrations in which high frequencies dominate. Recalling the laws of similitude presented in Chapter 2, the accelerations and frequencies of the simulated earthquake must be increased by a factor equal to the centrifugal acceleration on the model. In this study, all tests are performed at a centrifugal acceleration of 100 g. Therefore, an exciter plate that produces frequencies between 10 and 1000 Hz and peak accelerations of 20 to 50 g in the model soil deposit is desirable (these values correspond to prototype frequencies of 0.10 to 10 Hz and prototype accelerations of 0.2 to 0.5 g).

Coe [3.2] has tested plates made of various materials such as aluminum, plywood, dense foam rubber, and Duxseal, as well as composite plates made of plywood and lead. Most of these materials yielded accelerations in the soil that were too low and frequencies that were too high. The Duxseal plate produced frequencies that were the most earthquake-like, but had the disadvantage of suffering permanent deformations from each hammer blow. These deformations make the use of a Duxseal plate impractical because (1) the plate must be remolded after every couple of earthquakes and (2) the earthquakes are not very reproducible because the shape of the plate keeps changing. In a subsequent study Nagle [3.3] returned to examining a rigid aluminum plate. He set up an interference pattern of holes in the plate to try and attenuate high frequencies. This technique succeeded in narrowing the band of high frequencies produced by the plate, but it did not eliminate a dominant frequency at around 20 Hz (prototype scale). Based on the work done by these two researchers it is clear that a rigid plate made of dense material is needed to produce lower frequencies of vibration. Tests performed by this author show that a plate made of lead yields reasonable frequencies and amplitudes. The acceleration recorded at the plate in the direction of the blow of the hammer is shown in Figure 3.3 along with its Fourier Transform. The peak frequency is around 1000 Hz which includes damping effects due to the mounting of the plate on the steel rods. Although this frequency is a bit high for an earthquake, it is not unreasonable (see Section 4.1). To help damp out higher order frequencies that occur as smaller components of the vibration, a 1/8 inch thick piece of teflon is taped to the striker bar at the point of contact with the hammer.

As seen in Figure 3.2, the plate rests on nylon rollers and is theoretically free to slide once it is hit. However, the friction between the sand and the plate caused by the high centrifugal acceleration prevents the plate from moving even under relatively hard hammer blows. This was determined by using an LVDT to measure the displacement of the plate while the centrifuge was in flight and the simulated earthquake was being generated. The hammer is powered by 52 psi of

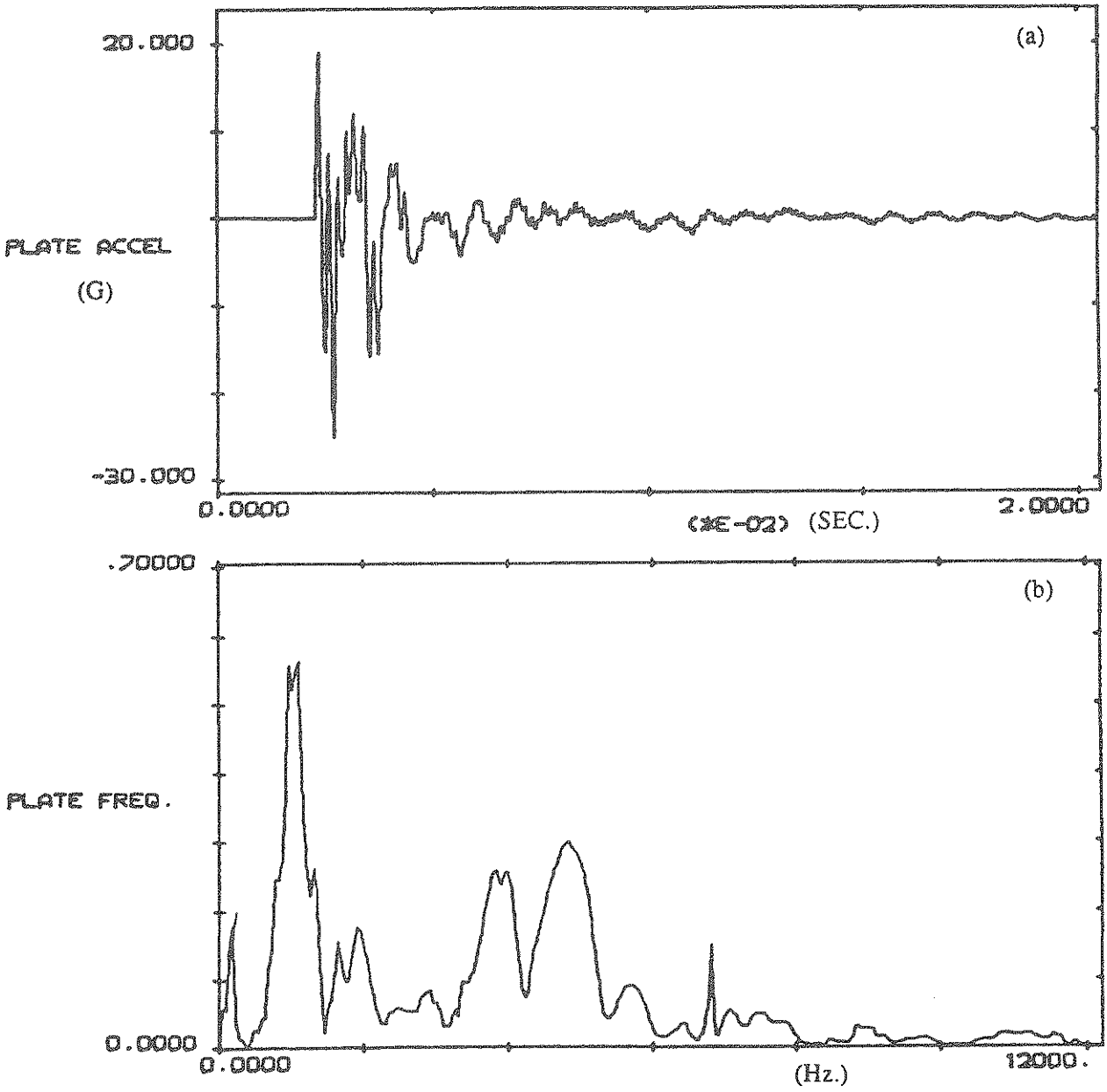

FIGURE 3.3
Acceleration Recorded at the Plate in the Direction of the Blow of theHammer.
(a) Acceleration Time History.
(b) Fourier Transform.

air pressure which is released through a solenoid valve. The opening and closing of this valve is triggered remotely from the centrifuge control room. The amplitude of the earthquake is not very sensitive to the exact amount of air pressure used. Pressures as high as 80 psi showed a negligible increase in peak accelerations in the soil. Larger amplitude earthquakes can be achieved if necessary by increasing the air pressure beyond 80 psi. Time histories of the simulated earthquake recorded in the soil deposit are presented in Section 4.1.

The nylon rollers and plate are inside an aluminum box built into the base of the bucket. An aluminum frame is placed on top of this box allowing a 4 inch by 4 inch contact area between the plate and the soil. This frame prevents the sand from getting in between the rollers and the plate. The channel around the aluminum box is filled with sand up to the top of the frame. The sand used is Monterey-0 which is a California beach sand. The mean grain size of a this sand is small enough so that the soil can still be regarded as a continuum under a 100 g acceleration. Table 3.1 shows various properties of Monterey-0 sand [3.4].

TABLE 3.1
SOIL PROPERTIES OF
MONTEREY-0 SAND

Shear Modulus*	$2.86\times10^5\ z^{1/2}\ psf$	
At $z=8.20ft$ (half width of footing used in experiments)		
Shear Modulus	$8.19\times10^5\ psf$	$3.92\times10^7\ N/m^2$
Shear Wave Velocity	$5.31\times10^2\ ft/sec$	$1.62\times10^2\ m/sec$
Median Grain Size	$1.18\times10^{-2}\ in$	$0.30\ mm$
Density	$93.7\ lb/ft^3$	$1.50\times10^3\ kg/m^3$

*Shear modulus varies with depth z.

The walls of the bucket are lined with two 1.5 inch thick layers of Duxseal which rest on the sand that is level with the aluminum frame. Experimental studies have been done to demonstrate the presence of standing waves during dynamic excitation due to wave reflection at the bucket walls [3.1, 3.2]. Coe has proven that the clay-like substance Duxseal, manufactured by the Johns-Manville Corporation, sufficiently absorbs these standing waves. As mentioned in Chapter

2, in most other centrifuge facilities nothing is done to attenuate wave reflections. Hence, the Duxseal lining is a unique and important feature of the Princeton Laboratory. The remaining cavity inside the Duxseal boundary is filled with Monterey-0 sand. Accelerometers are placed at various points in the model system to measure acceleration during the simulated earthquakes. Depending on the goal of the test, structures of various types may also be included.

3.2 Running a Test and Recording the Data

Once the soil or soil-structure system has been constructed, the next step is to subject it to a model earthquake. The centrifuge is accelerated to 100 g by bringing its rotation speed up to 289 rpm. The centrifuge is located on a slab that is isolated from the rest of the floor in order to reduce the vibration of the machine. The solenoid valve which provides the input pulse to the hammer is triggered from inside the control room. The striker bar is hit, and the impact is transmitted to the exciter plate which, in turn, vibrates, sending vertically propagating shear waves up through the soil. The same earthquake can be generated as often as necessary once the centrifuge is in flight, and acceleration traces are remarkably similar from experiment to experiment. This not only means that the results of a particular test are reproducible, but also that the same earthquake can be generated for a variety of soil-structure systems. This consistency is important to maintain and is one of the most valuable features of centrifugal modeling. Figure 3.4 shows the acceleration at 14.58 ft. below the soil surface during two tests on the same soil deposit performed at different times. The earthquakes are almost identical. The correlation coefficient between these two time histories is 0.945 which is very close to perfect correlation. The 10 Hz. peak that is evident in Figure 3.4b corresponds to the fundamental frequency of the lead plate (see Figure 3.3b).

The acceleration at various locations in the soil and on the structure is measured using Kistler model 8616 miniature accelerometers. The accelerometers are cylindrically shaped, with

a diameter of 0.20 inches (5.08 mm) and a length of 0.23 inches (5.8 mm), and weigh only 0.018 ounces (0.5 grams). It is important that all transducers be as small as possible because, under the centrifugal acceleration, all objects are 100 times larger. The accelerometers are sensitive to only one direction and have a good tolerance to cross information. The sensitivity varies from 3 to 5 millivolts/g, and all accelerometers are calibrated through a wide range of frequencies prior to use. Since a transducer measures acceleration by detecteding the motion of its top casing relative to its base, there is concern that the pressure of the sand would cause erroneous readings on a buried accelerometer. To prevent this, the buried accelerometers are enclosed in cases which do not restrict their movement. The cases are semicircular with the curved part facing upward so that stresses do not build up in the soil.

The accelerometers are piezoelectric and require a coupler to send an input voltage and to amplify the output signal. The couplers are also made by Kistler and are mounted on the centrifuge arm. They are powered by 28 volts DC coming from a supply box in the control room. The voltage supply is sent into the centrifuge through high voltage slip rings. A signal coming out of an accelerometer in the bucket is amplified by a coupler and sent out of the centrifuge through a low voltage slip ring. The gain of a coupler is about 5. The signal is recorded on the Norland 3001 digital processing oscilloscope which triggers automatically upon detection of a voltage increase. The output is digitized using 1024 points per wave usually with a sample interval of 10, 20, 50 or 100 μseconds. The data is sent to a MICRO VAX for further processing.

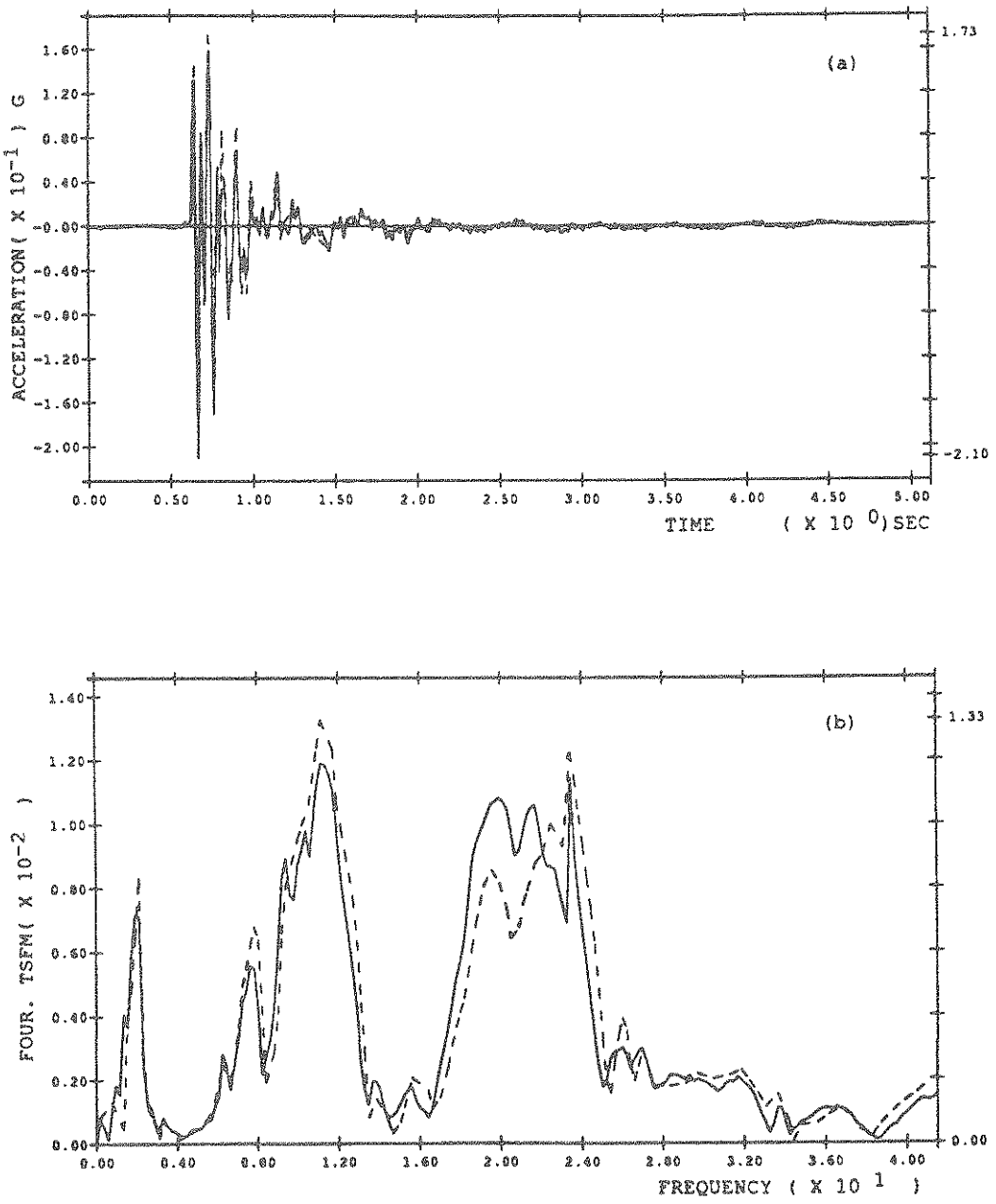

FIGURE 3.4

Acceleration Recorded 14.58 ft. Below the Soil Surface for Two Tests on the Same Soil Deposit Performed at Different Times. (Measurements are Given in Prototype Scale).

(a) Acceleration Time Histories.

(b) Fourier Transforms.

3.3 References for Chapter 3

3.1 Coe, C.J., Prevost, J.H., Scanlan, R.H., "Dynamic Stress Wave Reflections/Attenuation: Earthquake Simulation in Centrifuge soil models," *Earthquake Engineering and Structural Dynamics*, 1985, Vol. 13, pp 109-128.

3.2 Coe, Carlos, "On the Feasibility of Performing Dynamic Soil Tests in a Centrifuge," Ph.D. Thesis, Princeton University, Princeton, NJ, 1985.

3.3 Nagle, W.S., "Earthquake Simulation through Centrifugal Modeling and the Development of Experimental Control over the Hammer-Plate Excitor," B.S.E. Thesis, Princeton University, Princeton, NJ, 1985.

3.4 Lade, P.V., Duncan, J.M., "Cubical Triaxial Tests on Cohesionless Soil," *Journal of the Soil Mechanics and Foundations Division* , October, 1973, Vol. 99, No. GT10, pp. 793-812.

CHAPTER 4

CHARACTERIZATION OF THE CENTRIFUGE MODEL SYSTEM

4.1 Introduction

Before attempting to model soil-structure interaction effects, it is essential to characterize and understand the model system as thoroughly as possible in order to (1) verify that the earthquake simulated by the hammer-exciter plate and its propagational characteristics in the experimental soil deposit are representative of a realistic system, and (2) insure that the experimental data obtained from the model may be properly interpreted. In this chapter it is demonstrated through experimentation that the centrifuge model behaves realistically for a variety of soil and soil-structure systems. The tests discussed are divided into three categories, free field, scattered field and soil-structure interaction. The free field experiments examine the behavior of a horizontal soil layer during a simulated earthquake. The scattered field experiments focus on the effects of footing geometry on the input acceleration in a soil-structure system. The soil-structure interaction experiments investigate the response of a rigid circular footing to a simulated earthquake. To emphasize that the centrifuge model really represents a system that is 100 times larger, all measurements in this chapter are given in prototype scale unless otherwise indicated.

4.2 Free Field Experiments

The free field experiments examine the accelerations in a horizontal soil layer with a level free surface during a simulated earthquake. The goals of these experiments are (1) to demonstrate that the simulated earthquake is similar in amplitude and frequency content to a real earthquake, (2) to observe the dynamic characteristics of the soil deposit that might be noticeable during the earthquake, and (3) to show that the confined experimental soil deposit can be used to model a horizontal stratum of infinite lateral extent. To achieve these goals a 27.08 ft deep soil

stratum is instrumented with accelerometers as shown in Figure 4.1 and then subjected to a simulated earthquake. All accelerometers are oriented horizontally in the positive x direction (the direction of the blow of the hammer). This is done because the vibration of the exciter plate sends vertically incident shear waves up through the soil and, therefore, horizontal motion dominates in the system.

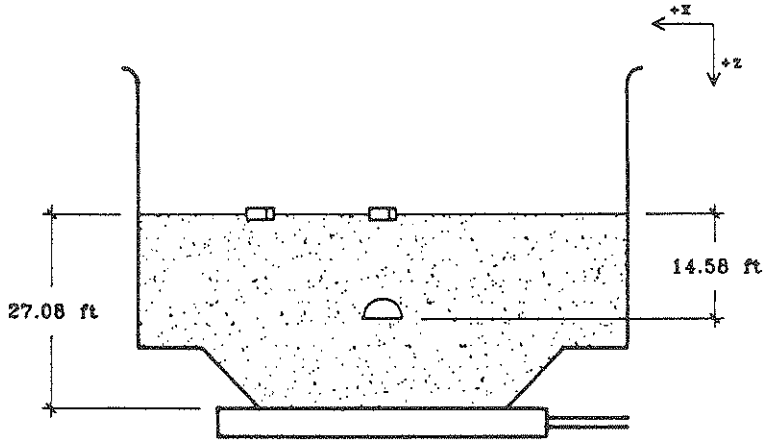

FIGURE 4.1
Accelerometer Configuration for Free Field Experiments

Figures 4.2 and 4.3 show the acceleration measured by each of the transducers (Figure 4.1) followed by their corresponding Fourier Transforms. The shaking induced by the exciter plate is similar to that which would be present near the source of a low magnitude earthquake. As an example, for the sake of comparison, the acceleration time history and the response spectra of the October 16, 1979 earthquake in Jenkinsville, S.C., recorded at the Monticello Dam site, are shown in Figure 4.4 along with the response spectra of the simulated earthquake. The earthquake at the Monticello Dam had a magnitude of 3.0, a hypocentral distance of 0.90 km and a depth of 0.07 km [4.1]. A comparison of the two response spectra in Figure 4.4 shows that the simulated and real earthquakes have similar, relatively high, frequency contents. The time history of the Monticello earthquake shown in Figure 4.4a may be compared to the time history of the simulated earthquake shown in Figure 4.2b. Both earthquakes are impulse-like (i.e. they have large amplitudes and short durations) with peak accelerations of about 0.35 g. Thus, the simulated

earthquake is similar in amplitude and frequency content to a real earthquake.

It is also evident from the free field measurements (Figures 4.2 and 4.3) that the earthquake is amplified as it travels towards the soil surface. The peak to peak amplitude of the acceleration increases by 71% between a depth of 14.58 ft (Figure 4.2a) and the soil surface (Figure 4.2b). The Fourier Transforms (Figures 4.3a and b) show that it is primarily the component at around 10 Hz that is amplified. The fundamental frequency of the soil layer in the horizontal direction is about 4.90 Hz (see Section 5.2) and is not present in the earthquake motion at depth. The 10 Hz component that is amplified corresponds to a higher order resonant frequency of the soil layer. Amplification is a resonance effect that has been observed in analogous prototype situations [4.2].

A comparison of the two signals recorded at different locations on the soil surface should provide an indication of how well the system is modeling a homogeneous horizontal stratum of infinite lateral extent. Ideally, vertically incident shear waves should yield the same acceleration at all points on the surface of a uniform soil layer. The acceleration at the soil surface to the left of the center (Figure 4.2c) is slightly smaller in amplitude but otherwise very similar to the acceleration measured at the center (Figure 4.2b). The coefficient of correlation of these two time histories is 0.716. The discrepancy between the acceleration at these two points is due to the fact that the exciter plate extends 16.67 ft from the center, but the outer accelerometer is 17.71 ft from the center (half-way between the center and the bucket wall). This off-center point sees a slightly weaker acceleration because it is not directly over the source of excitation. The distance between the two accelerometers is more than twice the radius of the footing of the structure used in the soil-structure interaction experiments described in Section 4.4 and Chapter 5. The acceleration is, therefore, fairly uniform for a region well beyond the dimensions of the base of the structure. Hence, wave reflections do not occur at the boundary walls when the walls are lined with Dux-seal.

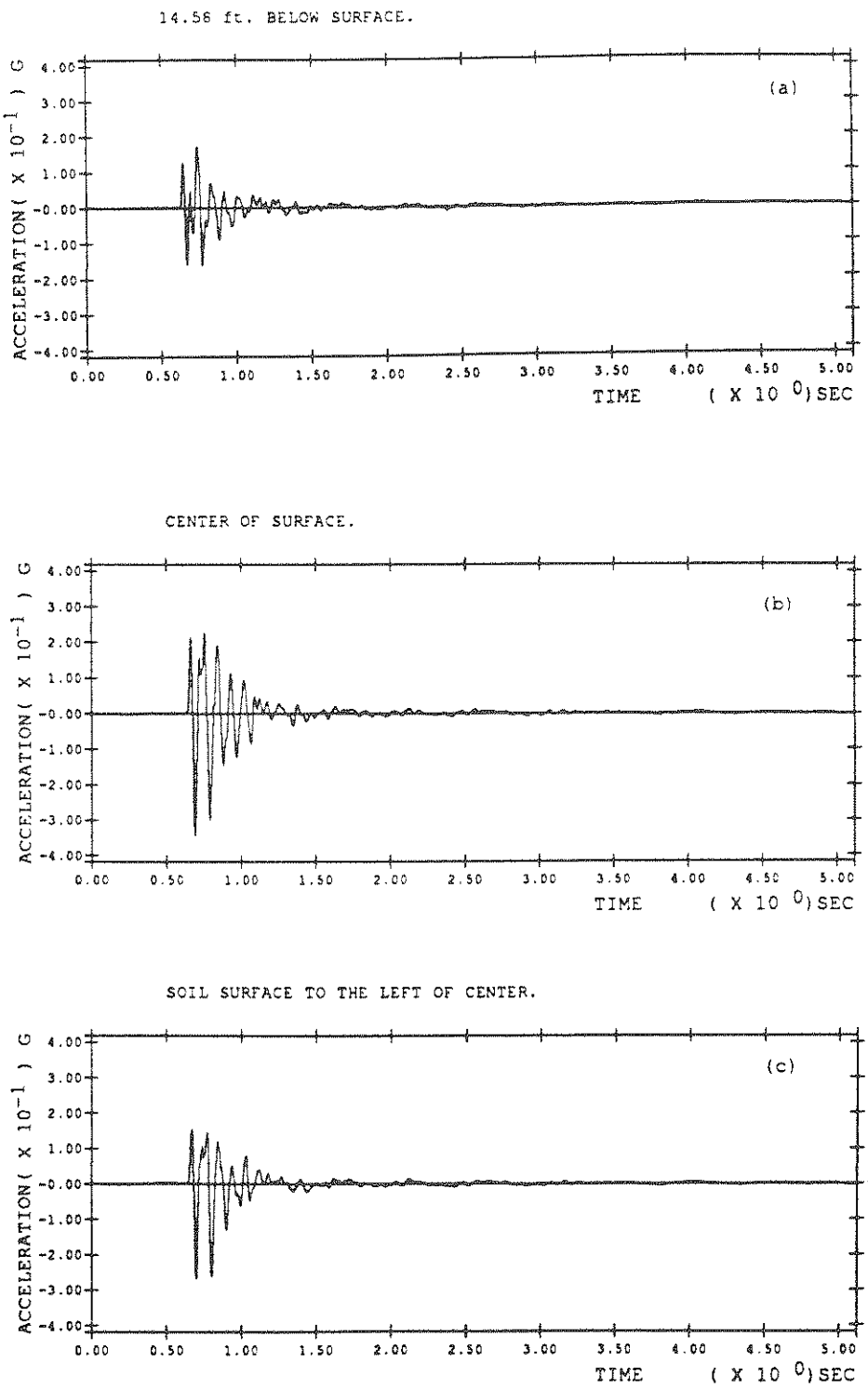

FIGURE 4.2
Free Field Test, Acceleration Recorded at Various Points in System.
(a) 14.58 ft. Below Surface.
(b) Center of Soil Surface.
(c) Soil Surface to the Left of Center.

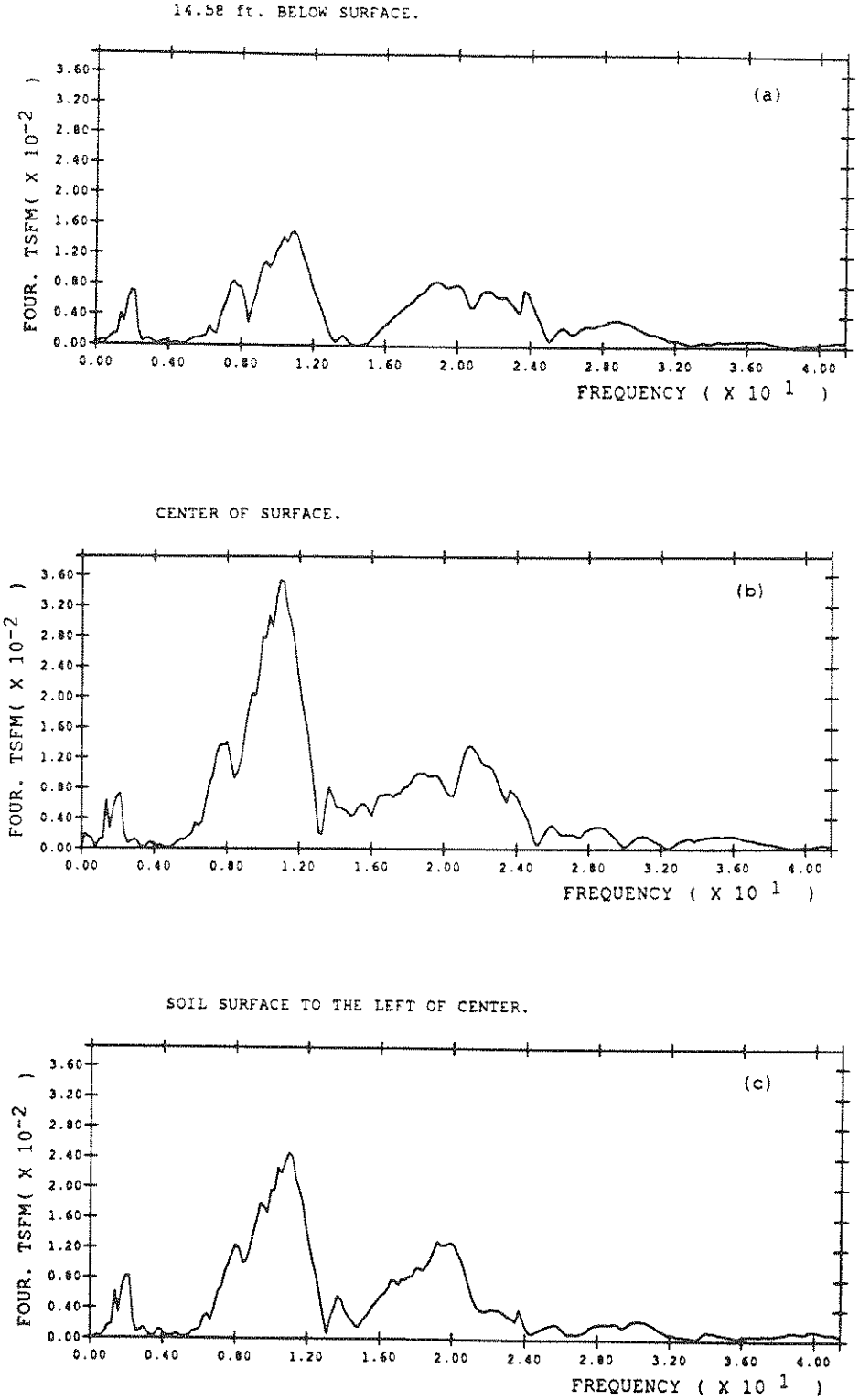

FIGURE 4.3

Free Field Test, Frequency Content of Acceleration at Various Points in System.

(a) 14.58 ft. Below Surface.

(b) Center of Soil Surface.

(c) Soil Surface to the Left of Center.

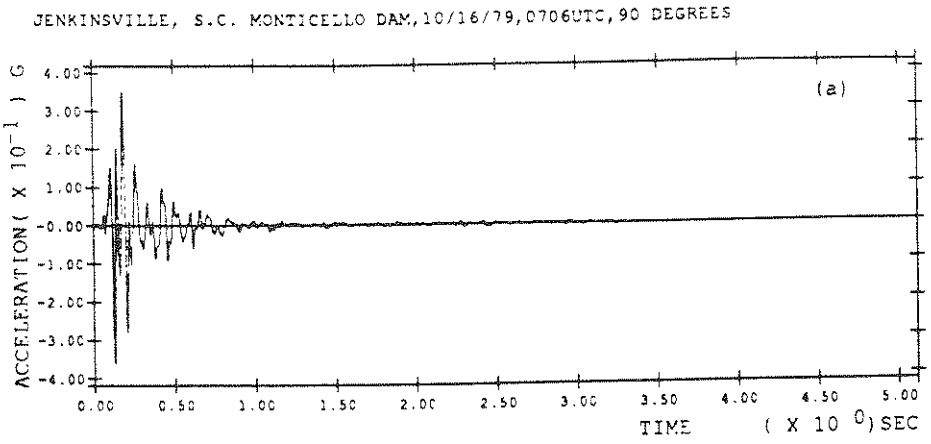

JENKINSVILLE, S.C. MONTICELLO DAM,
10/16/79,0706UTC,90 DEGREES.
0.0, 2.0, 5.0 ,10.0, 20.0 % DAMPING

SIMULATED EARTHQUAKE, HORIZONTAL COMPONENT
ON FREE SURFACE OF SOIL LAYER.
0.0, 2.0, 5.0 ,10.0, 20.0 % DAMPING

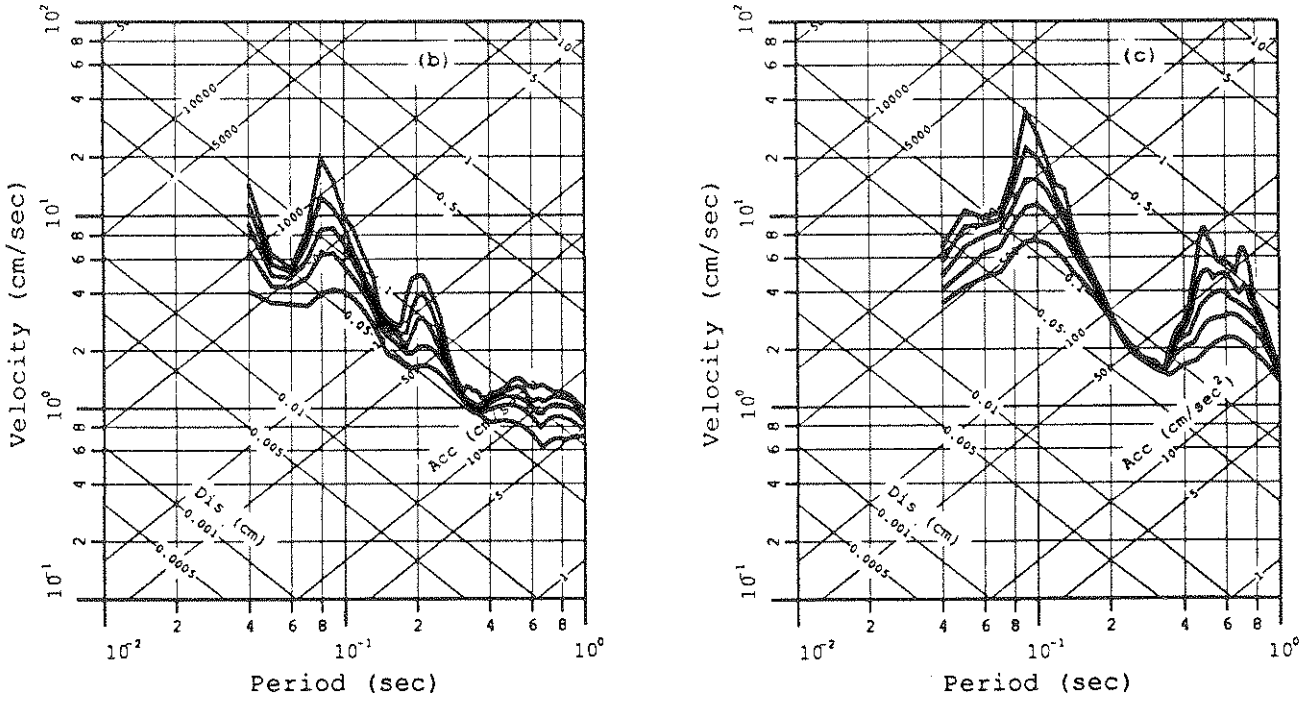

FIGURE 4.4
Comparison of Response Spectra of the Simulated Earthquake and
the October 16, 1978 Earthquake in Jenkinsville, S.C..
(a) Acceleration Time History of Jenkinsville Earthquake.
(b) Resonse Spectra of Jenkinsville Earthquake.
(c) Resonse Spectra of Earthquake Simulated by Hammer-Exciter Plate Technique.

4.3 Scattered Field Experiments

To further confirm the point that the surface accelerations are uniform, a comparison is made between the recorded free field motion at the center of the surface and the scattered field motion corresponding to a surface footing. The scattered field motion is the motion of the soil including the effects of the geometry of the structural foundation. For the case of a horizontal soil stratum of infinite lateral extent, the surface acceleration should be uniform and there should be no difference between the scattered and free field motions. Any difference between these two responses is, therefore, a measure of the error in the model system. Experimentally, the scattered field acceleration is obtained from an accelerometer mounted horizontally on a flat, plastic disk which is resting on the free soil surface. The disk has the same diameter as the base of the structure to be used and, with a thickness of 1/8 inch (model scale), it is essentially massless when compared to this structure. A layer of Monterey-0 sand is glued to the bottom of the disk to insure proper bonding between the disk and the soil surface. The measured scattered field acceleration is shown in Figure 4.5. The scattered field motion (Figure 4.5a) is found to be slightly larger than the free field motion (Figure 4.2b), but otherwise the two time histories are very similar. The correlation coefficient between the two motions is 0.857 which indicates a small amount of error in the experimental system. The results of the scattered field test for a surface footing clearly show that the model provides an accurate representation of a horizontal soil stratum of infinite lateral extent when the bucket walls are lined with Duxseal to attenuate wave reflections that would otherwise occur.

4.4 Soil-Structure Interaction Experiments

In this section a rigid circular footing on the surface of a 41.67 ft deep soil deposit is examined. The footing is made of brass and has a diameter of 16.4 ft, a height of 4.92 ft and a mass of $1.17\times10^4 \frac{lb}{ft/\sec^2}$. The configuration of accelerometers used to record the response at various

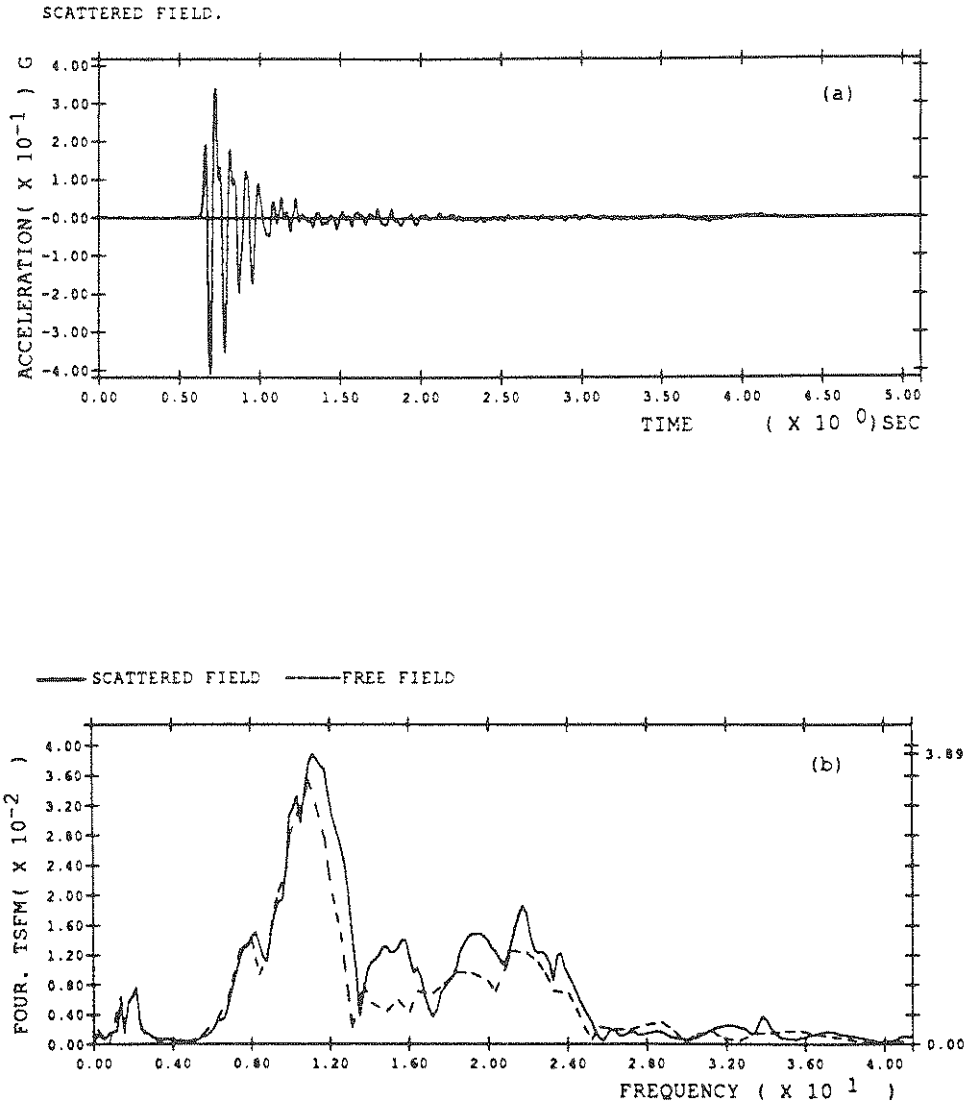

FIGURE 4.5
Scattered Field Acceleration.
(a) Acceleration Time History.
(b) Fourier Transforms of Scattered Field and Free Field Accelerations.

points in the system during a simulated earthquake is shown in Figure 4.6. There are horizontally oriented accelerometers 33.33 ft below the surface and on the side of the structure. There are vertically oriented accelerometers mounted on opposite ends of the structure. The measured accelerations are presented in Figure 4.7 The structure responds primarily in the horizontal mode (Fig. 4.6b). The vertical accelerations on opposite sides of the structure (Fig. 4.6c) are out of phase and slightly unequal in amplitude. This indicates that the structure undergoes some vertical and rocking motions. Although the peak amplitude of the vertical acceleration appears to be larger than the peak amplitude of the horizontal acceleration it is important to note that the vertical motion is recorded at a distance of 8.20 ft from the center of rotation and, therefore, represents a relatively small rotation.

The response of the footing in the centrifuge may be validated by comparing it to the response predicted analytically by a simple single degree of freedom model. The following equation of motion is used:

$$m\ddot{y} + c\dot{y} + ky = -m\ddot{u}_g$$

where m is the mass of the footing, u_g is the input ground motion given by the free field response of a soil deposit with a depth of 41.67 ft and y is the horizontal motion of the structure relative to u_g. A system identification method in which the error between the experimental and analytical response accelerations is minimized is used to extract appropriate values of c and k. The system identification technique is explained in detail in Chapter 6. The identified values of the damping and stiffness are found to be

$$c = 2.02\times10^5$$
$$k = 1.54\times10^7.$$

Figure 4.8 shows a comparison of the analytical and experimental accelerations. The experimental results are modeled very well by established theory. This demonstrates that the centrifuge model is capable of realistically representing a simple soil-structure system and can now be used with greater confidence to examine more complicated soil-structure systems.

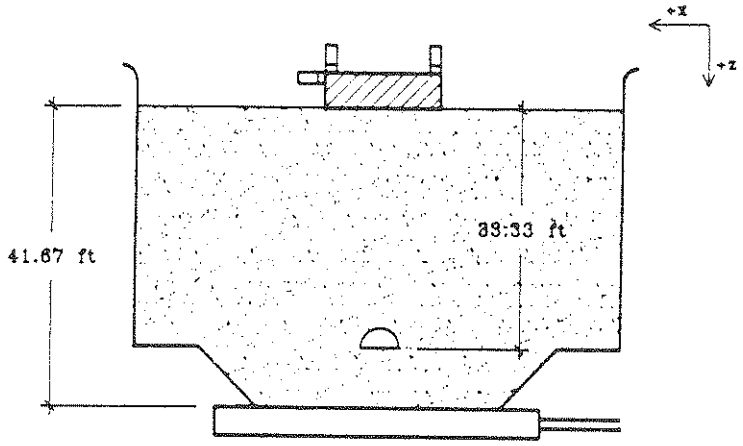

FIGURE 4.6
Accelerometer Configuration for Soil-Structure Interaction Experiments.

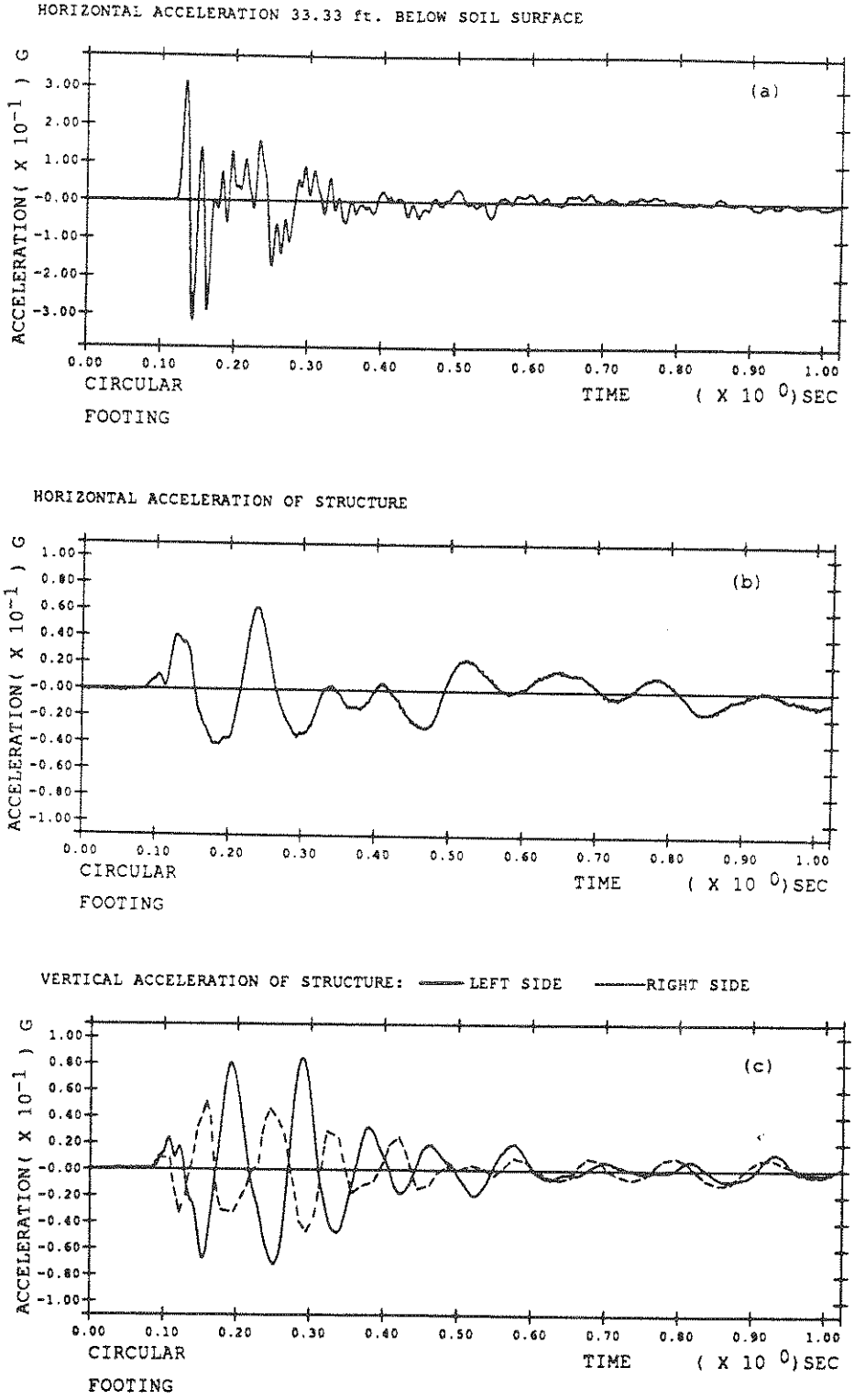

FIGURE 4.7

Soil-Structure Interaction Test, Acceleration Recorded at Various Points in System.

(a) Horizontal Acceleration 33.33 ft. Below Surface.

(b) Horizontal Acceleration of Structure.

(c) Vertical Acceleration of Structure.

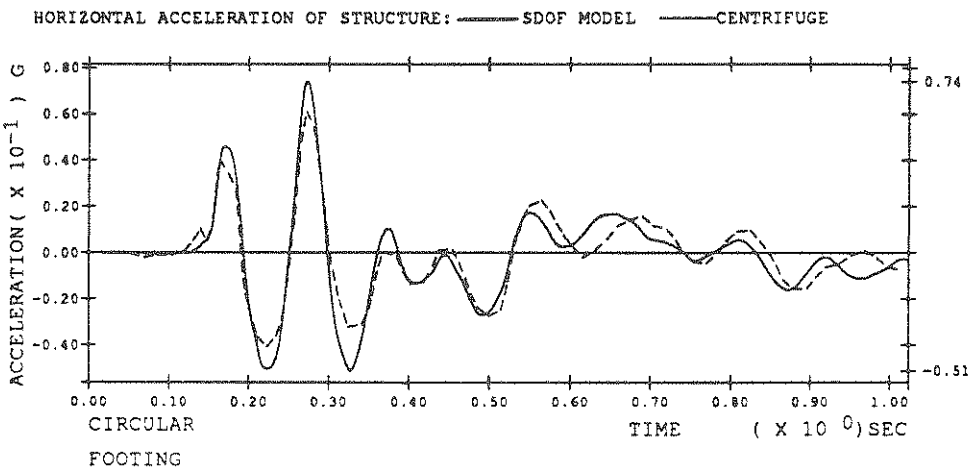

FIGURE 4.8
Horizontal Acceleration of Structure.
Comparison of ——Single Degree of Freedom Model and ----- Centrifuge Results.

4.5 Summary and Conclusions

The results of the experiments discussed in this chapter are summarized as follows:

1. The free field experiments show that the earthquake simulated by the hammer exciter plate technique is similar in amplitude and frequency content to a real earthquake (Fig. 4.4). The simulated earthquake is impulse-like having a large amplitude and a short duration. The free field experiments also show that the earthquake is amplified as it travels towards the soil surface, and that the acceleration is very similar at two different points on the soil surface just as it would be for a horizontal soil layer of infinite lateral extent.

2. The scattered field experiments demonstrate that the surface accelerations are in fact uniform over an area equal in size to the base of the structural footing.

3. The soil-structure interaction experiments show that the response of a rigid circular footing to a simulated earthquake can be accurately modeled by established lumped parameter theory.

The results of these experiments characterize the model system and are extremely important in demonstrating the value of this centrifuge model. The model consistently behaves as expected for simple, but realistic soil and soil-structure systems. It may now be used with confidence to examine more complicated systems. This is done in the experiments presented in Chapter 5.

4.6 References for Chapter 4

4.1 Fletcher, J.B., "A Comparison Between the Tectonic Stress Measured In Situ and Stress Parameters From Induced Seismicity at Monticello Reservoir, Sout Carolina," *Journal of Geophysical Research* , August 10, 1982, Vol. 87, No. B8, pp. 6931-6944.

4.2 Seed, H.B., and Lysmer, J., "The Seismic Soil-Structure Interaction Problem for Nuclear Facilities," *Soil-Strucure Interaction: The Status of Current Analysis Methods and Research*, Seismic Safety Margins Research Program, April 1980, p. II-26 - II-57.

CHAPTER 5

A STUDY OF RADIATION DAMPING AND SOIL-STRUCTURE INTERACTION EFFECTS IN THE CENTRIFUGE

5.1 Introduction

This chapter contains the details of an in depth experimental study of radiation damping and dynamic soil-structure interaction effects performed in the Princeton University Geotechnical Centrifuge. In the first part of this study (Section 5.3) the ability of the centrifuge model to represent soil-structure interaction effects is shown by using the model to demonstrate the phenomenon of radiation damping. When a structure is built on a half-space, energy is radiated away from it through the soil in all directions during vibration. This causes a damping of the structural response which is appropriately termed radiation damping. A soil deposit with a depth of three or four times the characteristic dimension of the structure (e.g the radius for a circular foundation) also behaves as a half-space as far as radiation damping is concerned [5.1]. If, however, a structure is built on a shallow layer over bedrock, radiation damping does not occur unless the natural frequency of the structure is greater than the fundamental frequency of the site (f_{soil}) [5.1, 5.2, 5.3] and surface waves can be generated at the soil-structure interface to radiate energy horizontally. The soil deposit in the centrifuge is used to model a shallow layer of soil and a structure with a variable natural frequency is introduced in order to demonstrate this phenomenon.

Once the capabilities of the model are established by this initial set of tests, further experiments are performed (Sections 5.4 and 5.5) in which the repeatability in the simulated earthquakes demonstrated in Chapter 4 is exploited in order to examine the response of various types of structures to the same earthquake. The experiments are designed to create a data pool which demonstrates the influence of

1. the frequencies of the structure

2. the foundation embedment, and

3. the foundation shape

on radiation damping and soil-structure interaction effects for a structure on a layer of soil over bedrock during an earthquake. This chapter presents the results of the experiments in the form of plots and qualitative observations. All quantitative analysis is left for Chapter 6. The emphasis in this chapter is on the experiments themselves and the wealth of data they provide. All the tests described herein are performed in a centrifuge at a centrifugal acceleration of 100g. All measurements in this chapter are given in prototype scale unless otherwise indicated.

5.2 Experimental Setup and Outline of Experiments

In all of the following experiments the model system consists of a single building-like structure on a horizontal soil stratum over "bedrock". The "bedrock" in the model is actually the exciter plate which provides the source of excitation. Previous experiments reported in Chapter 4 have demonstrated that the same simulated earthquake can be repeatedly generated. Therefore, by keeping the soil depth constant the earthquake input to the structure can be kept constant. This way the responses of a variety of independently tested structures may be directly compared as they are subjected to the same earthquake (i.e. the same amplitudes and frequencies of shaking). The soil deposit is a 27.08ft layer of Monterey-0 sand.

Similar structures are used in all of the experiments. They consist of a rigid base supporting a stem and a top mass. All components are made out of brass and, in all cases, the base is massive with respect to the superstructure. Figure 5.1 depicts the dimensions of the structure. The height of the top mass (h) can be changed in order to vary the natural frequency of the superstructure. The 16.4ft dimension of the base represents the diameter in the case of a circular footing and the width in the cases of square and rectangular footings. A strip footing with a width of

8.20ft is also tested. In all cases, the superstructure remains the same (except for the position of the top mass along the stem).

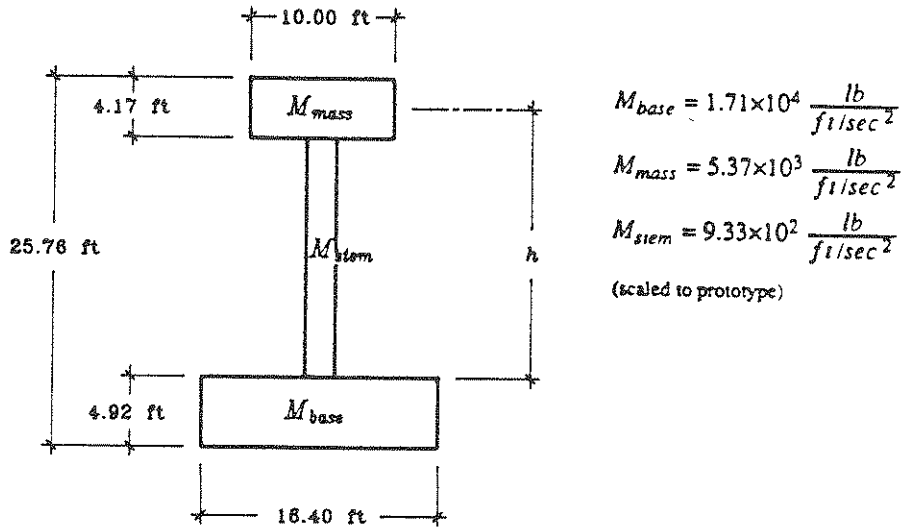

FIGURE 5.1
Dimensions of Structure.

Each structure can be viewed as having two primary frequencies, one associated with the horizontal motion of the superstructure and the other associated with the horizontal motion of the base. In order to explore the properties of radiation damping the frequency of the superstructure (henceforth denoted f_{str}) is varied above and below the fundamental frequency of the soil layer (which remains constant). The higher order structural frequency, which is associated with the base (f_b), remains the same. It is, therefore, necessary to determine approximate values of f_{str} and f_{soil}. These values only need to be exact enough to provide, *a priori*, an appropriate range of values of f_{str} which span the value of f_{soil}. This is done as follows:

f_{str} - The fixed base natural frequency of the structure is determined experimentally from a measurement of the free vibration acceleration of the superstructure while the base is clamped. A material damping ratio (ζ) is also estimated from this free vibration response using the log

decrement approximate method for small damping [5-4]:

$$\zeta = \frac{a_n - a_{n+m}}{2\pi m a_{n+m}} \times 100\%$$

where a_n and a_{n+m} are the amplitudes of the n^{th} and the $n+m^{th}$ cycles of acceleration respectively. Table 5.1 shows the results of these fixed base experiments for a variety of positions of the top mass. Each of these configurations is used in at least one of the experiments to be described in the next three sections.

TABLE 5.1
FIXED BASE FREQUENCIES
AND DAMPING RATIOS

h (ft.)	f_{str} (Hz.)	ζ (% of critical)
18.75	1.66	0.37
12.50	2.98	0.32
9.90	3.12	0.80
9.38	4.05	0.53
7.81	4.69	0.24
6.25	5.27	0.36

f_{soil} - The cutoff frequency above which radiation damping will occur is determined by the fundamental frequency of the site in the horizontal direction. This is because the dynamic excitation provided by the exciter plate consists primarily of vertically incident shear waves and, since the bottom heavy structure is not inclined towards rocking, it can be assumed that the structure will respond to these shear waves predominantly in the swaying mode. This value of f_{str} is calculated form the formula

$$f_{soil} = \frac{V_s}{4d} = 4.90Hz$$

where V_s is the shear wave velocity in the soil at a depth equal to half the cross sectional dimension of the base of the structure (531ft/sec, see Table 3.1) and d equals the depth of the layer (27.08ft). A shear column model such as the one presented in Reference 5.5 would account for the variation of shear wave velocity with depth in the calculation, giving an average value of f_{str}

for the stratum. However, the accuracy of this method is beyond the accuracy to which the shear modulus is known as a function of depth, so the extra effort involved in such a calculation is not worth while in this case.

It should be noted that the frequency of the massive rigid base should remain constant regardless of the value of f_{str}. It is, therefore, not necessary to have an *a priori* estimate of f_b as the value does not change and is most likely greater than f_{soil}. Hence radiation damping will be expected to occur at the base for all cases tested.

Uniaxial accelerometers are used to measure the response at various points in the system. Figure 5.2 shows the configuration of these transducers. There are horizontally oriented accelerometers placed at the soil surface, 14.5ft below the surface, the base of the structure and the superstructure. Vertically oriented accelerometers are placed on opposite ends of the base to detect rocking as well as vertical motion. The output is recorded on a NORLAND 3001 digital processing oscilloscope and stored on the MicroVAX for future analysis.

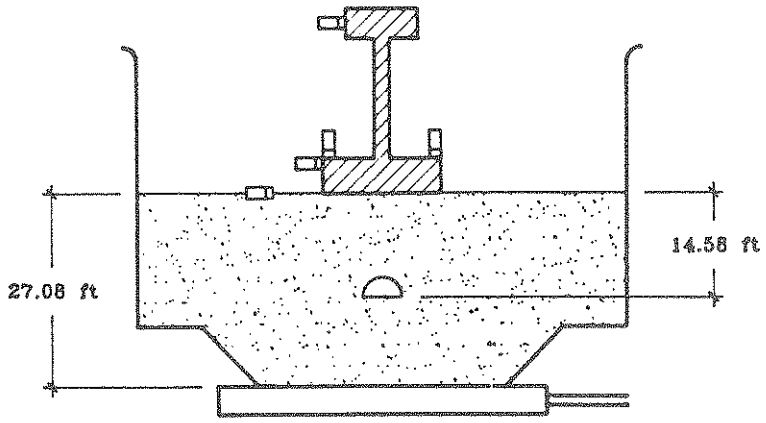

FIGURE 5.2
Accelerometer Configuration for Soil-Structure System.

Table 5.2 is a summary of the 32 test cases studied. The next three sections, in which the results of these tests are described, are organized as follows. In Section 5.3 the response of a structure with a surface footing is examined in detail, particularly for the influence of f_{str} and f_b on radiation damping and soil-structure interaction effects. Figure 5.3 shows a schematic diagram of a typical structure with a surface footing. The response of a similar structure with an embedded footing is presented for comparison in Section 5.4. Figure 5.4 shows a schematic diagram of a typical structure with an embedded footing. The responses of structures with surface and embedded foundations of various shapes are discussed in Section 5.5. Finally, the free field motion and the scattered field motions corresponding to each footing shape and level of embedment are presented in Section 5.6.

TABLE 5.2
SUMMARY OF TEST CASES

FOOTING SHAPE	SURFACE/ EMBEDDED	FREQUENCY OF SUPERSTRUCTURE (Hz)	FIGURE
Square	Surface	1.66	5.6
"	"	2.98	5.7
"	"	3.12	5.8
"	"	4.69	5.9
"	"	5.27	5.10
"	Embedded	1.66	5.11
"	"	2.98	5.12
"	"	3.12	5.13
"	"	4.69	5.14
"	"	5.27	5.15
Circular	Surface	1.66	5.16
"	"	4.05	5.17
"	"	4.69	5.18
"	"	5.27	5.19
Rectangular (L/W=2)	Surface	1.66	5.20
"	"	2.98	5.21
"	"	4.69	5.22
"	Embedded	1.66	5.23
"	"	2.98	5.24
"	"	4.69	5.25
Rectangular (L/W=4)	Surface	1.66	5.26
"	"	2.98	5.27
"	"	4.69	5.28
"	Embedded	1.66	5.29
"	"	2.98	5.30
"	"	4.69	5.31
Strip (L/W=8)	Surface	1.66	5.32
"	"	2.98	5.33
"	"	4.69	5.34
"	Embedded	1.66	5.35
"	"	2.98	5.36
"	"	4.69	5.37

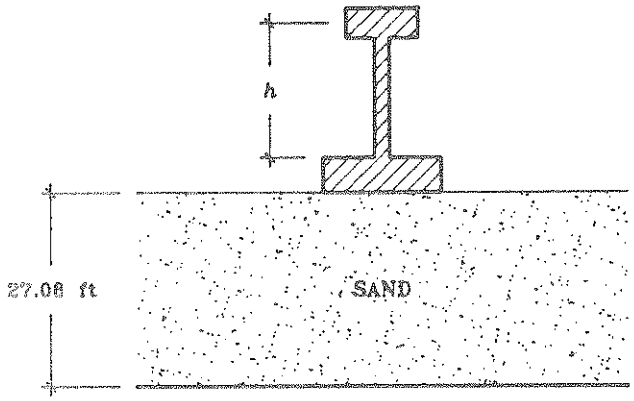

FIGURE 5.3
Schematic of Structure with Surface Footing.
Frequency of Superstructure Varies with Height of Top Mass (h).

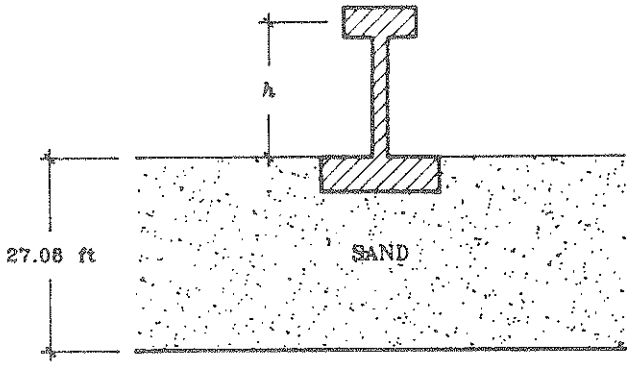

FIGURE 5.4
Schematic of Structure with Embedded Footing.

5.3 Structure With A Surface Square Footing

In the first set of experiments, the structure with a square base is placed on the surface of the soil deposit and subjected to a simulated earthquake. The height of the mass is moved down or up to induce or inhibit radiation damping respectively. Five values of f_{str} are tested:

(a) 1.66Hz < f_{soil}, (b) 2.98Hz < f_{soil},

(c) 3.12Hz < f_{soil}, (d) 4.69Hz ≈ f_{soil},

(e) 5.27Hz > f_{soil}.

Case (a) represents a situation where we would anticipate no radiation damping. Case (e) represents a situation where radiation damping is expected to occur. Cases (b), (c) and (d) fall in between these two extremes. In all cases, radiation damping is expected to occur at the base. Figure 5.5 shows the absolute acceleration of the superstructure plotted with the earthquake recorded below the soil surface for cases (a) through (e). It is clear from this comparison that in case (a) the superstructure is still accelerating after the earthquake is finished. This implies that energy is trapped in the structure and is not allowed to radiate away, thus radiation damping is small or nonexistent for case (a). In contrast to this, in case (e) the response of the superstructure dies out with the earthquake excitation indicating that radiation damping does exist for this case. Figures 5.5(b), (c) and (d) show that as f_{str} is increased above f_{soil} the amount of radiation damping increases. The concept derived from linear elastic theory that f_{soil} is a cutoff frequency perhaps suggests a more drastic jump between the occurrence and nonoccurrence of radiation damping than actually exists.

The acceleration is recorded at six different points in the soil-structure system for each test case (see Figure 5.2). As an example, Figure 5.6 shows the recorded accelerations along with their Fourier Transforms for case (a) where f_{str}=1.66Hz. The recorded accelerations for cases (b) through (e) are too numerous to be presented here but may be found in Reference 5.6. The

observations made from these recordings are summarized as follows.

The earthquake at 14.58 ft below the soil surface is similar for each case, therefore allowing direct comparisons to be made between the structural responses for different cases. A comparison of the five superstructure accelerations shows that the amplitude and frequency content of the strong motion response of the superstructure increases with f_{str}. The peak amplitude of the strong motion response increases by about 90% from case (a) to case (e). The dominant frequency component of the strong motion response is about 7.5Hz for case (a) and increases to about 22Hz for case (e). The strong motion response is damped out within about the first second of the earthquake for all five values of f_{str}.

In contrast to the superstructure, the horizontal motion of the base is very similar for all five test cases. The horizontal motion of the base dies out with the input earthquake. The Fourier Transforms of these signals indicate that the base responds with a dominant frequency of about 8.00Hz which is above the fundamental frequency of the soil layer. Thus, the heavy base is essentially acts independently of the superstructure and radiation damping occurs for this degree of freedom regardless of the height of the top mass.

The vertical accelerations recorded at opposite ends of the base are also quite similar for all five values of f_{str}. The signals on the right and left side are out-of-phase indicating that some rocking does occur. However, the vertical accelerations die out with the earthquake indicating that rocking does not contribute to the trapped energy observed in the superstructure when $f_{str} > f_{soil}$. The amplitudes of the two vertical accelerations are slightly unequal indicating that some purely vertical motion exists as well.

Finally, in addition to these observations on the soil-structure system, an important conclusion can be drawn about the ability of the bounded model to represent a layer of infinite lateral extent. The fact that radiation damping can be observed in the centrifuge model means that the

Duxseal lining the containment walls is indeed preventing waves from being reflected back into the system. This fact is crucial to the study of soil-structure interaction in the centrifuge.

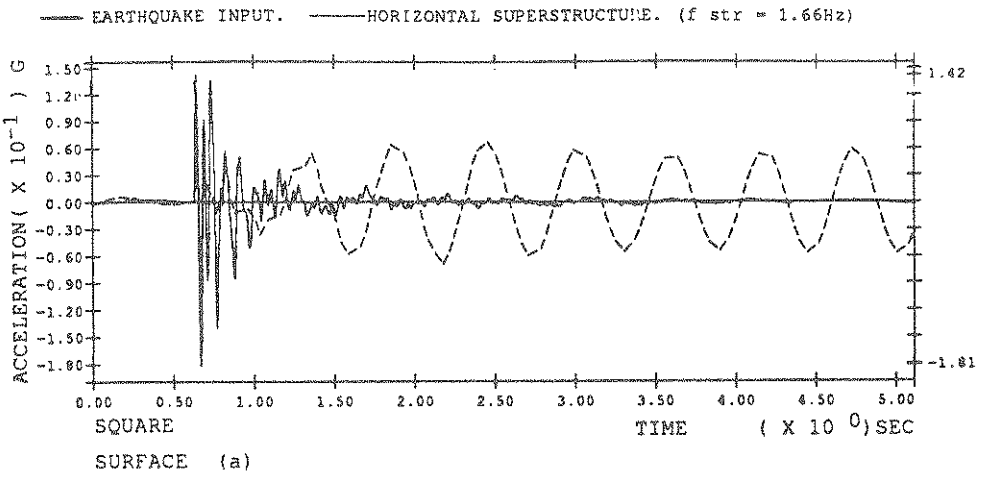

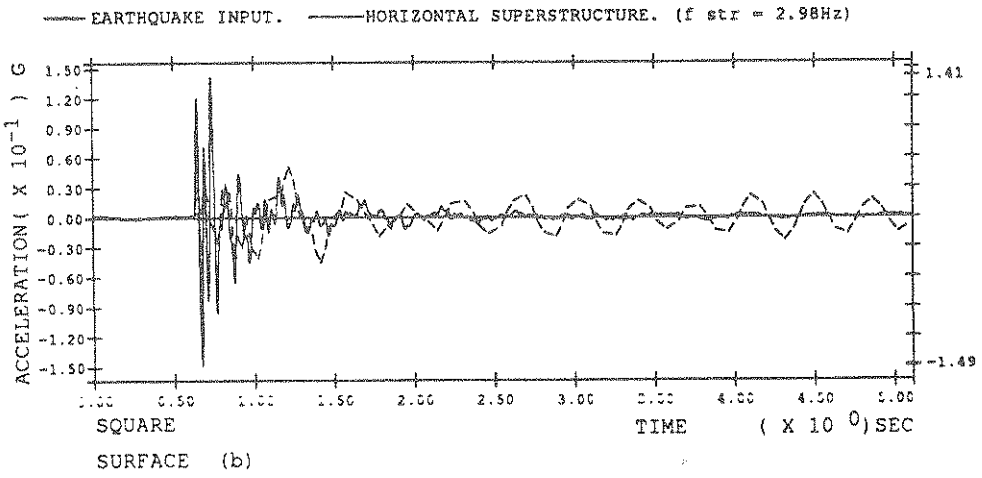

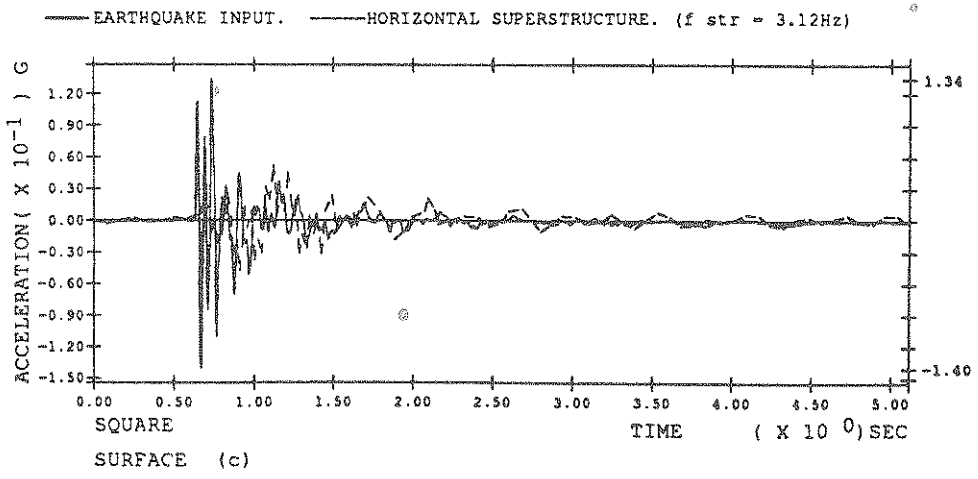

FIGURE 5.5
Horizontal Acceleration of Superstructure Plotted Against
Earthquake Input For Structure with Surface Square Footing.
(a) f_{str} = 1.66Hz.
(b) f_{str} = 2.98Hz.
(c) f_{str} = 3.12Hz.

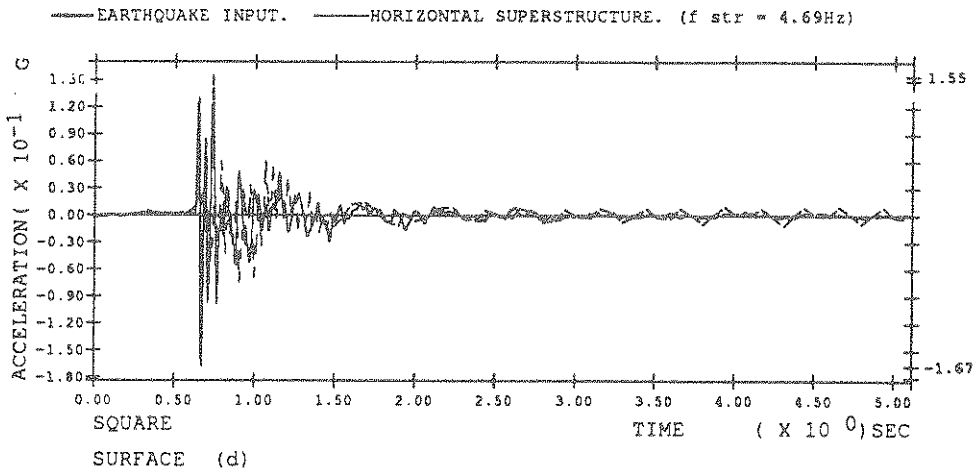

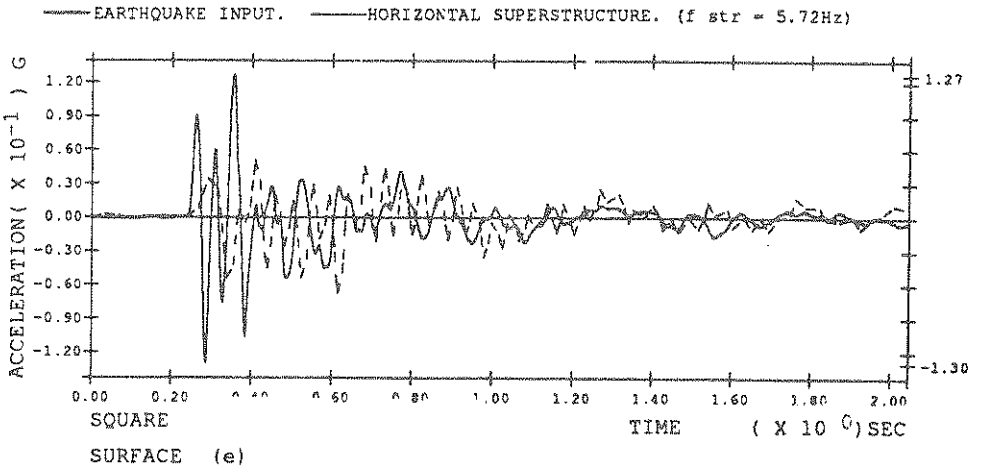

FIGURE 5.5 (cont'd)
Horizontal Acceleration of Superstructure Plotted Against
Earthquake Input For Structure with Surface Square Footing.
(d) f_{str} = 4.69Hz.
(e) f_{str} = 5.72Hz.

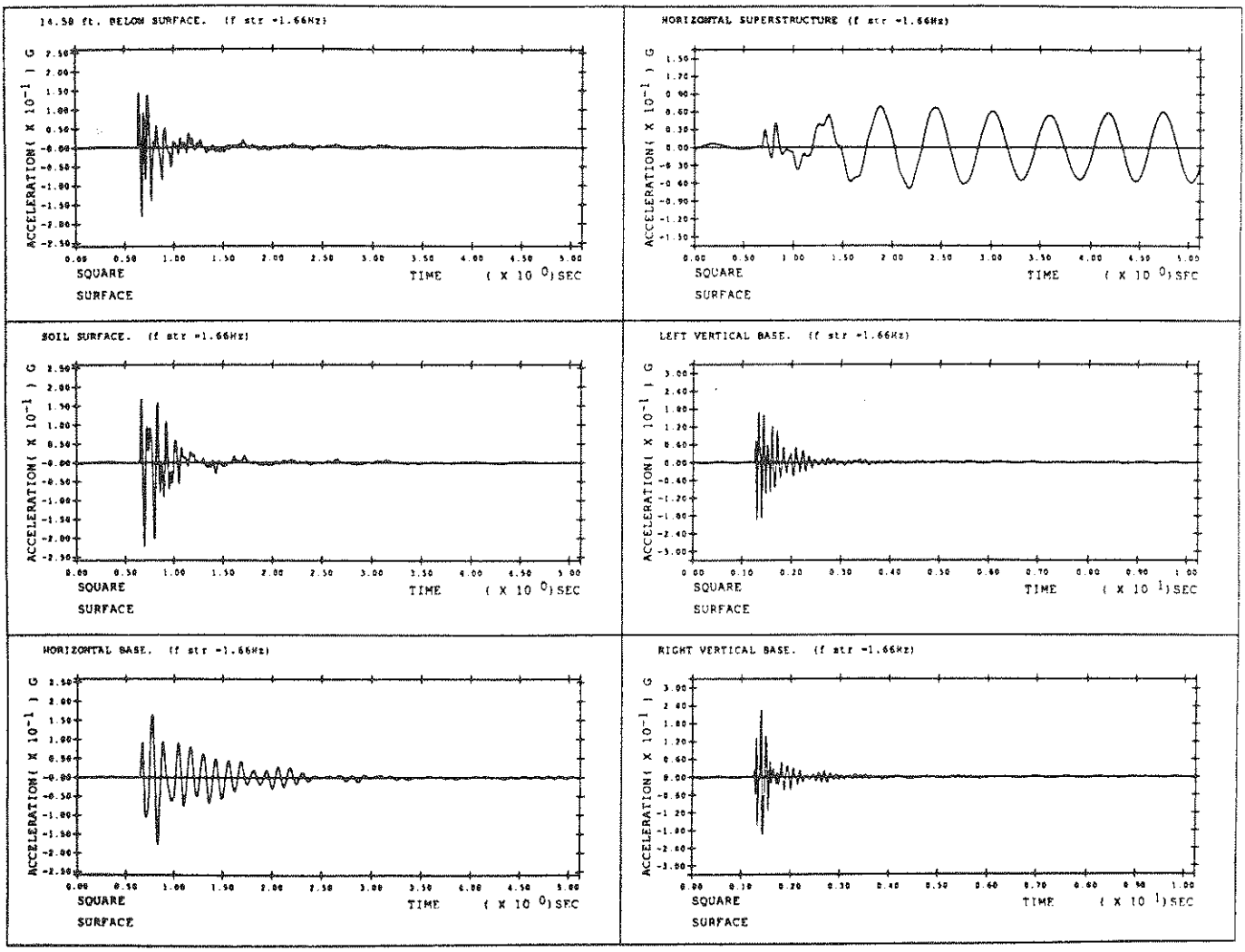

FIGURE 5.6
System with Surface Square Footing (f_{str} = 1.66Hz)

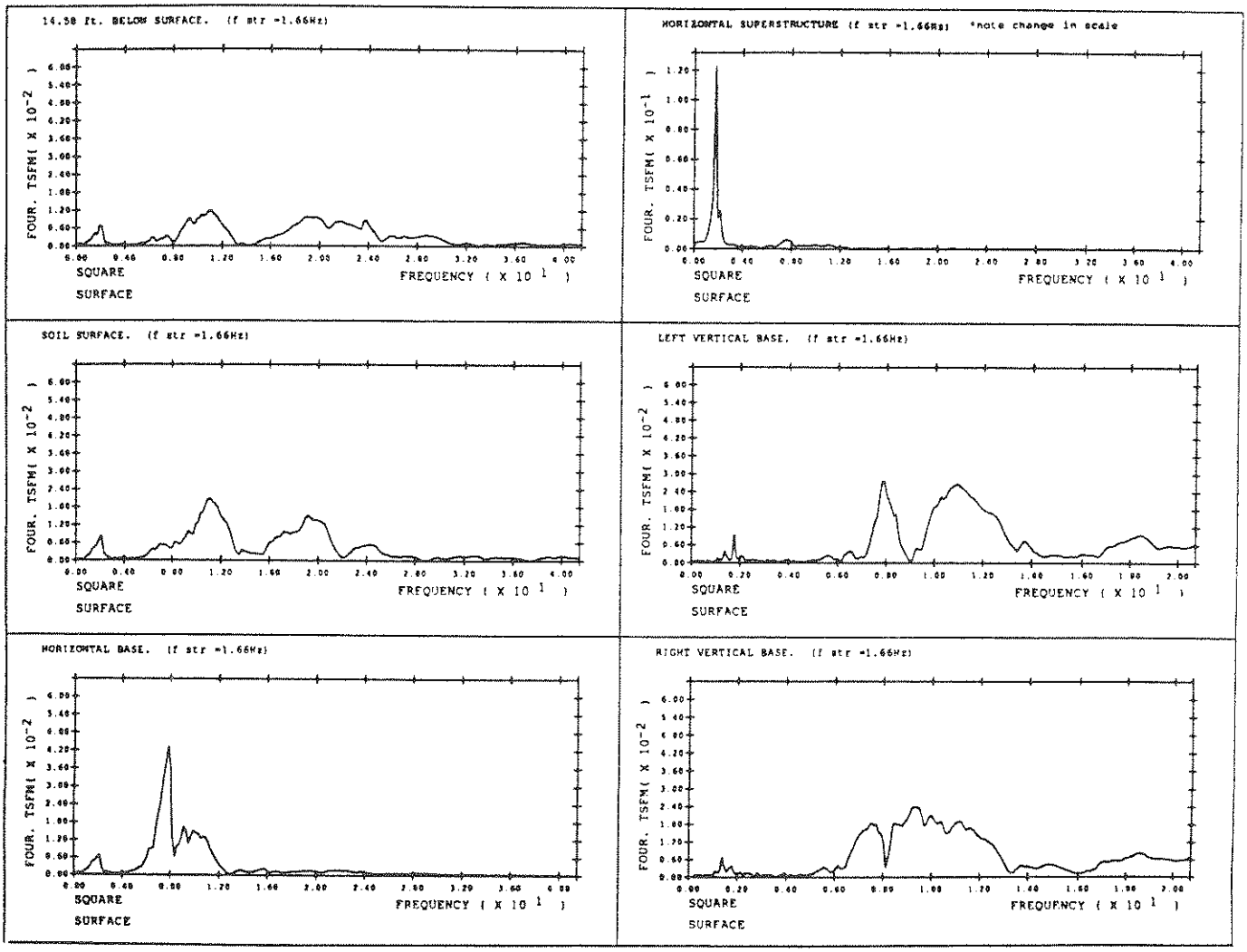

FIGURE 5.6 (cont'd)
System with Surface Square Footing (f_{str} = 1.66Hz)

5.4 Effects of Embedment

In the next set of experiments the structure with the square footing used in Section 5.3 is embedded up to the top of the base (see Figure 5.4). The depth of embedment, therefore, is 4.89ft. Sand is now glued to the side of the base as well as the bottom to ensure bonding between the side walls of the footing and the soil. The earthquake input is the same as it was for the surface structure experiments so direct comparisons of the structural response can be made between the two systems. The same five values of f_{soil} used in the surface footing experiments are tested with the embedded footing. Once again, the accelerations and Fourier Transforms for the case where f_{str}=1.66Hz are presented here (Figure 5.7) as an example, and the rest of the results may be found in Reference 5.6.

The horizontal motion of the superstructure shows the same general trends of radiation damping that were exhibited in the surface footing experiments; i.e. the amount of radiation damping increases as f_{str} increases. The amplitude and frequency content of the superstructure at the end of the signal (after two seconds) is similar for the embedded and the surface structures.

The strong motion response at the superstructure increases in amplitude and frequency as f_{str} is increased. This was generally true for the surface structures. However, the high frequencies present in the strong motion response are more heavily damped for the structures with embedded footings.

The horizontal motion of the base behaves similarly for the surface and embedded cases in that radiation damping exists for all values of f_{str}. However, the dominant frequency of the response, as seen from the Fourier Transforms, is slightly larger for the embedded structures (≈11Hz) than for the surface structures (≈8Hz). Thus the stiffness at the base-soil interface is larger for the embedded structure. The peak amplitude and damping at the base are also larger for the embedded structure.

The vertical motions on opposite sides of the base are similar for all five values of f_{str} and are again out-of-phase and of unequal amplitude. However, the vertical accelerations are smaller for the embedded structure than the surface structure. This is quite reasonable as the embedment provides some resistance to rocking, and the bonding between the side walls of the foundation and the soil restricts vertical motion.

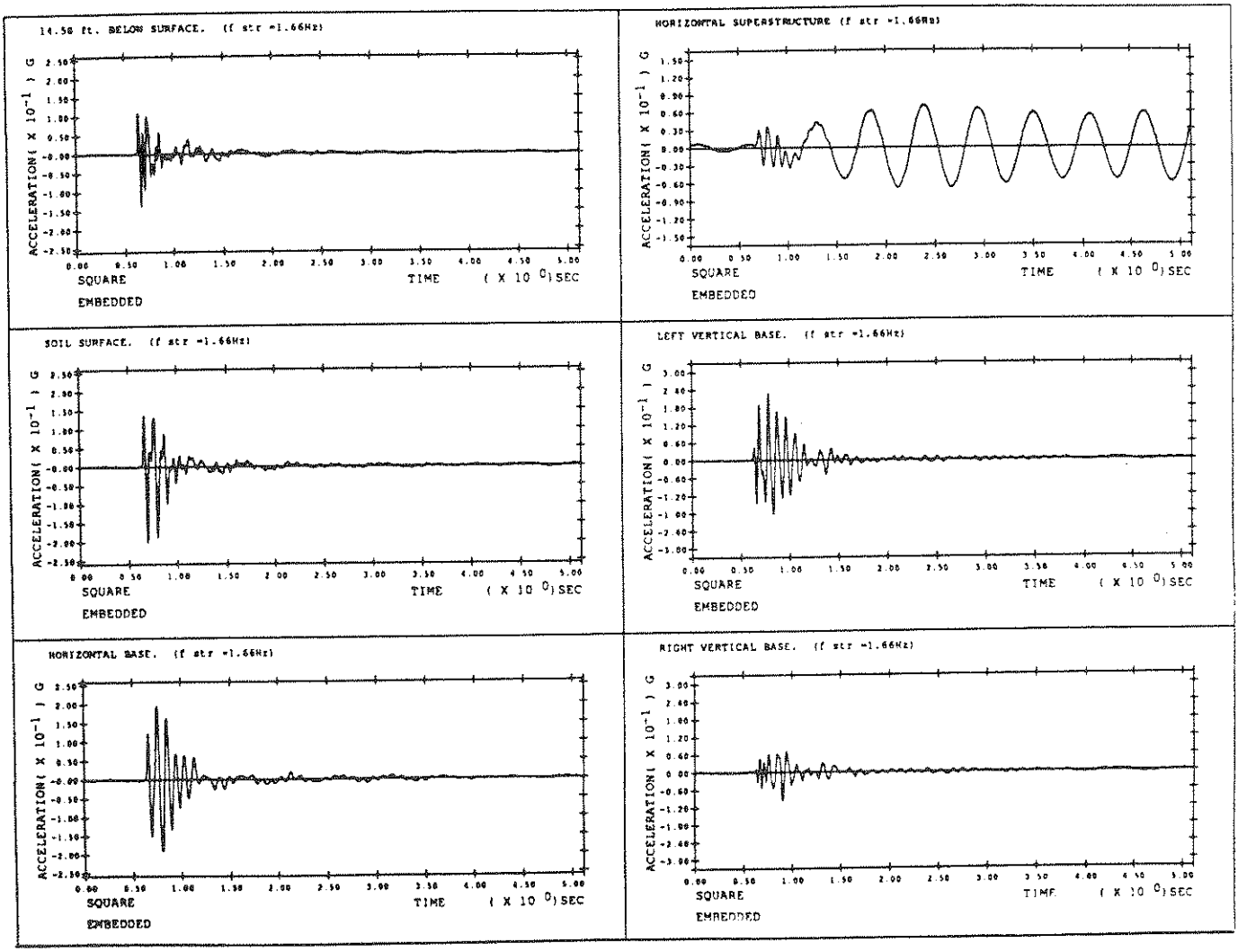

FIGURE 5.7
System with Embedded Square Footing (f_{str} = 1.66Hz)

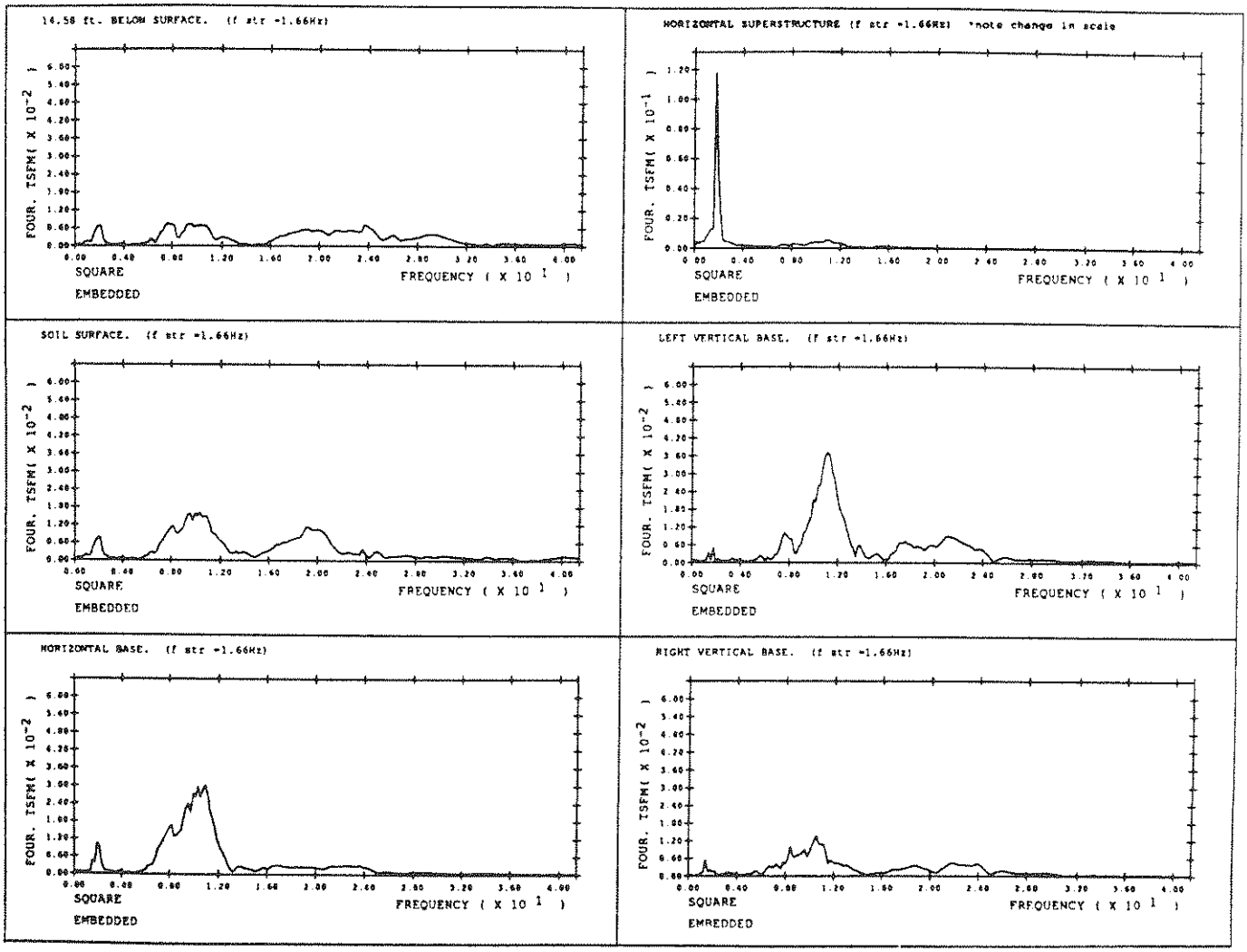

FIGURE 5.7 (cont'd)
System with Embedded Square Footing (f_{str} = 1.66Hz)

5.5 Effects of Foundation Shape

In order to establish the effects of foundation shape on radiation damping and soil-structure interaction, the experiments described in the preceding two sections are repeated for four additional foundation shapes. The additional shapes are a circle, a rectangle with an aspect ratio of 2, a rectangle with an aspect ratio of 4, and a strip (a long rectangle with an aspect ratio of 8). The same adjustable superstructure is used in each case. The circular and rectangular footings have a radius or half-width equal to the half-width of the square foundation (8.20ft). However, because of the limited dimensions of the model container, the half-width of the strip footing must be reduced (4.10ft) in order to obtain a large aspect ratio. In this section the results of the surface and embedded tests are presented simultaneously for each foundation. For the circular footing, tests are performed for values of f_{str} = 1.66Hz, 4.05Hz, 4.69Hz and 5.27Hz. For the two rectangular and the strip footings the tests are performed for values of f_{str} = 1.66Hz, 2.98Hz and 4.69Hz.

5.5.1 Circular

The accelerations of various points of the system with a circular footing and f_{str} =1.66Hz are shown in Figure 5.8 for the surface case (see Reference 5.6 for the results of all the surface tests). Unfortunately, the structure with the circular footing suffered damage during the embedded experiments so the results of the embedded tests must be excluded from the current study. The responses of the superstructure in the surface tests demonstrate the same relationship between radiation damping and f_{str} that is evident for the structure with a square footing. For $f_{str} < f_{soil}$ energy is still trapped in the structure after the earthquake ends whereas for $f_{str} > f_{soil}$ this energy is being radiated away.

The horizontal acceleration of the base is unaffected by the changes in the natural frequency of the superstructure. The dominant frequency of the base response for the surface structure is

7.8Hz. The vertical accelerations of the base are once again out-of-phase and unequal in amplitude signifying a combination of rocking and vertical motion.

5.5.2 Rectangular (Length/Width =2)

Examples of the response accelerations of the system with a surface and an embedded rectangular footing with an aspect ratio of 2 are shown in Figures 5.9 and 5.10, respectively. The rest of the results are given in Reference 5.6. The output at the superstructure indicates that the amount of radiation damping reflects changes in f_{str} much as it did in the previous tests with the square and circular footings. Like the square footing experiments, the strong motion response of the superstructure on this rectangular footing increases in amplitude and frequency content as f_{str} increases, and the high frequencies present in the strong motion response are more heavily damped for the embedded cases.

The horizontal acceleration at the base is distinctly larger for the embedded structure than for the surface structure. The peak amplitude differs by almost 100%. The dominant frequency of the base acceleration for the embedded structure (≈ 11Hz) is once again slightly larger than for the surface structure (≈ 8Hz). The vertical accelerations of the base follow the same trends as the vertical accelerations of the square and circular footings.

5.5.3 Rectangular (Length/Width=4)

Figures 5.11 and 5.12 show the results of the tests performed on structures with a rectangular base with an aspect ratio of 4 for f_{str}=1.66Hz. The rest of the results are given in Reference 5.6. The amplitude and frequency content of the horizontal acceleration of the superstructure are generally comparable for the surface and embedded cases. The trends in radiation damping discussed in previous sections are exhibited here as well. For the square footing and the other rectangular footing it was noticed that the higher frequencies present in the strong motion part of the

response are damped more heavily for the embedded structure than the surface structure. This is not true for the rectangular footing with an aspect ratio of 4.

The horizontal acceleration at the base is quite low for this rectangular footing, especially for the surface cases. This is most likely due to the fact that the base is now very large. Again, the horizontal acceleration at the base has a higher frequency content and more damping in the embedded experiments. The two vertical accelerations are out-of-phase, but are now very close in amplitude for both the surface and embedded cases and all values of f_{str}. It should be noted that the vertical accelerations decrease with embedment while the horizontal base accelerations increase.

5.5.4 Strip (Length/Width=8)

The results for the strip footing are shown in Figures 5.13 and 5.14 for f_{str}=1.66Hz. The rest of the results are given in Reference 5.6. The half-width of this footing is decreased by a factor of two in order to achieve a larger aspect ratio (half-width = 4.10ft). Thus the footing is narrower and less massive than the preceding rectangular footing and more rocking motion is likely to occur. This tendency is borne out in the large peak response of the superstructure and the large vertical accelerations of the base for the surface structure with f_{str} = 1.66Hz (Figure 5.13). although the vertical accelerations in this figure are comparable in absolute amplitude to the vertical accelerations of the other footing shapes, the rocking of the structure with the strip footing is actually twice as large as the figures indicate because the footing width is decreased by a factor of 2. When the structure is embedded, the soil offers a greater resistance to rocking and the peak amplitudes of the horizontal motion at the superstructure and the vertical motions at opposite sides of the base are smaller (Figure 5.14). Otherwise, the same trends of radiation damping are noticed for the response of the superstructure on the strip footing.

The peak horizontal response of the base is larger and has more damping and a higher dominant frequency for the embedded strip footing. The vertical motions are out-of-phase as they were for the other footing shapes.

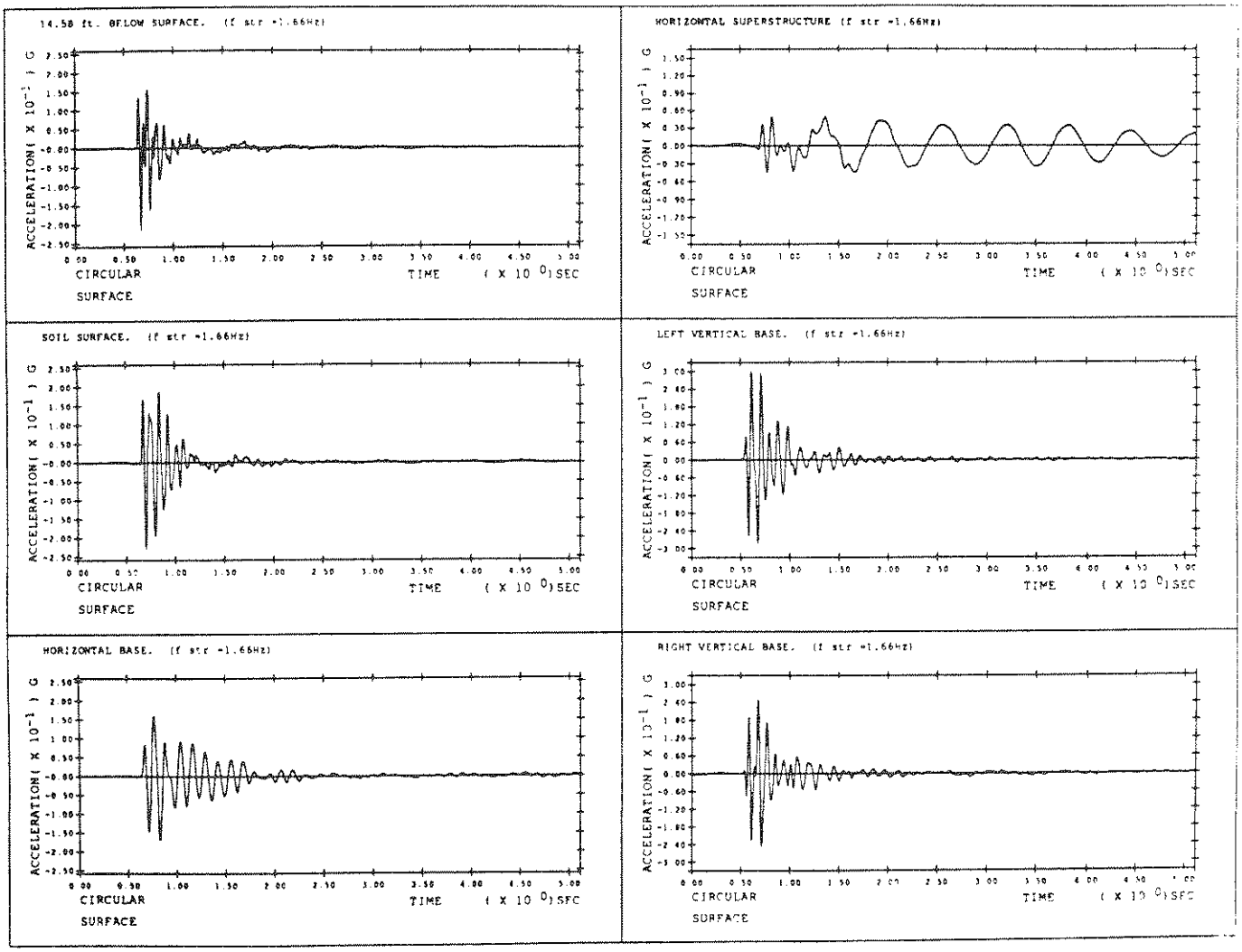

FIGURE 5.8
System with Surface Circular Footing (f_{str} = 1.66Hz)

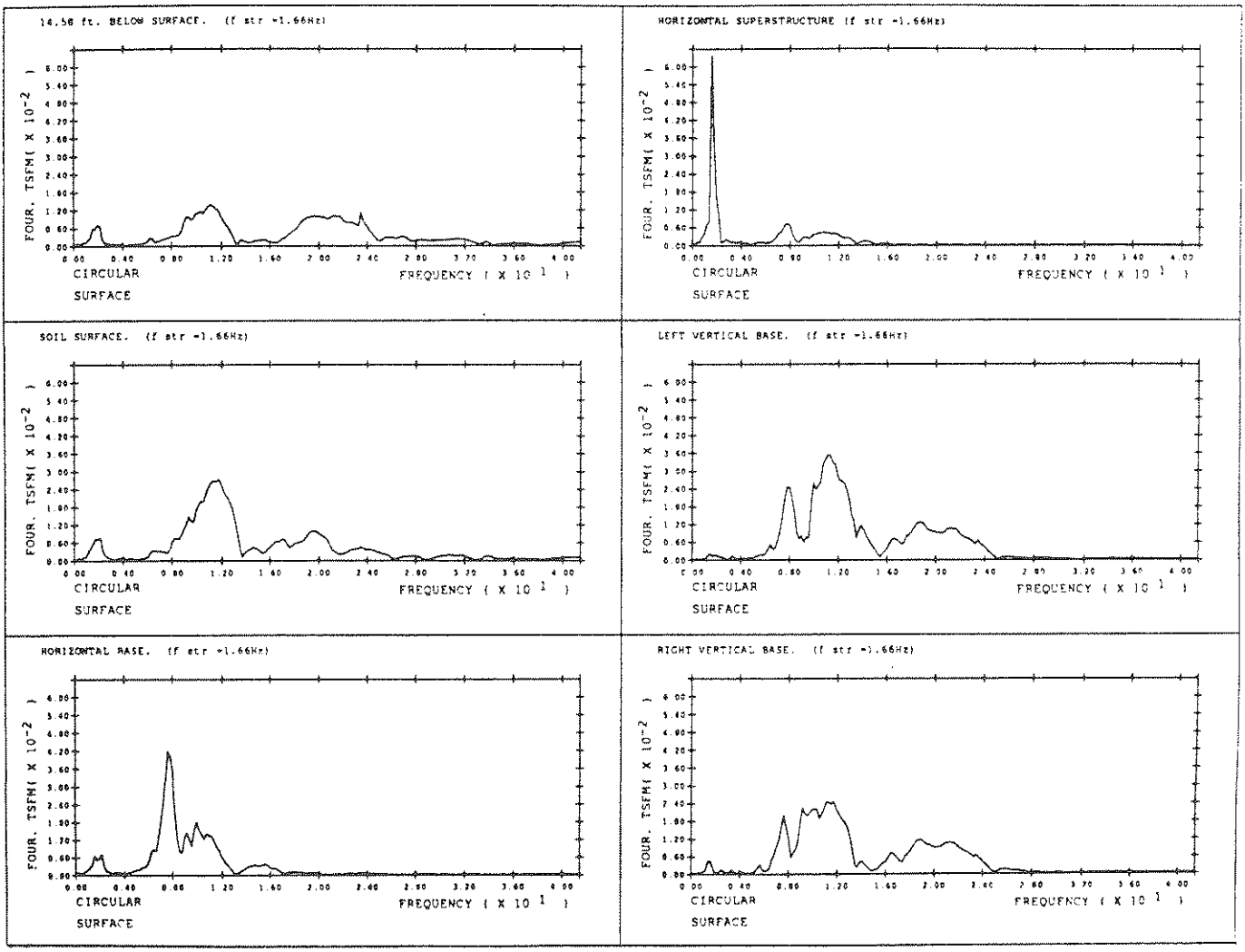

FIGURE 5.8 (cont'd)
System with Surface Circular Footing (f_{str} = 1.66Hz)

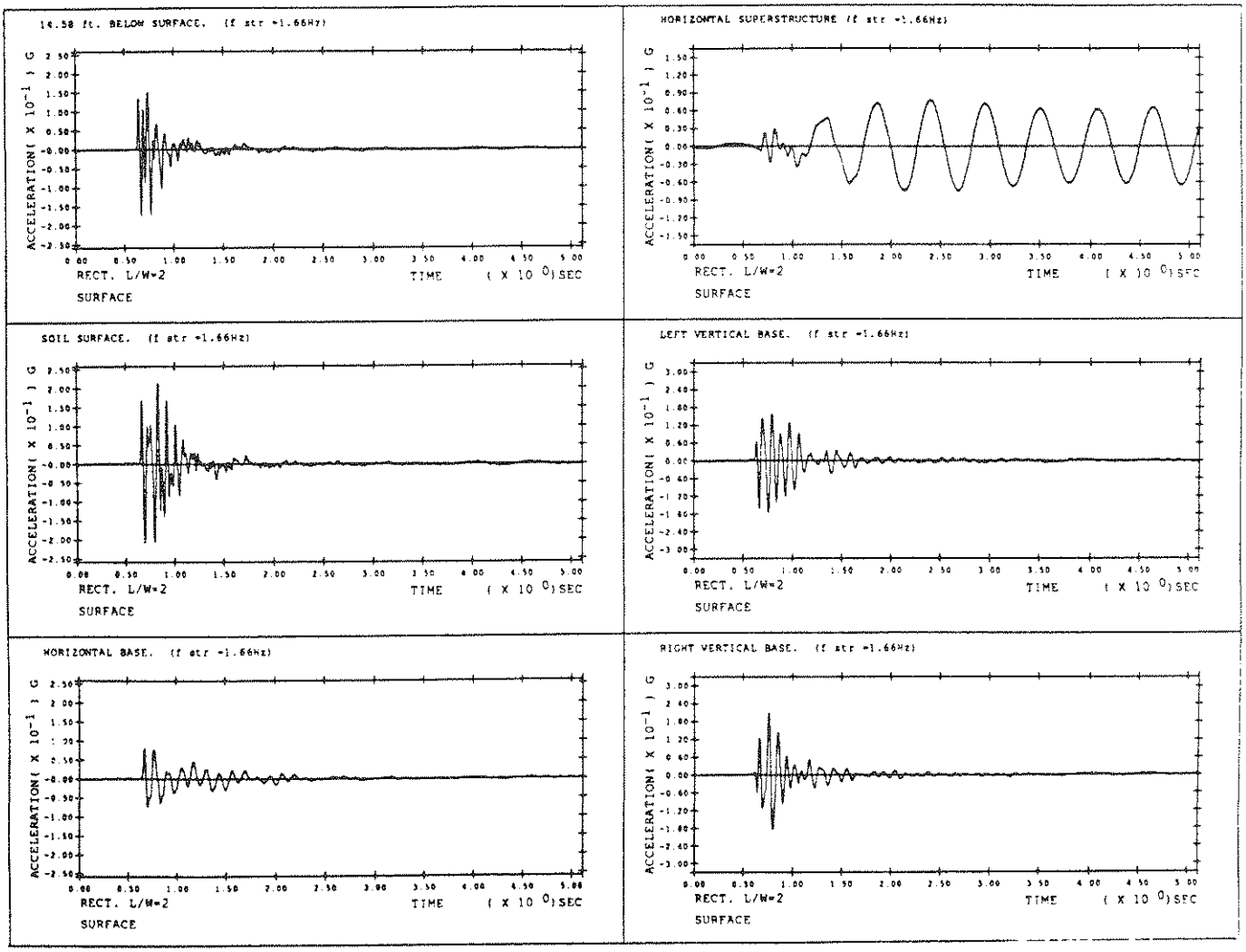

FIGURE 5.9
System with Surface Rectangular (L/W=2) Footing (f_{str} = 1.66Hz)

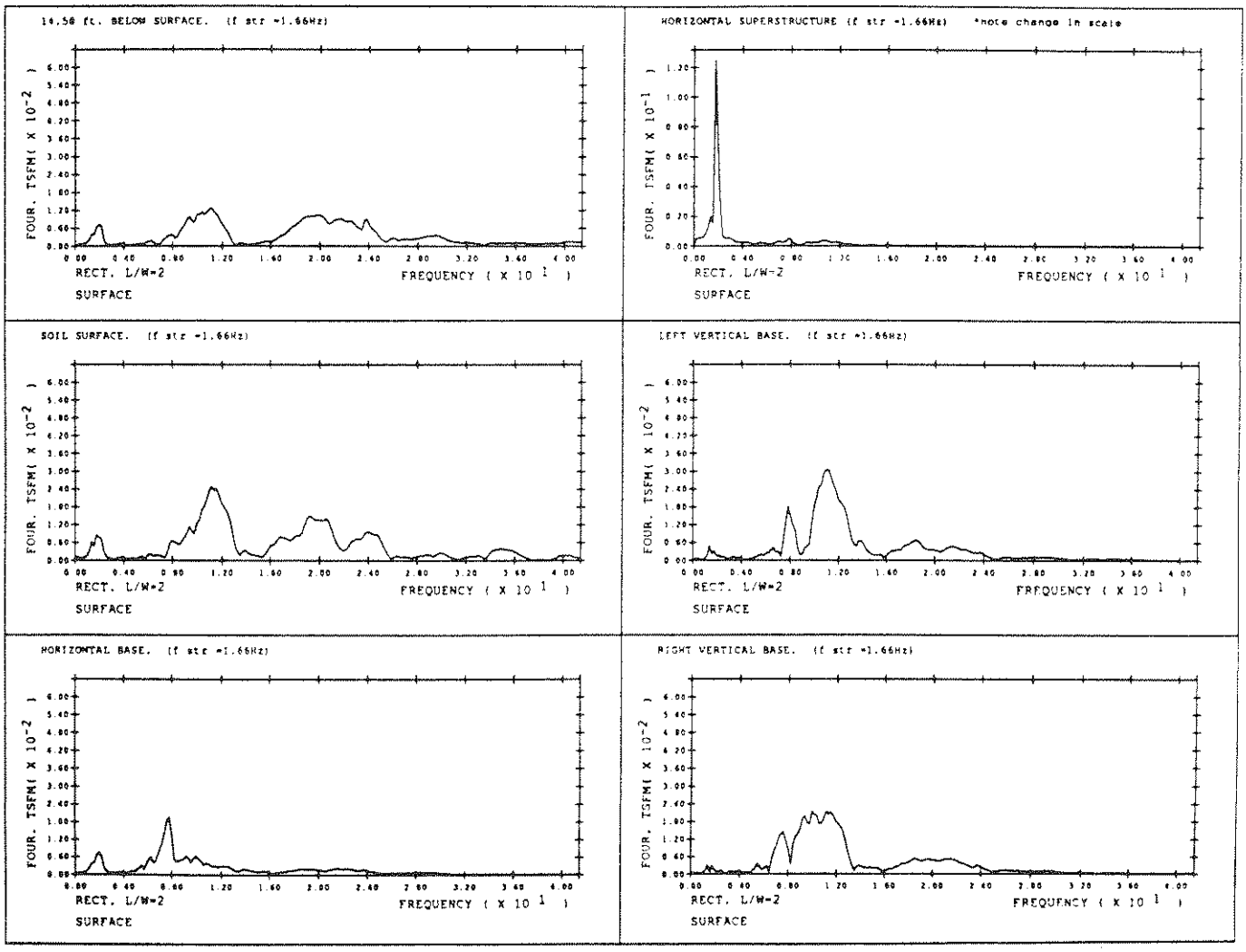

FIGURE 5.9 (cont'd)
System with Surface Rectangular (L/W=2) Footing (f_{str} = 1.66Hz)

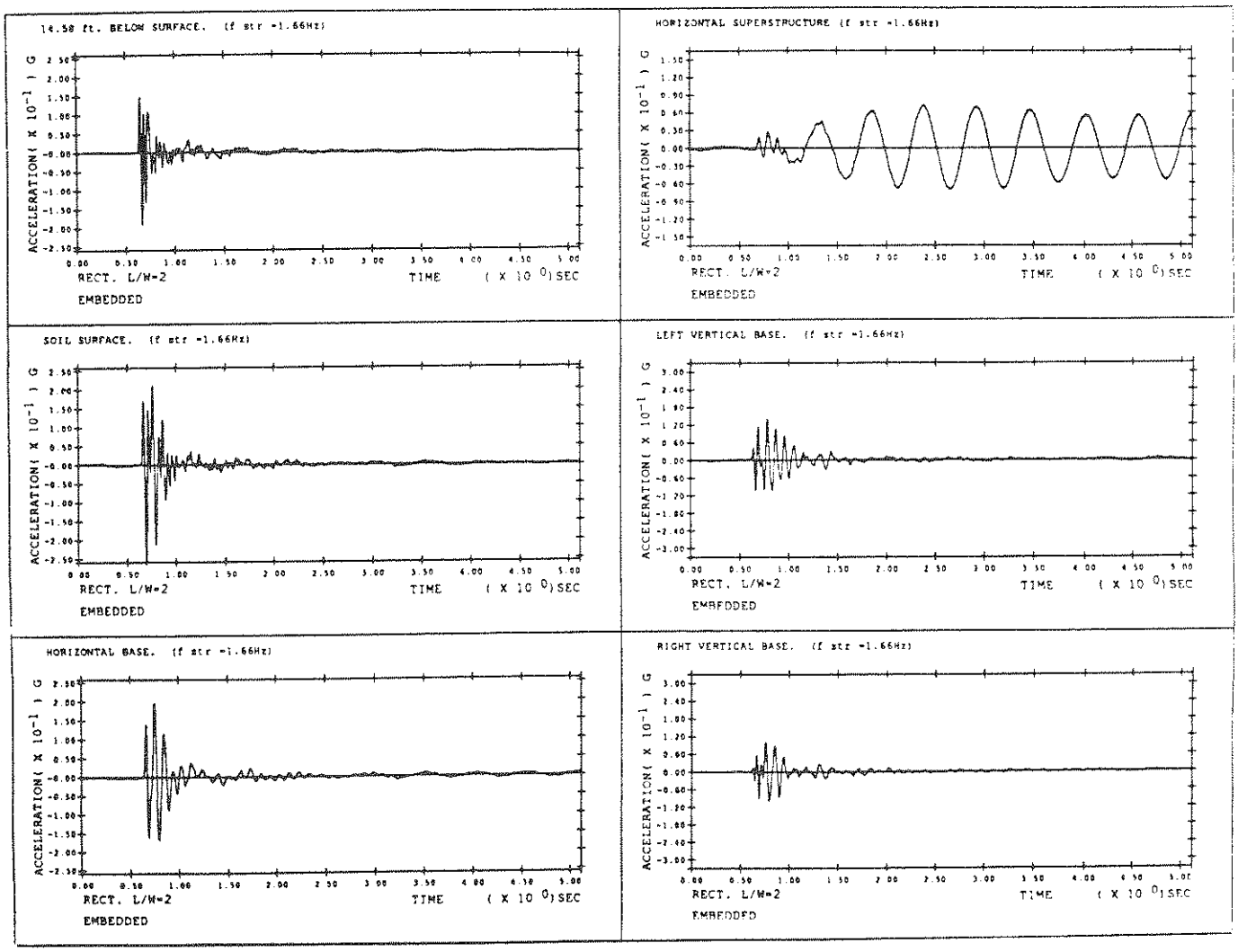

FIGURE 5.10
System with Embedded Rectangular (L/W=2) Footing (f_{str} = 1.66Hz)

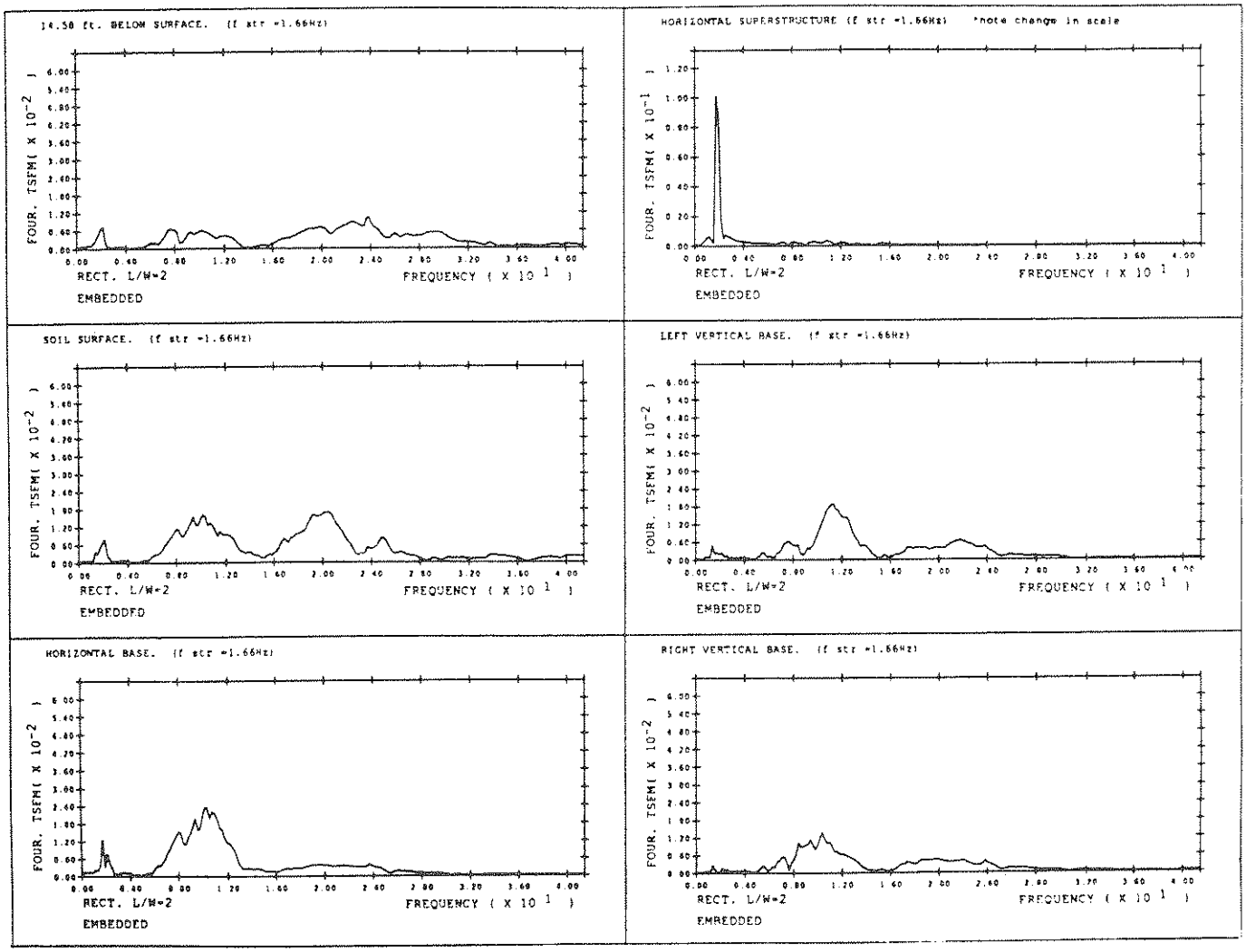

FIGURE 5.10 (cont'd)
System with Embedded Rectangular (L/W=2) Footing (f_{str} = 1.66Hz)

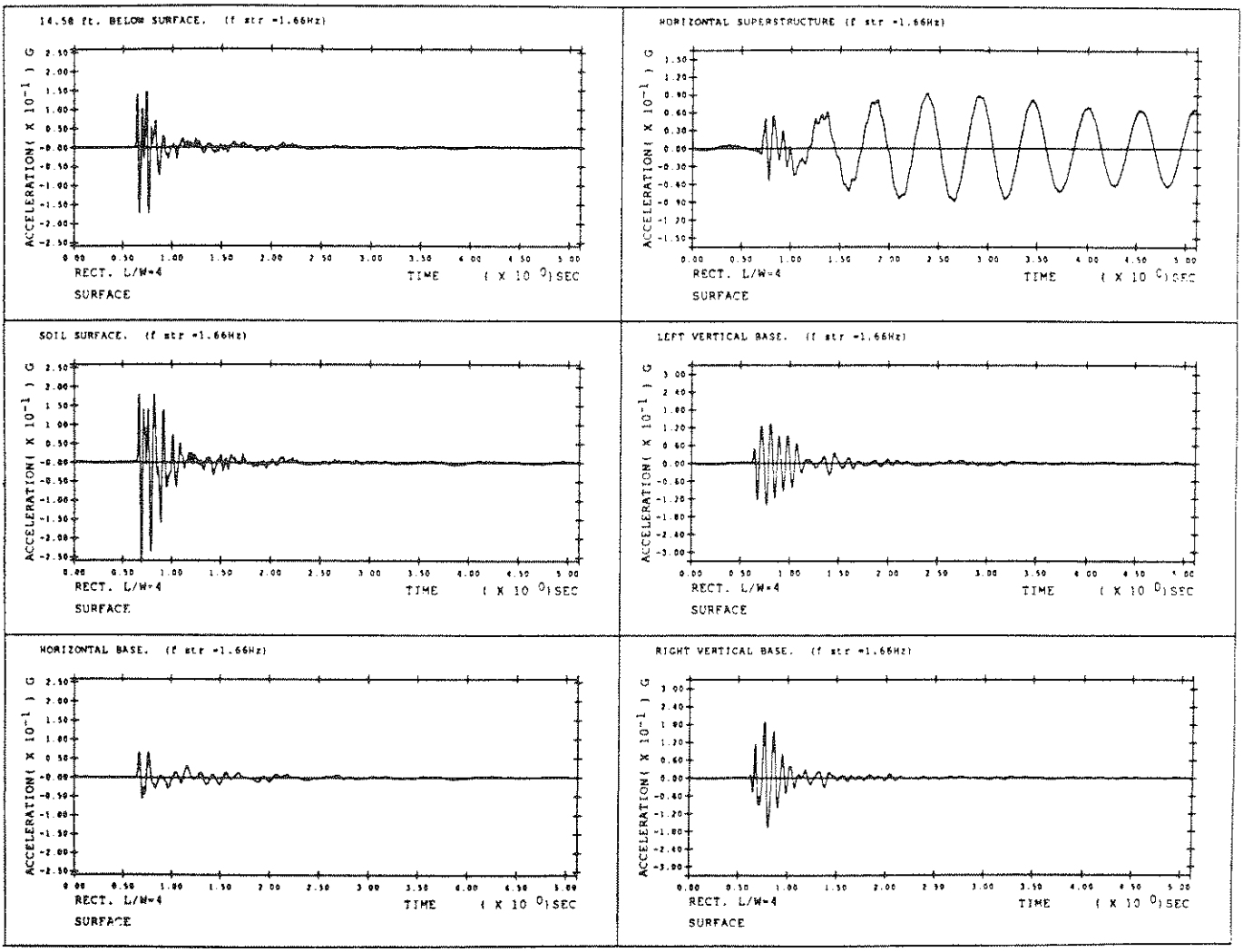

FIGURE 5.11
System with Surface Rectangular (L/W=4) Footing (f_{str} = 1.66Hz)

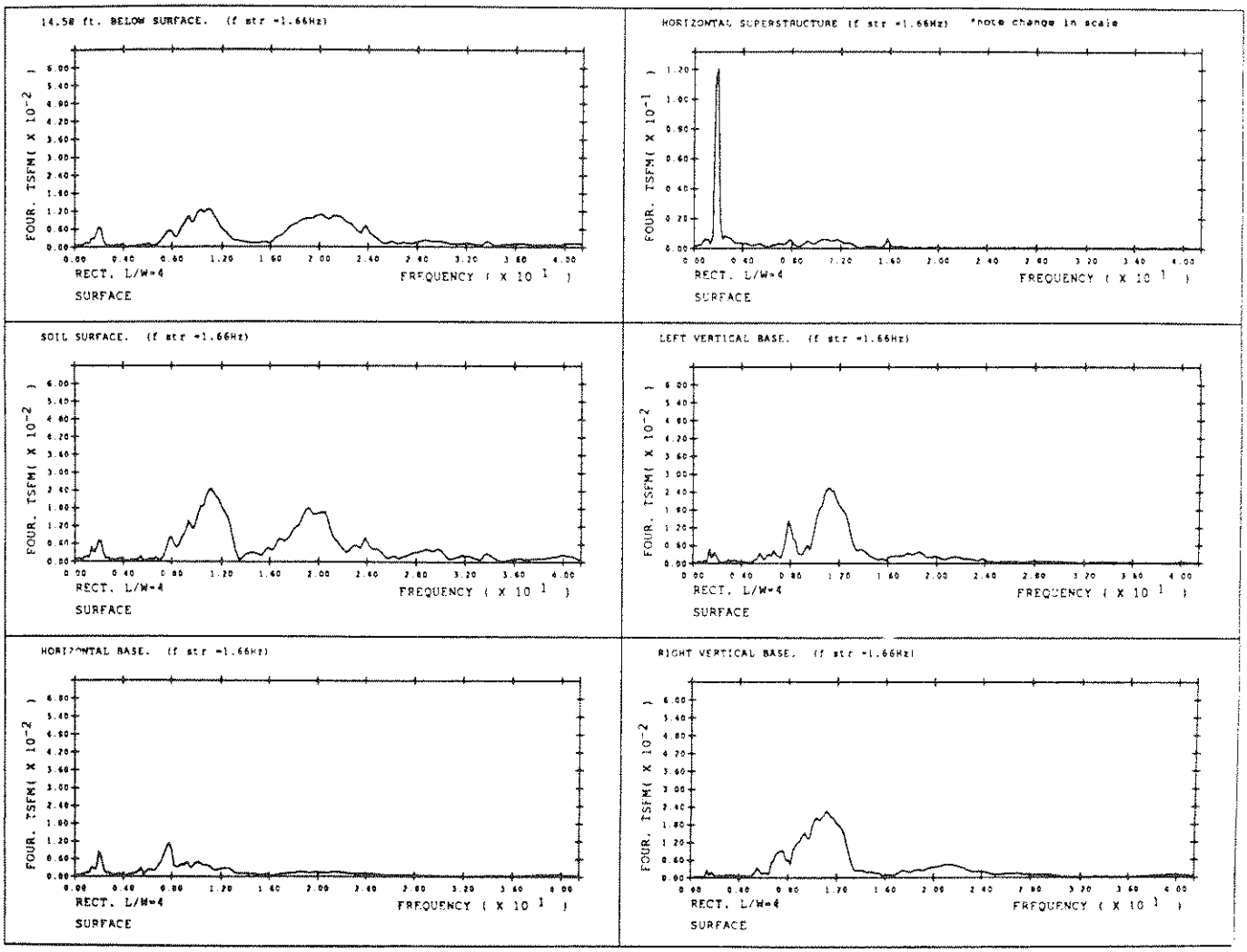

FIGURE 5.11 (cont'd)
System with Surface Rectangular (L/W=4) Footing (f_{str} = 1.66Hz)

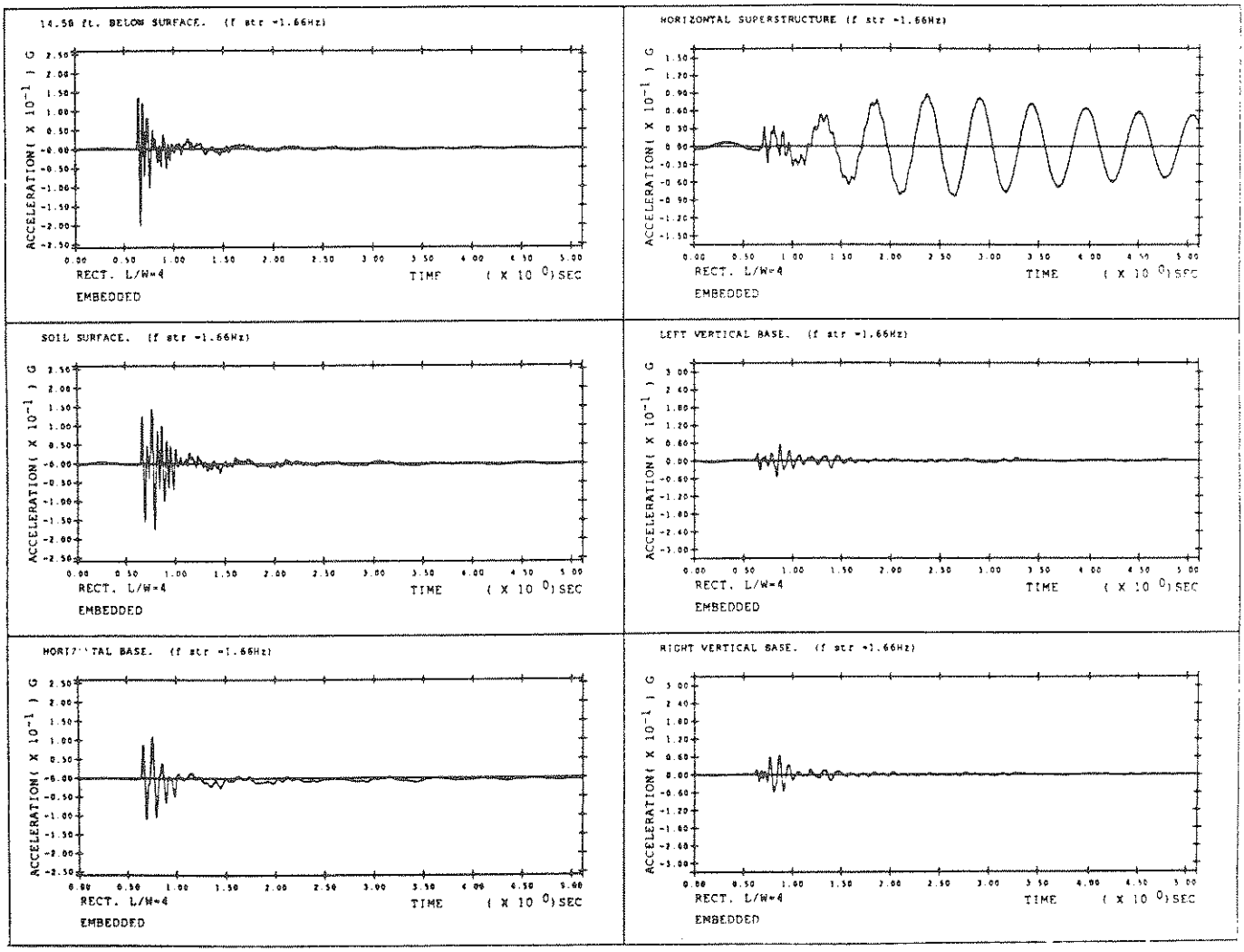

FIGURE 5.12
System with Embedded Rectangular (L/W=4) Footing (f_{STF} = 1.66Hz)

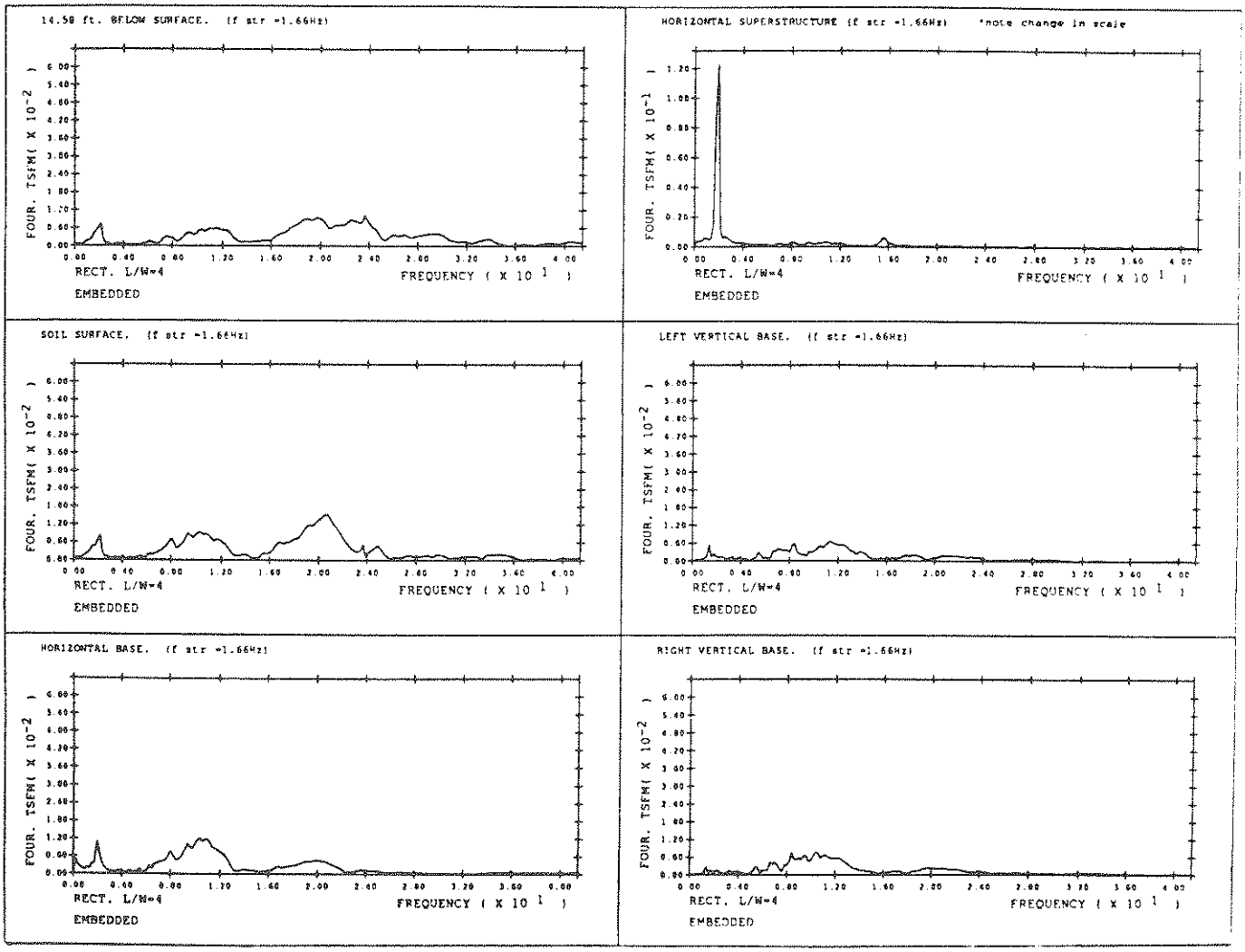

FIGURE 5.12 (cont'd)
System with Embedded Rectangular (L/W=4) Footing (f_{str} = 1.66Hz)

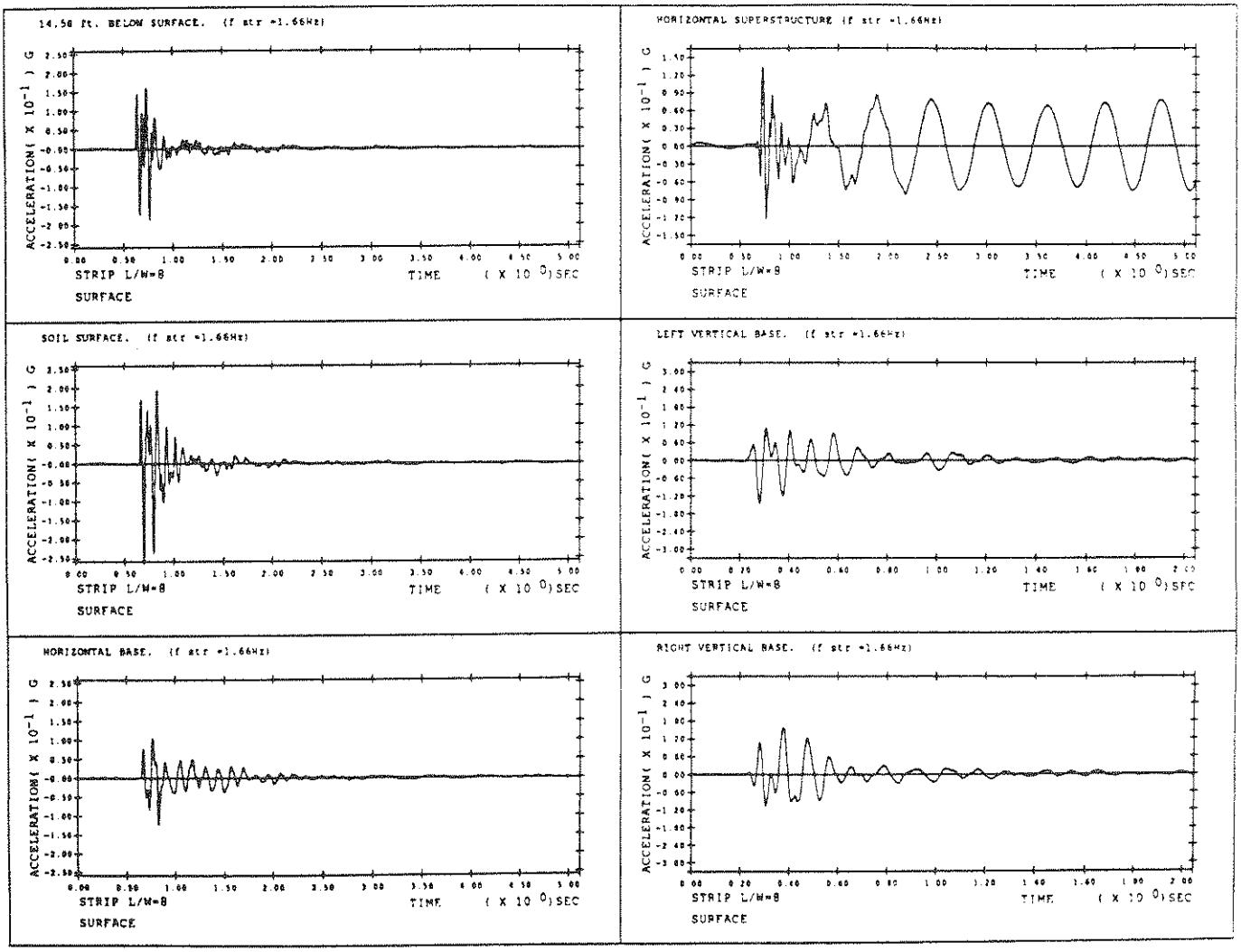

FIGURE 5.13
System with Surface Strip (L/W=8) Footing (f_{str} = 1.66Hz)

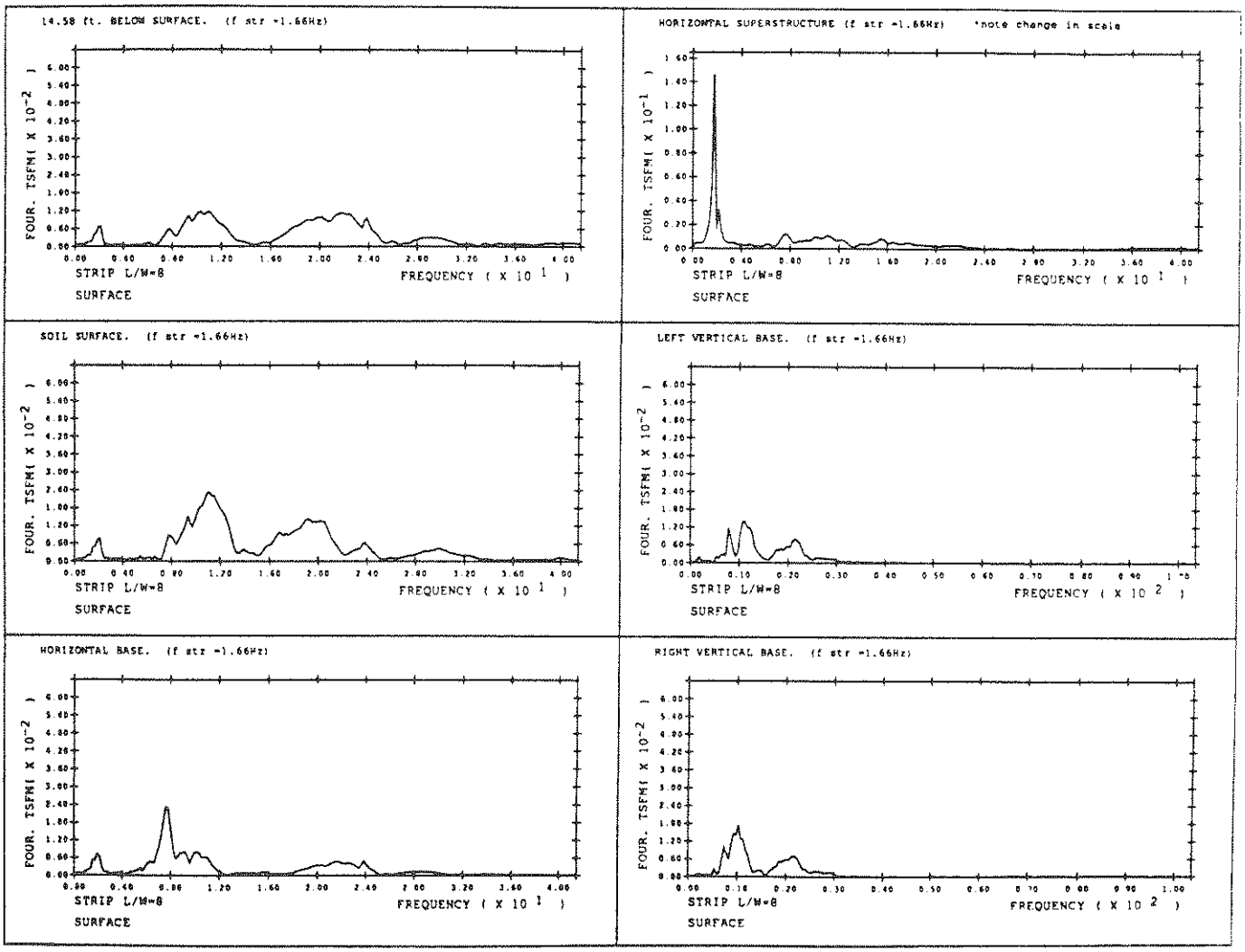

FIGURE 5.13 (cont'd)
System with Surface Strip (L/W=8) Footing (f_{str} = 1.66Hz)

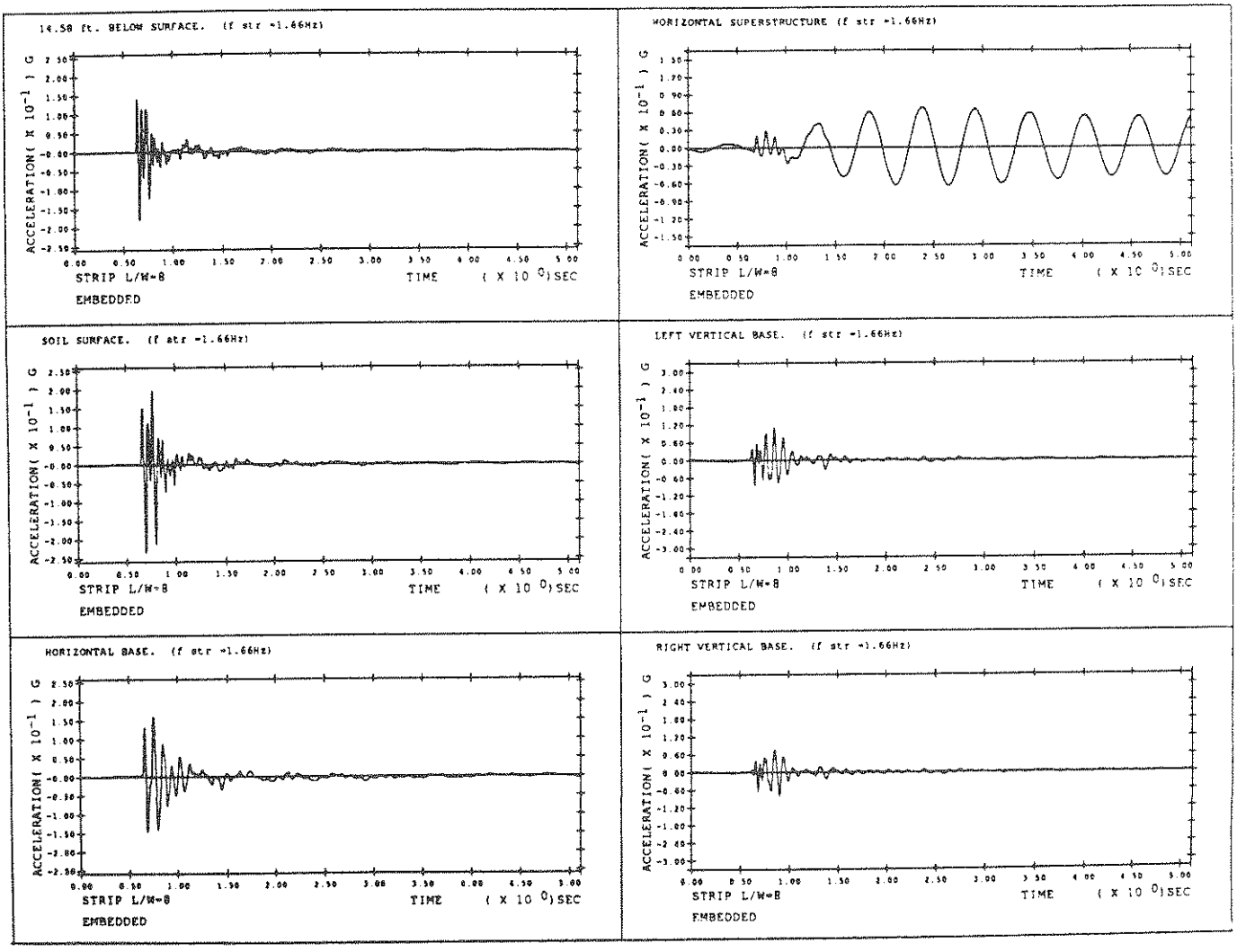

FIGURE 5.14
System with Embedded Strip (L/W=8) Footing (f_{str} = 1.66Hz)

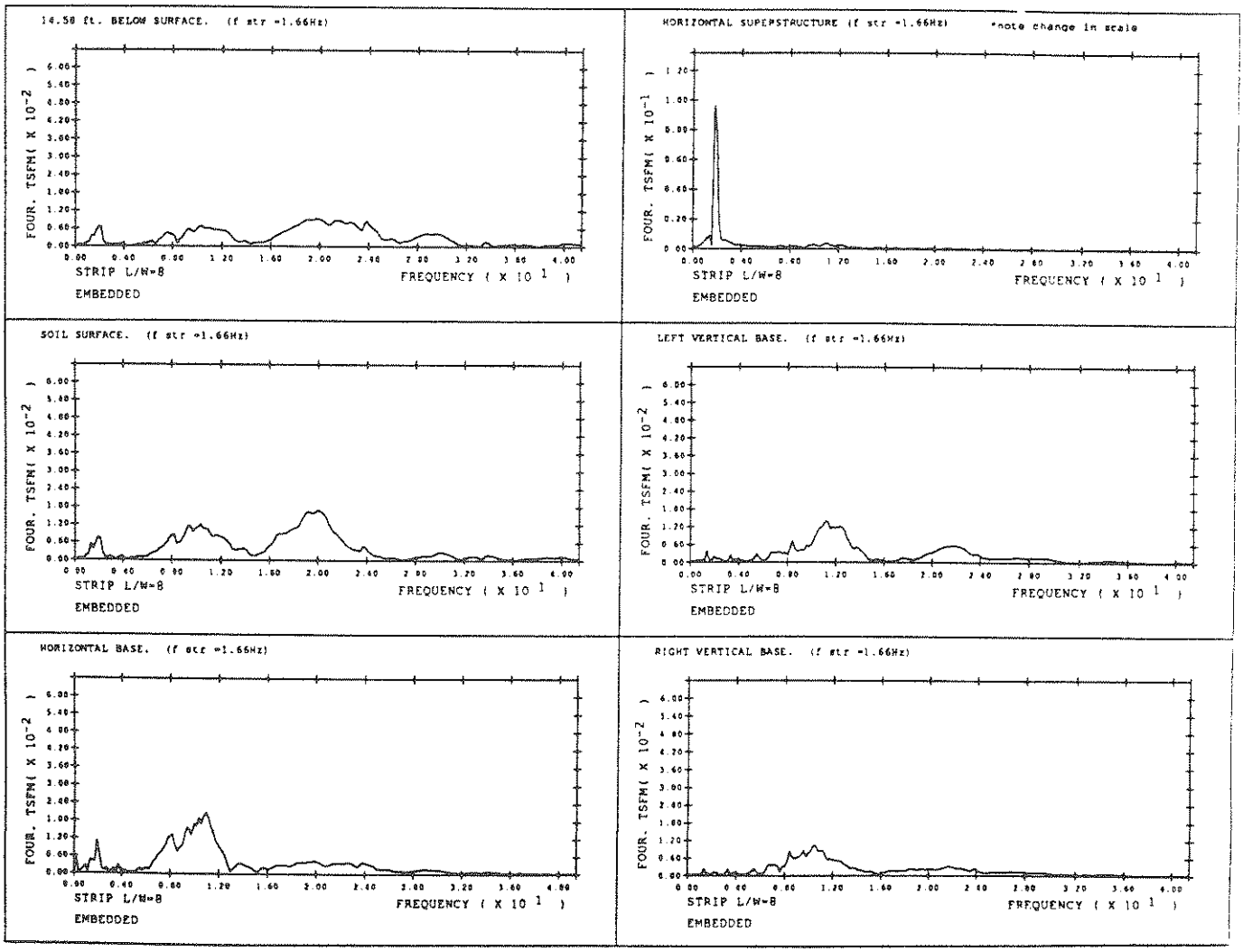

FIGURE 5.14 (cont'd)
System with Embedded Strip (L/W=8) Footing (f_{str} = 1.66Hz)

5.6 Free and Scattered Field Motions

To complete the data set, the free field and scattered field accelerations are presented in this section. The free field acceleration is the acceleration recorded on the surface of the soil deposit in the absence of a structure. The free field motion is given in Figure 5.15. The scattered field acceleration, which accounts for the footing geometry, is the input motion to the soil-structure system at the footing-soil interface. This input motion is necessary for the analysis performed in Chapter 6. Experimentally the scattered field motion is obtained by mounting an accelerometer in the center of a thin piece of light weight, rigid plastic that is cut to the same size and shape as the base of the footing. For a surface footing the plastic is flat and rests on the soil surface. For an embedded footing the plastic forms a hollow cup which is embedded into the soil. The accelerometer is mounted in the horizontal direction, and each scattered field system is subjected to a simulated earthquake.

The scattered field accelerations for the surface and embedded square footings are given in Figures 5.16 and 5.17, respectively. The scattered field motions for the circular, rectangular and strip footings may be found in Reference 5.6. In general the scattered field accelerations for the surface footings are very similar to the free field acceleration. As discussed in Section 4.3, this indicates that the surface motions are fairly uniform just as they would be for a horizontal soil deposit of infinite lateral extent excited by vertically incident shear waves. For the embedded footings there is a reduction in energy in the scattered field motion that is evident in both the amplitude of the acceleration time histories and the magnitude of the Fourier Transforms. Since the embedment is relatively shallow for the test cases herein, the scattered field motions for the embedded structures do not differ from the free field motion as much as they would for a deeply embedded structure. The correlation coefficients between the free field motion and the scattered field motions corresponding to each footing tested in this study are given in Table 5.3.

TABLE 5.3
CORRELATION COEFFICIENTS BETWEEN FREE AND SCATTERED FIELD MOTIONS

Footing	Surface	Embedded
Square	0.612	0.820
Circular	0.826	0.877
Rect. (L/W=2)	0.923	0.701
Rect. (L/W=4)	0.774	0.923
Strip (L/W=8)	0.830	0.927

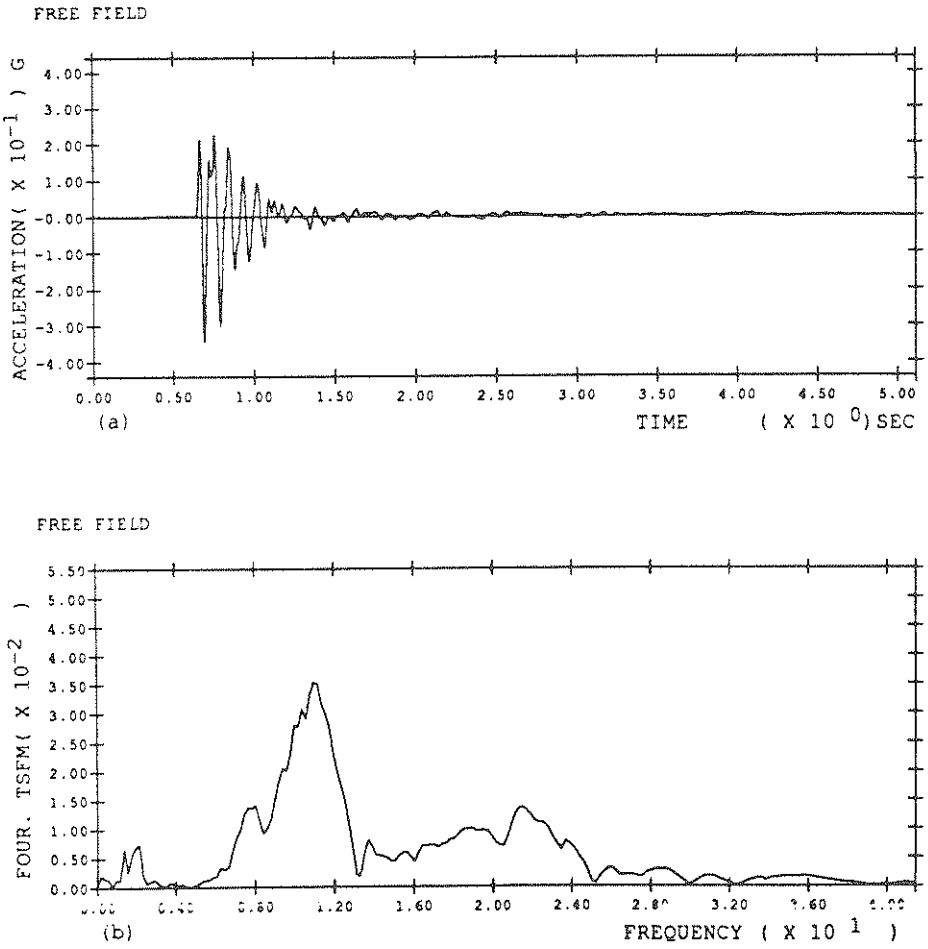

FIGURE 5.15
Free Field Motion.
(a) Acceleration Time History.
(b) Fourier Transform.

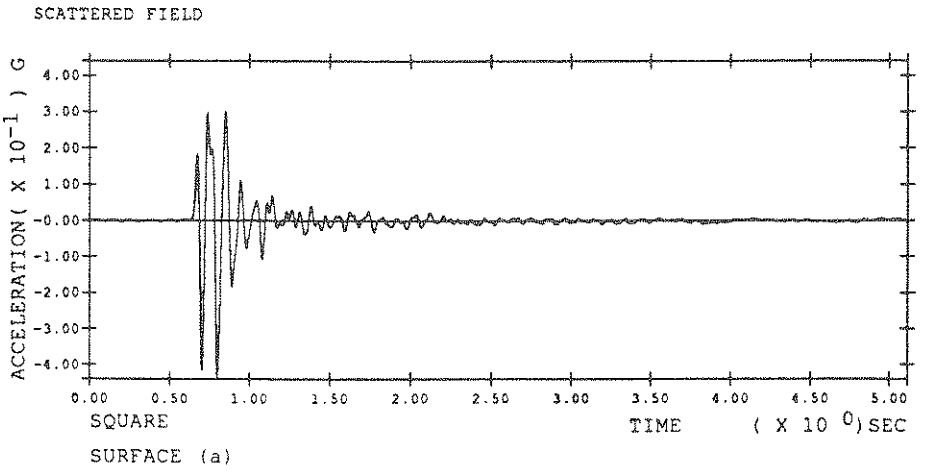

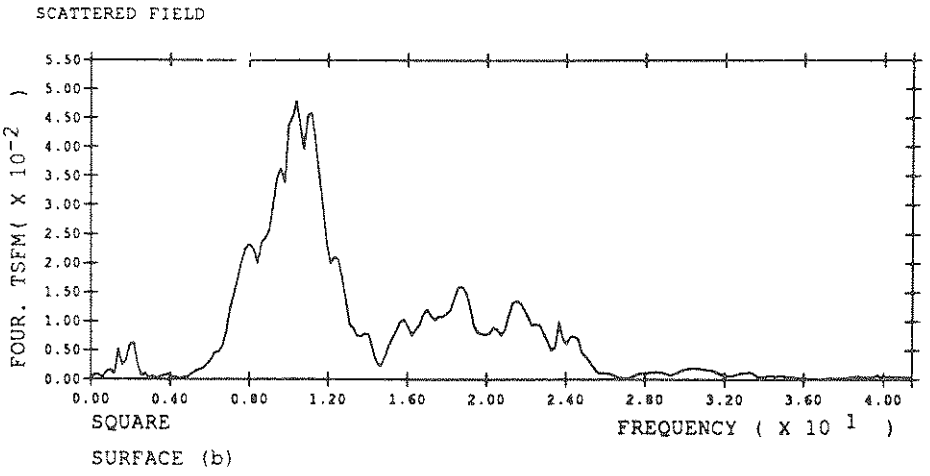

FIGURE 5.16
Scattered Field Motion for Square Surface Footing.
(a) Acceleration Time History.
(b) Fourier Transform.

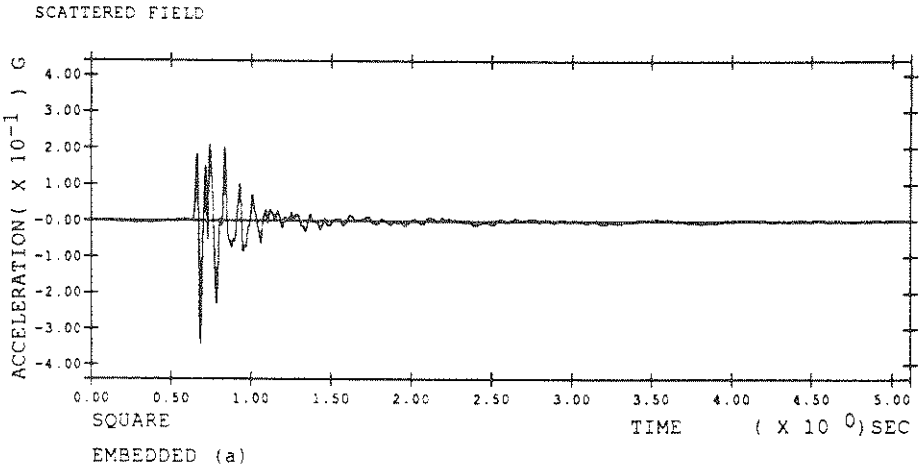

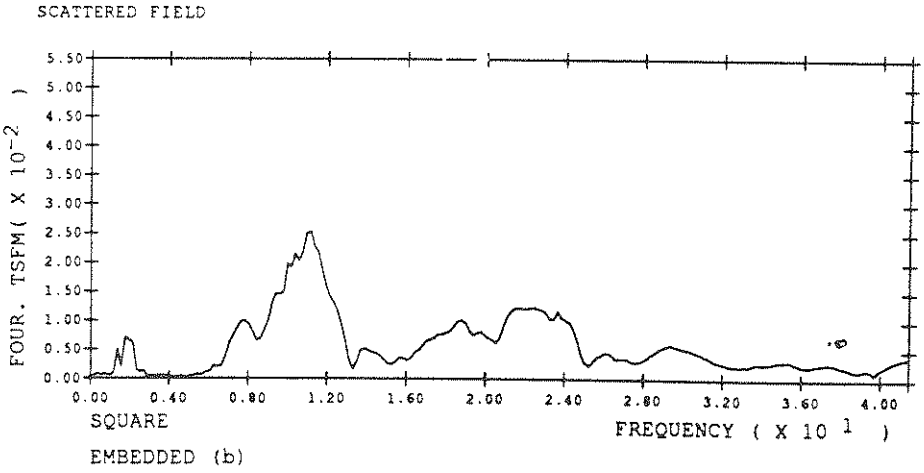

FIGURE 5.17
Scattered Field Motion for Square Embedded Footing.
(a) Acceleration Time History.
(b) Fourier Transform.

5.7 Summary and Conclusions

In this chapter the results of an extensive series of tests on radiation damping and soil-structure interaction performed in the centrifuge are organized and presented. Structures with surface and embedded square, circular, rectangular and strip footings are examined. In each case the natural frequency of the superstructure is varied but the higher order frequency associated with the motion of the base is kept constant. It is found that, regardless of the foundation shape or level of embedment, the amount of radiation damping depends on the natural frequency of the vibrating modes of the structure relative to the fundamental frequency of the soil layer (f_{soil}). The amount of radiation damping at the superstructure gradually increases as the natural frequency of the superstructure is increased above f_{soil}. Radiation damping is always present in the horizontal motion of the base as the frequency associated with this motion is consistently greater than f_{soil}.

Comparisons of stiffness and damping between surface and embedded structures can be made by observing changes in response frequency and response amplitude decay. In general, embedment of the base does not affect the amount of radiation damping associated with the natural frequency of the superstructure, but does affect the response of the superstructure to the strong motion part of the earthquake. Embedment causes an increase in the damping, stiffness and peak amplitude of the horizontal acceleration of the base, and a decrease in the peak amplitude of the vertical accelerations (and hence rocking) of the base.

Unfortunately, direct comparisons are not valid between the structures of different footing shapes because the mass of the footing and the contact area between the footing and the soil are different for each case. It can be seen that the general properties of radiation damping are not affected by the foundation shape but any further conclusions must be based on numerical analysis. The response must in some way be normalized by the footing size before comparisons

can be made. Such analysis is performed in Chapter 6.

Comparisons between the free and scattered field motions show that the free field motion is similar to the scattered field motions for the systems presented in this chapter. The scattered field motions for the structures with surface footings have amplitudes of acceleration that are slightly larger than the amplitudes of the free field motion. For the embedded footings, the amplitudes of the scattered field motion decrease.

The centrifuge experiments described in this chapter yield a large data pool which demonstrates the influence of the structural frequency, the foundation embedment, and the foundation shape on radiation damping and soil-structure interaction for a structure on a layer of soil over bedrock during an earthquake. A good deal of insight is gained from the direct qualitative observations just described. The next step is to use this data pool to verify and improve existing analytical methods for predicting soil-structure interaction effects during earthquakes.

5.8 References for Chapter 5

5.1 Roesset, J.M., "A Review of Soil-Structure Interaction," *Soil-Structure Interaction: The Status of Current Analysis Methods and Research*, Seismic Safety Margins Research Program, June 1980, p. 95.

5.2 Wolf, J.P., *Dynamic Soil-Structure Interaction*, Prentice Hall, Englewood Cliffs, N.J., 1985, pp 18-50, 295, 405.408.

5.3 Gazetas, G., "Analysis of Machine Foundation Vibrations: State of the Art," *Soil Dynamics and Earthquake Engineering*, 1983, Vol. 2, No.

5.4 Clough, R.W., Penzien, J., *Dynamics of Structures*, McGraw-Hill, New York, 1975, pp. 47-48.

5.5 Das, B.M., *Fundamentals of Soil Dynamics*, Elsevier, New York, 1983, pp. 270-275.

5.6 Weissman, K., Prevost, J.H., "A Study Of Radiation Damping and Soil-Structure Interaction Effects in the Centrifuge," Technical Report NCEER-88-0013, National Center for Earthquake Engineering Research, May 24, 1989.

CHAPTER 6

NUMERICAL ANALYSIS AND SYSTEM IDENTIFICATION USING THE EXPERIMENTAL RESULTS

6.1 Introduction

In this chapter a numerical analysis of the experimental results is performed in order to demonstrate that the centrifuge system can be modeled by established analytical procedures. In Section 6.2 a simple two degree of freedom lumped parameter model is introduced to represent the experimental system. The damping and stiffness coefficients of this numerical model are computed by methods of system identification from the results of the soil-structure interaction experiments performed in Chapter 5. The system identification procedure is described in Section 6.3. The identified damping and stiffness values are presented in Sections 6.4 and 6.5 for the structures with surface and embedded footings, respectively. Plots comparing the structural response in the experiments to the response calculated numerically using the identified parameter values show the accuracy in fit of the two degree of freedom model to the experimental results. Also contained in these sections is a comparison of the identified parameter values and those computed by classical text book formulas. This comparison further demonstrates that the behavior of the centrifuge model is consistent with established theory. The relative error between the experimental and textbook values is given in order to facilitate this comparison. Finally, in Section 6.6 the accuracy of the system identification scheme is investigated. A sensitivity analysis is performed in order to measure the correlation between two parameters. The stability of the parameter estimates is examined in order to show that the identified parameters are representative of the soil-structure system in general, and not dependent on the specific earthquake used in the data set. Conclusions are drawn in Section 6.7.

6.2 A Simple Two Degree of Freedom Model

A two degree of freedom, lumped parameter, linear model is used to represent the soil-structure systems tested in Chapter 5. A free body diagram of the model is shown in Figure 6.1. Degrees of freedom one and two are assigned to the horizontal motions of the base and the superstructure, respectively. Note that y_1 and y_2 are *relative* motions. The absolute motion of the superstructure is $(y_2 + y_1 + u_g)$ and the absolute motion of the base is $(y_1 + u_g)$. The input to the soil-structure system $(\ddot{u}_g)$ is the scattered field motion (Figures 5.44-5.53). A rotational mode is not included because rocking motion only exists during the strong motion response and does not contribute to the steady state response (see the vertical accelerations plotted for each case in Chapter 5).

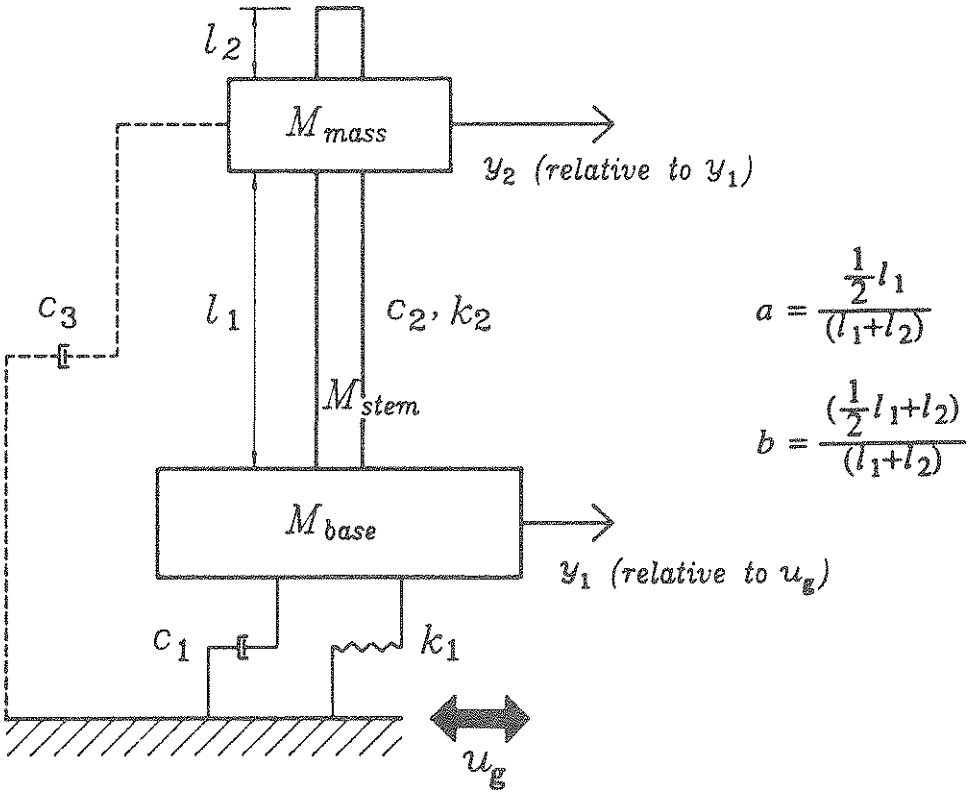

FIGURE 6.1
Two Degree of Freedom Model System

Since radiation damping is a frequency dependent phenomenon it is necessary to have a radiation damping term associated with each frequency of the model system. Thus, radiation damping terms are assigned to the motion of the base (c_1) and the motion of the superstructure (c_3). In Figure 6.1 the dashpot representing c_3 is drawn with a broken line so that it does not imply a physical connection between the superstructure and the ground. The figure merely reflects the fact that radiation damping is a soil-structure interaction parameter which acts on the motion of the superstructure relative to the ground ($\dot{y}_1+\dot{y}_2$). Material damping in the soil foundation is neglected in the model. However, material damping associated with the motion of the superstructure $\dot{y}_2$ (=structural distortion) is accounted for with the term c_2. The resulting equations of motion for the system are as follows:

$$\begin{bmatrix} m_1+m_2 & m_2 \\ m_2 & m_2 \end{bmatrix} \begin{bmatrix} \ddot{y}_1 \\ \ddot{y}_2 \end{bmatrix} + \begin{bmatrix} c_1+c_3 & c_3 \\ c_3 & c_2+c_3 \end{bmatrix} \begin{bmatrix} \dot{y}_1 \\ \dot{y}_2 \end{bmatrix} + \begin{bmatrix} k_1 & 0 \\ 0 & k_2 \end{bmatrix} \begin{bmatrix} y_1 \\ y_2 \end{bmatrix} = \begin{bmatrix} -(m_1+m_2) \\ -m_2 \end{bmatrix} \ddot{u}_g . \qquad (6.1)$$

The system identification procedure is described in the next section.

6.3 System Identification

6.3.1 Definition of Unknown and Deterministic Parameters

The first step in a system identification problem is to specify which parameters may be determined from known properties and which parameters are unknown and must be identified from the experimental results. The coefficients of the mass matrix (*viz.*, m_1 and m_2) are determined from measurable quantities by lumping the mass of the stem to the top and bottom degrees of freedom as follows:

$$m_1 = M_{base} + aM_{stem} \qquad (6.2a)$$

$$m_2 = M_{mass} + bM_{stem} \qquad (6.2b)$$

where a and b vary according to the location of the top mass along the stem (see Figure 6.1). The stiffness and material damping parameters of degree of freedom number two (*viz.*, k_2 and c_2)

may be calculated from material properties as well using the following formulas:

$$k_2 = (2\pi f_{str})^2 m_2 \tag{6.3a}$$

$$c_2 = 2\zeta_{str}\sqrt{k_2 m_2}. \tag{6.3b}$$

where f_{str} and ζ_{str} are the frequency and damping ratio obtained from the fixed base free vibration experiments (see Table 5.1). However, it is found by examining the experimental results that the value of k_2 in the coupled system (Equation 6.1) is slightly different from the fixed base value given by Equation 6.3a. Therefore, k_2 is considered an unknown parameter and is identified from the experimental results. The material damping of the superstructure (c_2) is slightly different for the coupled system as well, but it is found that the model is very insensitive to small changes in this parameter (see Section 6.6.1). Therefore, it is not necessary to identify c_2 because the improvement in the fit of the model is negligible.

The remaining soil-structure interaction coefficients c_1, k_1 and c_3 together with k_2 form the components of the vector of unknown parameters

$$\mathbf{q} = \{c_1, k_1, c_3, k_2\}$$

whereas m_1, m_2 and c_2 are always considered deterministic quantities.

Initial estimates of the unknown parameters are required as input to the optimization routine. The initial estimate of k_2 is determined by Equation 6.3a. The initial estimates of c_1, k_1, and c_3 are determined from a system identification technique proposed by Distefano and Rath [6.3] that leads to an explicit calculation of the parameters. Distefano and Rath's technique requires measurements of the acceleration, velocity and displacement at each degree of freedom as input. The resulting parameter values are used as first estimates and not as final solutions because their accuracy is contingent on the accuracy of this input. Only the acceleration is recorded in the experimental system so the velocity and displacement must be calculated by digitally integrating the acceleration an appropriate number of times. Errors associated with the digital integration procedure cause substantial inaccuracies in the velocity and displacement. These

inaccuracies are passed on to the resulting parameter estimates.

6.3.2 Measure of Fit

The vector of unknown parameters $\mathbf{q}$ is identified by minimizing the following acceleration dependent error function:

$$S = \int_{T_o}^{T_f} \left[\left[\frac{\ddot{y}_1 - \ddot{y}_1^*}{\ddot{y}_{1\,\max}} \right]^2 + \left[\frac{\ddot{y}_2 - \ddot{y}_2^*}{\ddot{y}_{2\,\max}} \right]^2 \right] dt \tag{6.4}$$

where $\ddot{y}_1$ and $\ddot{y}_2$ are the relative accelerations of degrees of freedom one and two measured experimentally, $\ddot{y}_1^*$ and $\ddot{y}_2^*$ are the accelerations calculated numerically by integrating Equation 6.1 using trapezoidal integration, and $(T_o - T_f)$ is the duration of the interval over which the parameters are to be identified. The difference between the measured and calculated accelerations is normalized by the maximum amplitude of the measured acceleration over the interval T_o to T_f. The error function S is minimized with respect to $\mathbf{q}$ by the IMSL routine ZXMIN which employs a quasi-Newton method of optimization.

6.4 Structures with Surface Footings

6.4.1 Identified Experimental Parameter Values

Initially the experimental system is assumed to behave linearly and the error function S (Equation 6.4) is minimized over the entire duration of the response signal. The parameter values identified from the experimental results for two of the test cases with a surface circular footing, one case without radiation damping (f_{str}=1.66Hz) and one with radiation damping (f_{str}=4.69Hz) in the superstructure, are presented in Table 6.1. The accelerations $\ddot{y}_1^*$ and $\ddot{y}_2^*$ computed using these parameters (by integrating Equation 6.1) are plotted against the experimental results in Figures 6.2 and 6.3 for the cases with no radiation damping and radiation damping respectively. Overall the fit is good in both cases for both degrees of freedom except that the linear model overpredicts the amplitude of the response to the strong motion. This indicates that there is some

nonlinearity in the response, i.e. the soil may be softening during the strong motion part of the earthquake.

TABLE 6.1
EQUATION PARAMETERS OF LINEAR 2DOF MODEL
STRUCTURE WITH A SURFACE CIRCULAR FOOTING
($M_{base} = 1.71\times10^4$ $M_{mass} = 5.37\times10^3$ $M_{stem} = 9.33\times10^2$ $\frac{lb}{ft/sec^2}$)

PARAMETER	FREQUENCY OF SUPERSTRUCTURE (f_{str}) 1.66 Hz	4.69 Hz	UNITS
Deterministic Values			
a	0.500	0.172	-
b	0.500	0.828	-
m_1	1.76×10^4	1.73×10^4	$\frac{lb}{ft/sec^2}$
m_2	5.84×10^3	6.14×10^3	$\frac{lb}{ft/sec^2}$
c_2	4.37×10^2	8.68×10^2	$\frac{lb-sec}{ft}$
Identified Values			
k_2	5.96×10^5	2.67×10^6	$\frac{lb}{ft}$
c_1	2.67×10^5	2.67×10^5	$\frac{lb-sec}{ft}$
k_1	4.00×10^7	4.00×10^7	$\frac{lb}{ft}$
c_3	0.00	1.50×10^5	$\frac{lb-sec}{ft}$

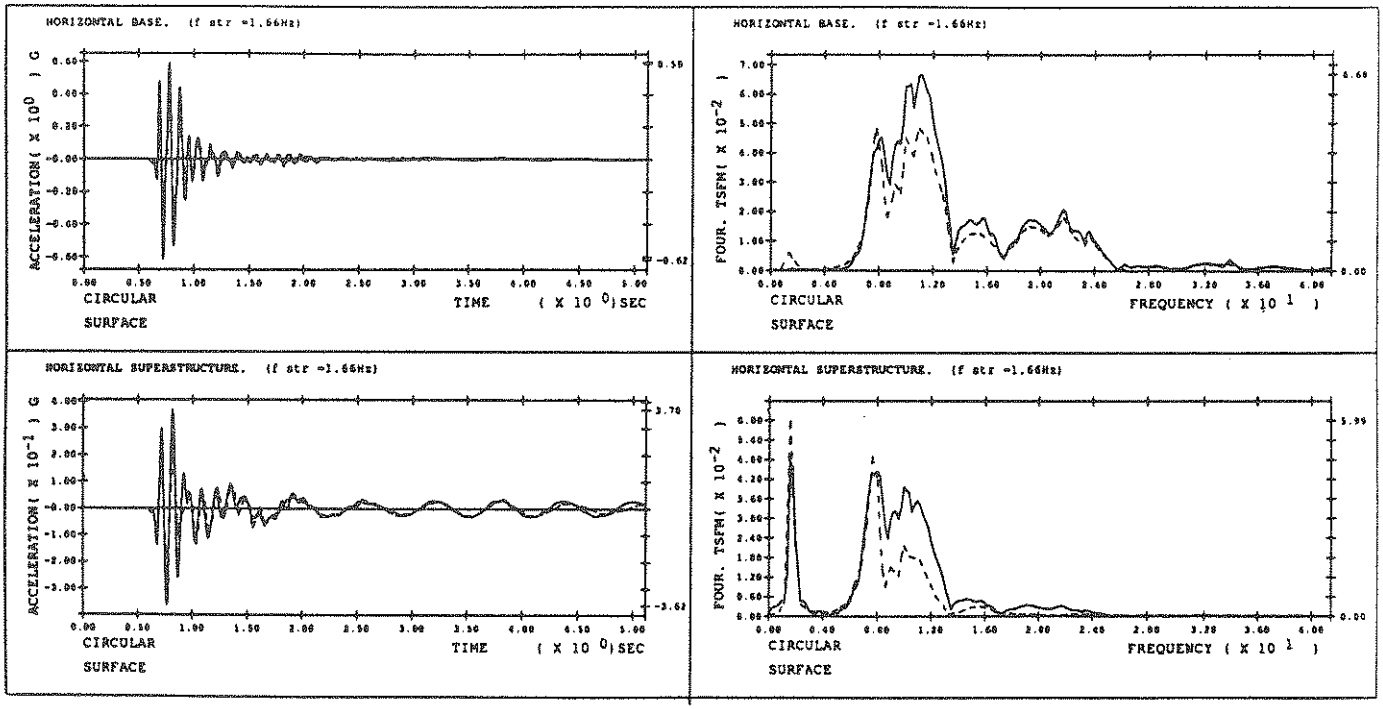

FIGURE 6.2
Linear Model: Circular Surface Footing, f_{str} =1.66Hz
Comparison of —Two Degree of Freedom Model and ----Centrifuge Results

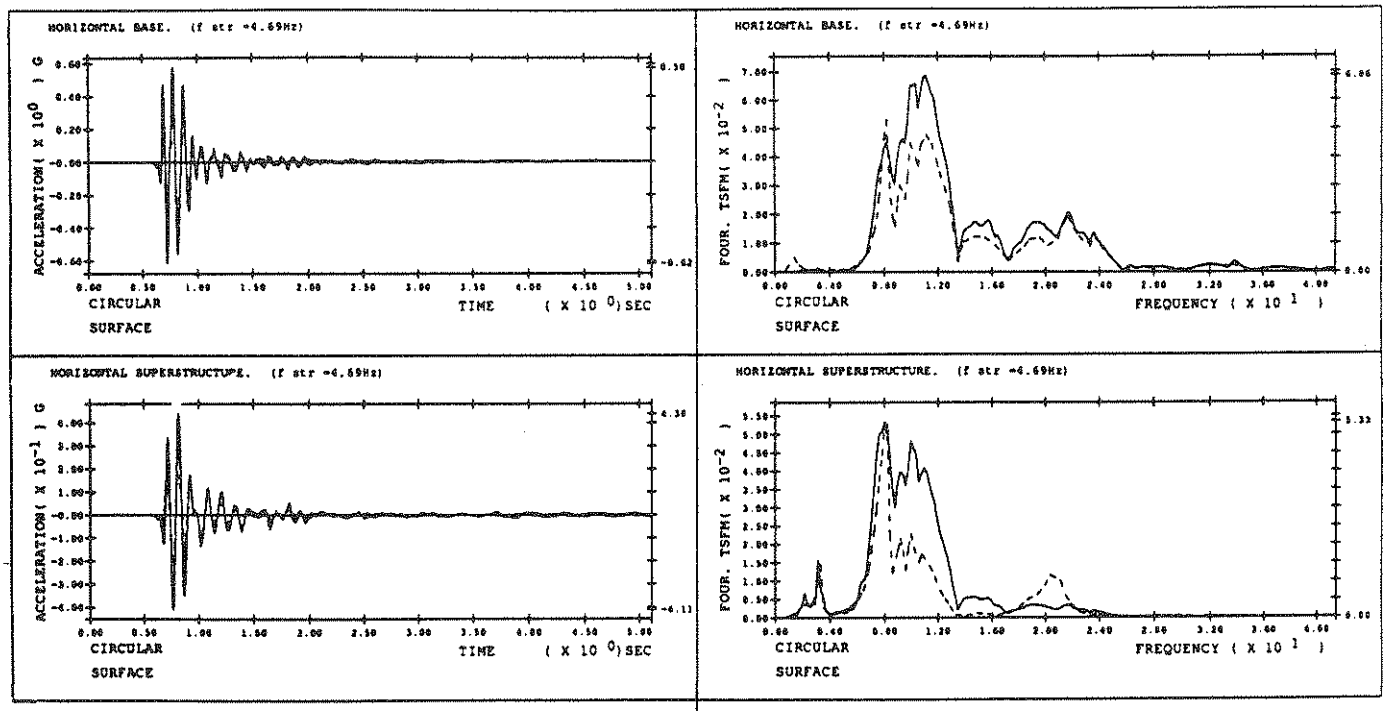

FIGURE 6.3
Linear Model: Circular Surface Footing, f_{str} =4.69Hz
Comparison of —Two Degree of Freedom Model and ----Centrifuge Results

To account for the nonlinearity, a piecewise linear approach is adopted in which the duration of the response is divided into three intervals. The first interval, which contains the strong motion response, is between 0.0 and 1.0 seconds, the second interval is between 1.0 and 2.5 seconds, and the third interval is between 2.5 and 5.0 seconds. The error function S is minimized over each interval separately, and three sets of parameters are obtained. It should be noted, however, that k_2 remains the same for all of the intervals because it depends primarily on structural properties and is essentially unaffected by nonlinearities at the soil-structure interface. The parameters identified using the piecewise linear models of the four test cases with surface circular footings are given in Table 6.2[1]. In each case the value of k_1 is about 33% smaller during the first interval than during the second and third where it remains constant. The acceleration time histories calculated using the parameter values in Table 6.2 for f_{str}=1.66Hz and f_{str}=4.69Hz are plotted in Figures 6.4 and 6.5 respectively (see Reference 6.12 for cases with f_{str}=4.05Hz and 5.72Hz). The improvement in the fit for the piecewise linear model over the linear model (Figures 6.2 and 6.3) can be readily observed.

The fit provided by the piecewise linear model is a good one for all the footing shapes tested in Chapter 5. The parameters identified using the piecewise linear models of the structures with square, rectangular (L/W=2), rectangular (L/W=4) and strip surface footings are given in Tables 6.3 through 6.6. The acceleration time histories calculated using these parameter values are shown in Reference 6.12. For the strip footing and the rectangular footing with an aspect ratio of 4, the response to the strong motion is slightly underestimated by the two degree of

[1]For systems where the top mass is located close to the base, the two degree of freedom idealization becomes less accurate. Because of this, the identified stiffness values are less exact, in some case causing a slight phase lag between $\ddot{y}$ and $\ddot{y}^*$. By definition, the error function, S, becomes larger due to such a phase lag and the optimization routine compensates by increasing the damping. This problem is most noticeable during the steady state response (between 1.0 and 5.0 seconds) for systems with $f_{str} \geq 4.69$ Hz. For the purposes of this study, the artificially high damping value is misleading, whereas, the slight phase lag is insignificant. Because of this, some of the values of c_3 presented in Tables 6.2-6.6 are one or two orders of magnitude smaller than the values actually obtained from minimizing the error function in Equation 6.4 in order to model the amplitude of the steady state response more accurately.

model. This is because the rocking motion is larger for such footing geometries. The steady state response in these cases is, however, accurately modeled by the two translational degrees of freedom.

A measure of the error in fit is given in Tables 6.2-6.6 along with the identified values for each segment. This number is equal to the value of the error function S (Equation 6.4) evaluated at the parameter values given in the tables and normalized by the length of the segment in seconds. Since S is already normalized by the peak amplitude of acceleration within the segment, the values of the error in fit may be directly compared regardless of the test case or segment. The error in fit is typically less than 10% for the first two segments, and somewhat larger (15-20%) for the final segment where the earthquake input, and in most cases the response, become very small. The error in fit is also consistently lower for the cases with little or no radiation damping. This is because the structure most closely resembles a two degree of freedom system when the top mass is at the very top of the stem. When the top mass is lowered in order to increase the value of f_{str}, the stem sticking out above the mass introduces additional modes into the system.

6.4.2 Comparison With Text Book Values

In order to further demonstrate that the behavior of the centrifuge model is consistent with established theory, the parameter values identified from the experimental results are compared with the corresponding values computed from classical text book formulas. In general, the text book formulas reflect the fact that soil-structure interaction parameters vary with frequency [e.g see 6.2]. For earthquake excitation it is difficult to isolate a single driving frequency, so often frequency independent formulas are used to approximate the parameters [6.4]. In the current model system (Figure 6.1) the damping and stiffness of degree of freedom number one (c_1, and k_1) may be approximated by the following frequency independent formulas developed for a rigid, circular

footing on the surface of a horizontal stratum [6.4, 6.5]:

$$c_1 = \frac{4.6\rho V_s r^2}{2-\nu}\left[1+\frac{1}{2}\frac{r}{d}\right] \tag{6.5a}$$

$$k_1 = \frac{8Gr}{2-\nu}\left[1+\frac{1}{2}\frac{r}{d}\right] \tag{6.5b}$$

G = Shear Modulus of Soil Evaluated at Depth r (See Table 3.1)

ν = Poisson's Ratio of Soil (= 0.33)

r = Radius of Base of Structure

d = Depth of Soil

V_s = Shear Wave Velocity in Soil

ρ = Density of Soil.

For the case of the square and rectangular footings, r is replaced by the equivalent radius in the above formulas, and the resulting values of c_1 and k_1 are multiplied by a correction factor which is proportional to the aspect ratio (L/W) of the footing [6.2, 6.6, 6.7]. The strip footing requires a two dimensional analysis and is discussed later on in this section. The frequency independent approximations of c_1 and k_1 for the circular, square and rectangular footings are shown under *Text Book Values* in Tables 6.2 through 6.5. For these footing shapes the text book values of c_1 and k_1 are remarkably close to the values extracted from the experimental results for the steady state part of the response.

Unfortunately, similar formulas which isolate the soil-structure interaction effects for the superstructure have not yet been developed. Hence, there is no quick and easy formula to calculate the radiation damping term c_3 in the model system (Figure 6.1). It is common practice, however, to account for soil-structure interaction effects for the base and the superstructure together by idealizing the entire structure as a single degree of freedom oscillator, and using frequency dependent formulas to calculate the stiffness and damping at the frequency of the resulting oscillator [6.4]. In order to estimate c_3, this procedure is slightly modified by assuming that the frequency of the single degree of freedom oscillator is equal to the fixed base natural frequency of

the superstructure. Thus, the mass of the footing is neglected in this approximation. The dynamic damping of the oscillator is commonly expressed as the imaginary part of the following

$$K = k_1\{k_{dyn} + ia_o c_{dyn}\} \tag{6.6}$$

where k_1 is the static stiffness calculated by Equation 6.5b, $i=\sqrt{-1}$, and k_{dyn} and c_{dyn} are the dynamic stiffness and damping coefficients which are functions of the dimensionless frequency a_o. The dimensionless frequency is equal to $a_o = (\omega r)/V_s$, where ω is the frequency of vibration. The damping term c_3 may be extracted from the imaginary part of Equation 6.6 as follows:

$$c_3 = \frac{k_1 r c_{dyn}}{V_s}. \tag{6.7}$$

Values of c_{dyn} may be obtained for a structure with a rigid, surface footing on a horizontal stratum from charts developed by Kausel *et.al.* [6.8].

The text book values of c_3 for the circular, square and rectangular footings are also presented in the Tables 6.2 through 6.5. In general the text book values of c_3 are close to the values identified from the experimental results for the cases with little or no radiation damping. As the radiation damping in the system increases, the text book formulas often over predict the values of c_3 by as much as a factor of 100. These results are consistent with the findings of Lin [6.1] who performed similar experiments on a full scale model. Lin finds that the horizontal dynamic stiffness obtained experimentally is close to the static stiffness (frequency independent) value given by text book theory, but the dynamic damping obtained experimentally differs by an order of magnitude from the analytical value given by text book theory.

The comparisons between the identified and text book parameter values can be seen more clearly from the relative error which is given in Tables 6.7-6.10 for the circular, square and rectangular footings. This error is calculated by the following formula:

$$\frac{Identified\ Value - Text\ Book\ Value}{Text\ Book\ Value}. \tag{6.8}$$

The text book values apply to linear systems so it is understandable that the relative error may be fairly large for the parameters identified over the first interval (0.0-1.0 seconds) where the response exhibits some nonlinearity. For the second and third intervals, where the response is essentially linear, the relative errors in the damping and stiffness of the base, c_1 and k_1, are generally smaller for the circular and square footings than for the two rectangular footings. This is reasonable because the equivalent circular model used to compute the text book values is more accurate for the circular and square footings than for the rectangular footings with larger aspect ratios. The relative error is typically less than 50% for c_1 and less than 12% for k_1. The relative error in c_3, however, is more dependent on the value of f_{str} than the footing shape. The relative error for c_3 ranges from 0 for cases with no radiation damping in the superstructure, to 100% for cases with substantial radiation damping in the superstructure.

For the strip footing a two dimensional formulation is used to calculate the stiffness and damping terms. The static stiffness value may be used as a frequency independent approximation to k_1, and is calculated as follows [6.2]:

$$\frac{k_1}{(unit\ length)} = \frac{2.1G}{2-\nu}\left[1+2\frac{w}{d}\right] \tag{6.9}$$

where w is the half-width of the footing. For the strip footing, the frequency dependent formula in Equation 6.7 is used to compute the value of c_1 as well as c_3. The text book values of c_1, k_1 and c_3 for the strip footing are given in Table 6.6. There are more discrepancies between the identified and text book values for the structures with strip footings (see Table 6.11 for relative error) than there are for the structures with other footing shapes. This is particularly true for the parameter k_1. One possible reason for the large relative errors is that the footing may be behaving more like a rectangle than a strip. The equivalent circular model used for the square and rectangular footings is no longer appropriate because the aspect ratio of the strip footing is large (L/W=8), so a true rectangular model may be necessary.

TABLE 6.2
EQUATION PARAMETERS OF 2DOF MODEL
STRUCTURE WITH A SURFACE CIRCULAR FOOTING
($M_{base} = 1.71\times10^4$ $M_{mass} = 5.37\times10^3$ $M_{stem} = 9.33\times10^2$ $\frac{lb}{ft/sec^2}$)

PARAMETER	FREQUENCY OF SUPERSTRUCTURE (f_{str}) 1.66 Hz	4.05 Hz	4.69 Hz	5.72 Hz	UNITS
	Deterministic Values				
a	0.500	0.219	0.172	0.125	-
b	0.500	0.781	0.828	0.875	-
m_1	1.76×10^4	1.73×10^4	1.73×10^4	1.72×10^4	$\frac{lb}{ft/sec^2}$
m_2	5.84×10^3	6.10×10^3	6.14×10^3	6.19×10^3	$\frac{lb}{ft/sec^2}$
c_2	4.37×10^2	1.65×10^3	8.68×10^2	1.48×10^3	$\frac{lb-sec}{ft}$
	Identified Values				
k_2	5.96×10^5	2.00×10^6	2.67×10^6	3.36×10^6	$\frac{lb}{ft}$
0.0-1.0 sec.					
c_1	2.21×10^5	2.70×10^5	3.87×10^5	4.33×10^5	$\frac{lb-sec}{ft}$
k_1	2.74×10^7	2.95×10^7	2.27×10^7	2.27×10^7	$\frac{lb}{ft}$
c_3	2.10×10^3	1.10×10^4	3.67×10^4	8.73×10^4	$\frac{lb-sec}{ft}$
error in fit	0.0217	0.0308	0.0688	0.0754	
1.0-2.5 sec.					
c_1	1.38×10^5	2.37×10^5	2.82×10^5	3.08×10^5	$\frac{lb-sec}{ft}$
k_1	4.00×10^7	4.00×10^7	4.00×10^7	4.58×10^7	$\frac{lb}{ft}$
c_3	0.00	1.05×10^3	1.42×10^3	1.33×10^4	$\frac{lb-sec}{ft}$
error in fit	0.0215	0.0588	0.0637	0.0873	
2.5-5.0 sec.					
c_1	2.65×10^5	2.20×10^5	2.22×10^5	1.26×10^5	$\frac{lb-sec}{ft}$
k_1	4.00×10^7	4.00×10^7	4.00×10^7	4.00×10^7	$\frac{lb}{ft}$
c_3	0.00	9.00×10^4	1.25×10^5	1.33×10^4	$\frac{lb-sec}{ft}$
error in fit	0.1409	0.2293	0.1560	0.1408	
	Text Book Values				
c_1	3.29×10^5	3.29×10^5	3.29×10^5	3.29×10^5	$\frac{lb-sec}{ft}$
k_1	3.70×10^7	3.70×10^7	3.70×10^7	3.70×10^7	$\frac{lb}{ft}$
c_3	0.00	5.72×10^4	1.54×10^5	2.00×10^5	$\frac{lb-sec}{ft}$

TABLE 6.3
EQUATION PARAMETERS OF 2DOF MODEL
STRUCTURE WITH A SURFACE SQUARE FOOTING
($M_{base} = 2.17\times10^4$ $M_{mass} = 5.37\times10^3$ $M_{stem} = 9.33\times10^2$ $\frac{lb}{ft/sec^2}$)

PARAMETER	FREQUENCY OF SUPERSTRUCTURE (f_{str}) 1.66 Hz	2.98 Hz	3.12 Hz	4.69 Hz	5.72 Hz	UNITS
			Deterministic Values			
a	0.500	0.313	0.234	0.172	0.125	-
b	0.500	0.688	0.766	0.828	0.875	-
m_1	2.22×10^4	2.20×10^4	2.19×10^4	2.19×10^4	2.18×10^4	$\frac{lb}{ft/sec^2}$
m_2	5.84×10^3	6.01×10^3	6.08×10^3	6.14×10^3	6.19×10^3	$\frac{lb}{ft/sec^2}$
c_2	4.37×10^2	7.20×10^2	1.90×10^3	8.68×10^2	1.48×10^3	$\frac{lb-sec}{ft}$
			Identified Values			
k_2	7.00×10^5	2.00×10^6	3.10×10^6	5.33×10^6	4.73×10^6	$\frac{lb}{ft}$
0.0-1.0 sec.						
c_1	4.95×10^5	5.64×10^5	4.53×10^5	6.07×10^5	6.51×10^5	$\frac{lb-sec}{ft}$
k_1	1.47×10^7	7.63×10^6	4.18×10^6	2.85×10^6	6.99×10^6	$\frac{lb}{ft}$
c_3	2.49×10^3	9.23×10^3	6.00×10^3	3.95×10^4	7.23×10^4	$\frac{lb-sec}{ft}$
error in fit	0.0604	0.0786	0.0967	0.0835	0.1136	
1.0-2.5 sec.						
c_1	2.87×10^5	3.50×10^5	2.50×10^5	2.87×10^5	1.92×10^6	$\frac{lb-sec}{ft}$
k_1	5.00×10^7	5.15×10^7	5.10×10^7	5.00×10^7	5.95×10^7	$\frac{lb}{ft}$
c_3	0.00	4.00×10^2	1.15×10^4	1.64×10^4	3.58×10^4	$\frac{lb-sec}{ft}$
error in fit	0.0671	0.1140	0.2430	0.5012	0.7328	
2.5-5.0 sec.						
c_1	3.27×10^5	1.41×10^5	1.81×10^5	3.27×10^5	*	$\frac{lb-sec}{ft}$
k_1	5.00×10^7	5.15×10^7	5.10×10^7	5.00×10^7	*	$\frac{lb}{ft}$
c_3	0.00	4.00×10^2	1.19×10^4	1.97×10^4	*	$\frac{lb-sec}{ft}$
error in fit	0.1875	0.1335	0.1412	0.1479		
			Text Book Values			
c_1	4.39×10^5	4.39×10^5	4.39×10^5	4.39×10^5	4.39×10^5	$\frac{lb-sec}{ft}$
k_1	4.58×10^7	4.58×10^7	4.58×10^7	4.58×10^7	4.58×10^7	$\frac{lb}{ft}$
c_3	0.00	4.66×10^4	4.66×10^4	2.33×10^5	4.26×10^5	$\frac{lb-sec}{ft}$

*Time history only available to 2 seconds.

TABLE 6.4
EQUATION PARAMETERS OF 2DOF MODEL

STRUCTURE WITH A SURFACE RECTANGULAR (L/W=2) FOOTING

($M_{base} = 4.36\times10^4$ $M_{mass} = 5.37\times10^3$ $M_{stem} = 9.33\times10^2$ $\frac{lb}{ft/sec^2}$)

PARAMETER	FREQUENCY OF SUPERSTRUCTURE (f_{str}) 1.66 Hz	2.98 Hz	4.69 Hz	UNITS
	Deterministic Values			
a	0.500	0.313	0.172	-
b	0.500	0.688	0.828	-
m_1	4.40×10^4	4.39×10^4	4.37×10^4	$\frac{lb}{ft/sec^2}$
m_2	5.84×10^3	6.01×10^3	6.14×10^3	$\frac{lb}{ft/sec^2}$
c_2	4.37×10^2	7.20×10^2	8.68×10^2	$\frac{lb-sec}{ft}$
	Identified Values			
k_2	7.45×10^5	1.90×10^6	5.00×10^6	$\frac{lb}{ft}$
0.0-1.0 sec.				
c_1	7.06×10^5	5.10×10^5	7.34×10^5	$\frac{lb-sec}{ft}$
k_1	3.13×10^7	1.78×10^7	2.69×10^7	$\frac{lb}{ft}$
c_3	0.00	0.00	2.29×10^4	$\frac{lb-sec}{ft}$
error in fit	0.1107	0.1650	0.1253	
1.0-2.5 sec.				
c_1	6.28×10^5	5.19×10^5	9.47×10^5	$\frac{lb-sec}{ft}$
k_1	8.00×10^7	8.28×10^7	1.00×10^8	$\frac{lb}{ft}$
c_3	0.00	0.00	1.60×10^3	$\frac{lb-sec}{ft}$
error in fit	0.0582	0.1376	0.1236	
2.5-5.0 sec.				
c_1	1.99×10^6	3.74×10^5	5.76×10^5	$\frac{lb-sec}{ft}$
k_1	1.01×10^8	8.28×10^7	1.00×10^8	$\frac{lb}{ft}$
c_3	0.00	0.00	4.45×10^3	$\frac{lb-sec}{ft}$
error in fit	0.1314	0.1908	0.2533	
	Text Book Values			
c_1	1.02×10^6	1.02×10^6	1.02×10^6	$\frac{lb-sec}{ft}$
k_1	8.48×10^7	8.48×10^7	8.48×10^7	$\frac{lb}{ft}$
c_3	0.00	8.70×10^4	7.48×10^5	$\frac{lb-sec}{ft}$

TABLE 6.5
EQUATION PARAMETERS OF 2DOF MODEL

STRUCTURE WITH A SURFACE RECTANGULAR (L/W=4) FOOTING

($M_{base} = 8.68\times10^4$ $M_{mass} = 5.37\times10^3$ $M_{stem} = 9.33\times10^2$ $\frac{lb}{ft/sec^2}$)

PARAMETER	FREQUENCY OF SUPERSTRUCTURE (f_{str}) 1.66 Hz	2.98 Hz	4.69 Hz	UNITS
	Deterministic Values			
a	0.500	0.313	0.172	-
b	0.500	0.688	0.828	-
m_1	8.73×10^4	8.71×10^4	8.70×10^4	$\frac{lb}{ft/sec^2}$
m_2	5.84×10^3	6.01×10^3	6.14×10^3	$\frac{lb}{ft/sec^2}$
c_2	4.37×10^2	7.20×10^2	8.68×10^2	$\frac{lb-sec}{ft}$
	Identified Values			
k_2	8.00×10^5	2.15×10^6	5.33×10^6	$\frac{lb}{ft}$
0.0-1.0 sec.				
c_1	1.16×10^6	1.51×10^6	1.24×10^6	$\frac{lb-sec}{ft}$
k_1	4.08×10^7	5.00×10^7	5.06×10^7	$\frac{lb}{ft}$
c_3	0.00	0.00	5.77×10^3	$\frac{lb-sec}{ft}$
error in fit	0.0782	0.0786	0.0911	
1.0-2.5 sec.				
c_1	4.94×10^6	3.14×10^6	3.69×10^6	$\frac{lb-sec}{ft}$
k_1	2.00×10^8	2.21×10^8	2.21×10^8	$\frac{lb}{ft}$
c_3	0.00	6.42×10^1	3.42×10^3	$\frac{lb-sec}{ft}$
error in fit	0.0638	0.0641	0.1546	
2.5-5.0 sec.				
c_1	6.29×10^5	5.67×10^6	3.69×10^6	$\frac{lb-sec}{ft}$
k_1	2.00×10^8	2.21×10^8	2.21×10^8	$\frac{lb}{ft}$
c_3	0.00	0.00	6.42×10^3	$\frac{lb-sec}{ft}$
error in fit	0.2043	0.1146	0.1515	
	Text Book Values			
c_1	2.25×10^6	2.25×10^6	2.25×10^6	$\frac{lb-sec}{ft}$
k_1	1.79×10^8	1.79×10^8	1.79×10^8	$\frac{lb}{ft}$
c_3	0.00	5.10×10^4	1.53×10^6	$\frac{lb-sec}{ft}$

TABLE 6.6
EQUATION PARAMETERS OF 2DOF MODEL
STRUCTURE WITH A SURFACE STRIP (L/W=8) FOOTING
($M_{base} = 4.36\times10^4$ $M_{mass} = 5.37\times10^3$ $M_{stem} = 9.33\times10^2$ $\frac{lb}{ft/sec^2}$)

PARAMETER	FREQUENCY OF SUPERSTRUCTURE (f_{str}) 1.66 Hz	2.98 Hz	4.69 Hz	UNITS
	Determinisuc Values			
a	0.500	0.313	0.172	-
b	0.500	0.688	0.828	-
m_1	4.40×10^4	4.39×10^4	4.37×10^4	$\frac{lb}{ft/sec^2}$
m_2	5.84×10^3	6.01×10^3	6.14×10^3	$\frac{lb}{ft/sec^2}$
c_2	4.37×10^2	7.20×10^2	8.68×10^2	$\frac{lb-sec}{ft}$
	Identified Values			
k_2	6.86×10^5	1.64×10^6	4.06×10^6	$\frac{lb}{ft}$
0.0-1.0 sec.				
c_1	3.72×10^5	4.91×10^5	9.38×10^5	$\frac{lb-sec}{ft}$
k_1	2.46×10^7	3.00×10^7	4.15×10^7	$\frac{lb}{ft}$
c_3	0.00	0.00	8.16×10^4	$\frac{lb-sec}{ft}$
error in fit	0.1082	0.0991	0.0875	
1.0-2.5 sec.				
c_1	8.90×10^5	5.45×10^5	1.01×10^6	$\frac{lb-sec}{ft}$
k_1	1.06×10^8	7.83×10^7	9.38×10^7	$\frac{lb}{ft}$
c_3	0.00	3.40×10^3	5.14×10^3	$\frac{lb-sec}{ft}$
error in fit	0.1222	0.0271	0.0506	
2.5-5.0 sec.				
c_1	2.08×10^6	2.96×10^6	2.87×10^6	$\frac{lb-sec}{ft}$
k_1	1.06×10^8	2.67×10^7	9.37×10^7	$\frac{lb}{ft}$
c_3	0.00	4.21×10^2	1.06×10^4	$\frac{lb-sec}{ft}$
error in fit	0.1341	0.0952	0.2399	
	Text Book Values			
c_1	2.46×10^7	2.46×10^7	2.46×10^7	$\frac{lb-sec}{ft}$
k_1	3.11×10^7	3.11×10^7	3.11×10^7	$\frac{lb}{ft}$
c_3	0.00	2.86×10^6	5.13×10^6	$\frac{lb-sec}{ft}$

TABLE 6.7
RELATIVE ERROR BETWEEN IDENTIFIED AND TEXT BOOK VALUES
STRUCTURE WITH A SURFACE CIRCULAR FOOTING

PARAMETER	FREQUENCY OF SUPERSTRUCTURE (f_{str})			
	1.66 Hz	4.05 Hz	4.69 Hz	5.72 Hz
0.0-1.0 sec.				
c_1	-0.328	-0.179	0.176	0.316
k_1	-0.260	-0.203	-0.387	-0.387
c_3	-	-0.808	-0.762	-0.564
1.0-2.5 sec.				
c_1	-0.581	-0.280	-0.143	-0.064
k_1	0.081	0.081	0.081	0.238
c_3	0.000	-0.982	-0.991	-0.934
2.5-5.0 sec.				
c_1	-0.195	-0.331	-0.325	-0.617
k_1	0.081	0.081	0.081	0.081
c_3	0.000	0.573	-0.188	-0.934

TABLE 6.8
RELATIVE ERROR BETWEEN IDENTIFIED AND TEXT BOOK VALUES
STRUCTURE WITH A SURFACE SQUARE FOOTING

	FREQUENCY OF SUPERSTRUCTURE (f_{str})				
PARAMETER	1.66 Hz	2.98 Hz	3.12 Hz	4.69 Hz	5.72 Hz
0.0-1.0 sec.					
c_1	0.128	0.285	0.032	0.383	0.483
k_1	-0.679	-0.833	-0.909	-0.938	-0.847
c_3	-	-0.802	-0.871	-0.830	-0.830
1.0-2.5 sec.					
c_1	-0.346	-0.203	-0.431	-0.346	3.374
k_1	0.092	0.124	0.114	0.092	0.299
c_3	0.000	-0.991	-0.753	-0.930	-0.916
2.5-5.0 sec.					
c_1	-0.255	-0.679	-0.588	-0.255	*
k_1	0.092	0.124	0.114	0.092	*
c_3	0.000	-0.991	-0.745	-0.915	*

*Time history only available to 2 seconds.

TABLE 6.9
RELATIVE ERROR BETWEEN IDENTIFIED AND TEXT BOOK VALUES
STRUCTURE WITH A SURFACE RECTANGULAR (L/W=2) FOOTING

	FREQUENCY OF SUPERSTRUCTURE (f_{str})		
PARAMETER	1.66 Hz	2.98 Hz	4.69 Hz
0.0-1.0 sec.			
c_1	-0.308	-0.500	-0.280
k_1	-0.631	-0.790	-0.683
c_3	0.000	-1.000	-0.969
1.0-2.5 sec.			
c_1	-0.384	-0.491	-0.072
k_1	-0.057	-0.024	0.179
c_3	0.000	-1.000	-0.998
2.5-5.0 sec.			
c_1	0.951	-0.633	-0.435
k_1	0.191	-0.024	0.179
c_3	0.000	-1.000	-0.994

TABLE 6.10
RELATIVE ERROR BETWEEN IDENTIFIED AND TEXT BOOK VALUES
STRUCTURE WITH A SURFACE RECTANGULAR (L/W=4) FOOTING

PARAMETER	FREQUENCY OF SUPERSTRUCTURE (f_{str})		
	1.66 Hz	2.98 Hz	4.69 Hz
0.0-1.0 sec.			
c_1	-0.484	-0.329	-0.449
k_1	-0.772	-0.721	-0.717
c_3	0.000	-1.000	-0.996
1.0-2.5 sec.			
c_1	1.196	0.396	0.640
k_1	0.117	0.235	0.235
c_3	0.000	-0.999	-0.998
2.5-5.0 sec.			
c_1	-0.720	1.520	0.640
k_1	0.117	0.235	0.235
c_3	0.000	-1.000	-0.996

TABLE 6.11
RELATIVE ERROR BETWEEN IDENTIFIED AND TEXT BOOK VALUES
STRUCTURE WITH A SURFACE STRIP (L/W=8) FOOTING

PARAMETER	FREQUENCY OF SUPERSTRUCTURE (f_{str})		
	1.66 Hz	2.98 Hz	4.69 Hz
0.0 0.0 sec.			
c_1	-0.985	-0.980	-0.962
k_1	-0.209	-0.035	0.334
c_3	0.000	-1.000	-0.984
1.0-2.5 sec.			
c_1	-0.964	-0.978	-0.959
k_1	2.408	1.518	2.016
c_3	0.000	-0.999	-0.999
2.5-5.0 sec.			
c_1	-0.915	-0.880	-0.883
k_1	2.408	-0.141	2.013
c_3	0.000	-1.000	-0.998

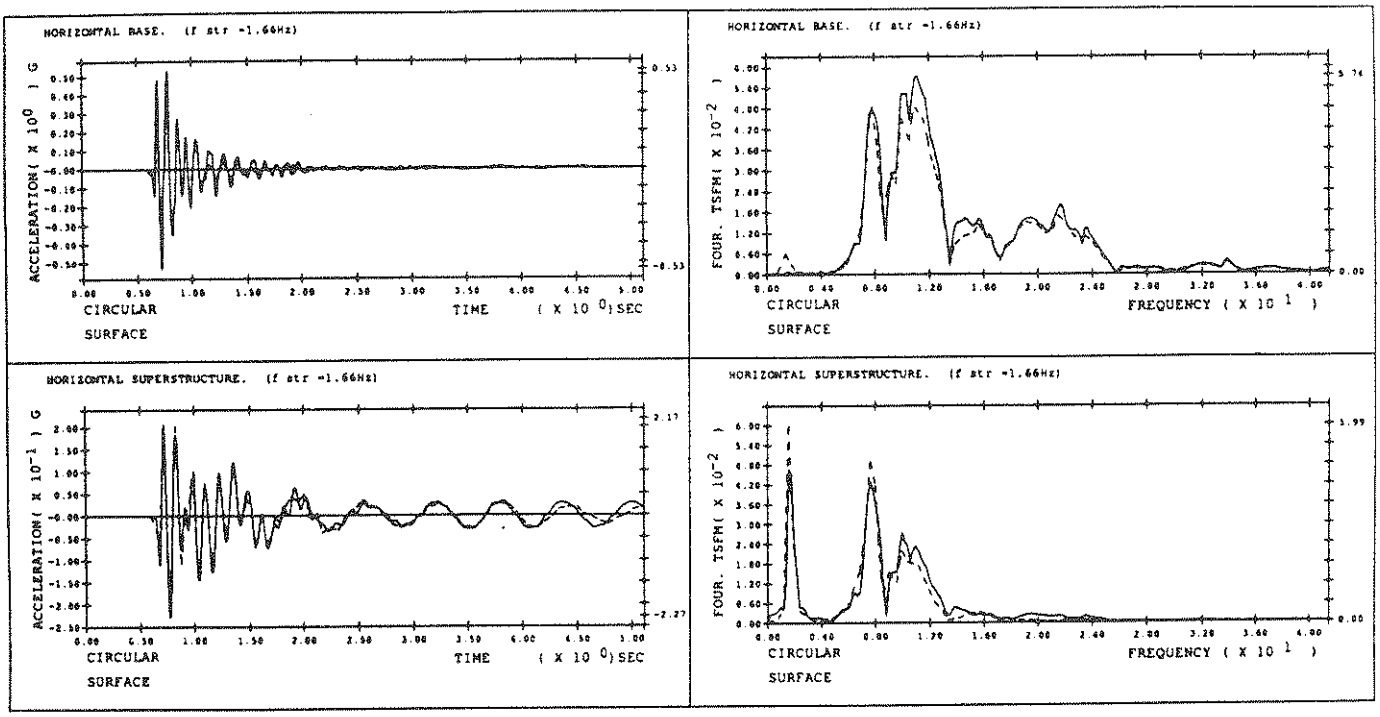

FIGURE 6.4
Circular Surface Footing, f_{str} =1.66Hz
Comparison of —Two Degree of Freedom Model and ----Centrifuge Results

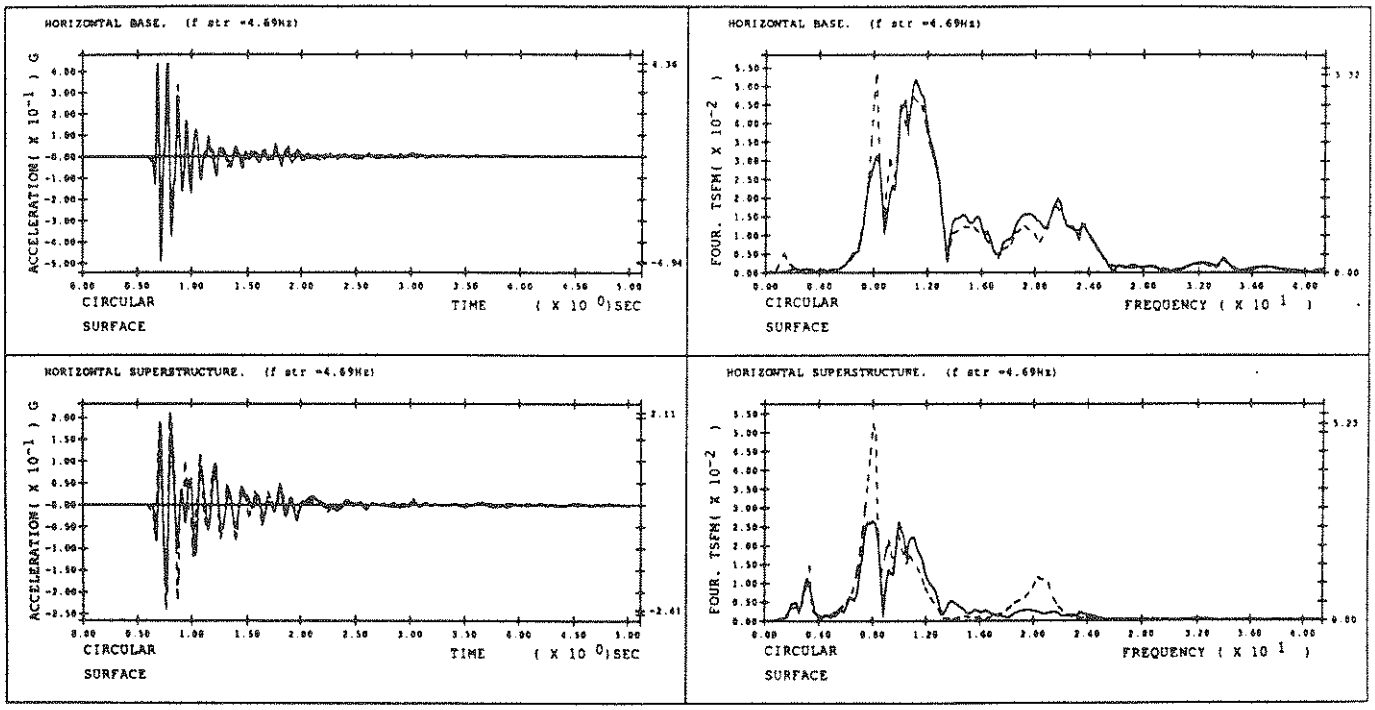

FIGURE 6.5
Circular Surface Footing, f_{str}=4.69Hz
Comparison of —Two Degree of Freedom Model and ----Centrifuge Results

6.5 Structures With Embedded Footings

6.5.1 Identified Experimental Parameter Values

The parameters identified from the results of the experiments on structures with embedded footings using the piecewise linear two degree of freedom model (see Equation 6.1) are given in Tables 6.12 through 6.15. The damping of the base of the structure, c_1, is anywhere from three to seven times larger for the structures with embedded footings than for the structures with surface footings. The stiffness of the base, k_1, is about two to three times larger for the structures with embedded footings. The damping of the superstructure, c_3, is generally similar for the embedded and surface cases. The acceleration time history calculated using the identified parameter values for the embedded square footing (Table 6.12) with f_{str} = 1.66Hz is shown as an example in Figure 6.6. The computed time histories for the remaining cases may be found in Reference 6.12.

A measure of the error in fit for each segment is also given in Tables 6.12-6.15. The error in fit for the embedded cases is similar to the error in fit for the surface cases. It is typically less than 10% for the first two segments, and somewhat larger (15-20%) for the final segment. The error in fit is also consistently lower for the cases with little or no radiation damping.

6.5.2 Comparison with Text Book Values

For the embedded square and rectangular footings, frequency independent approximations are used to determine the text book values of c_1 and k_1. The frequency independent damping and static stiffness are computed from the following formulas for a rigid cylindrical footing embedded in a horizontal soil stratum [6.8, 6.9]:

$$c_1 = \pi \rho V_s r^2 \left[1+1.3\frac{e}{r}\left[1+\frac{3.6}{\pi(1-\nu)}\right]\right]\left[1+\frac{1}{2}\frac{r}{d}\right]\left[1+\frac{5}{4}\frac{e}{d}\right] \tag{6.10a}$$

$$k_1 = \frac{8Gr}{2-\nu}\left[1+\frac{1}{2}\frac{r}{d}\right]\left[1+\frac{2}{3}\frac{e}{r}\right]\left[1+\frac{5}{4}\frac{e}{d}\right] \tag{6.10b}$$

where e is depth of embedment (4.92 ft) and r is the equivalent radius of the square and rectangular footings. In reality, the sensitivity of the static stiffness to the embedment ratio (e/r or e/w, w= footing half-width) is smaller for rectangular footings than for circular footings [6.7]. Therefore, the coefficient of e/r in Equation 6.10b should really be smaller than 2/3. However, the embedment ratio is small ($e/r \leq 0.53$) for the all the footings in this study so the error introduced by the large coefficient in the equivalent circular model should be small. The values of c_1 and k_1 computed from Equations 6.10a and 6.10b for the embedded square and rectangular footings are shown under *Text Book Values* in Tables 6.12-6.14.

The damping of the superstructure, c_3, is computed from the frequency dependent formula given in Equation 6.7. The text book values of c_3 for the structures with embedded square and rectangular footings are also given in Tables 6.12-6.14.

The two dimensional formula for the frequency independent approximation to the stiffness of a rigid, embedded strip footing is [6.10]:

$$k_1 = \frac{2.1G}{2-\nu}\left[1+2\frac{w}{d}\right]\left[1+\frac{1}{3}\frac{e}{w}\right]\left[1+\frac{4}{3}\frac{e}{d}\right] \tag{6.11}$$

Equation 6.7 is used to compute the text book values of the damping terms c_1 and c_3. The text book values of the parameters for the structures with embedded strip footings are given in Table 6.15.

The relative errors (Equation 6.8) between the identified and text book values for the structures with embedded footings are given in Tables 6.16-6.19. On the whole, the relative errors in c_1 and k_1 are larger for the embedded cases than the surface cases (Tables 6.7-6.10). The frequency independent formula given in Equation 6.10b tends to underestimate the damping value k_1 for the embedded footings, while the frequency independent formula in Equation 6.5b gave very accurate predictions of the experimental values for the surface footings. The frequency independent approximation of k_1 is less accurate for the embedded footings because the true

dynamic value of k_1 actually exhibits large oscillations about the static value in the high frequency range for embedded footings [6.8]. For surface footings, the dynamic value of k_1 exhibits much smaller oscillations in this range and can, therefore, be more closely approximated by the static value. The relative error in c_3 is very similar for the embedded and surface cases. The relative error in c_3 is smaller when there is little or no radiation damping in the super structure, but rather large when there is substantial radiation damping in the super structure.

TABLE 6.12
EQUATION PARAMETERS OF 2DOF MODEL
STRUCTURE WITH AN EMBEDDED SQUARE FOOTING
($M_{base} = 2.17\times10^4$ $M_{mass} = 5.37\times10^3$ $M_{stem} = 9.33\times10^2$ $\frac{lb}{ft/sec^2}$)

PARAMETER	FREQUENCY OF SUPERSTRUCTURE (f_{str}) 1.66 Hz	2.98 Hz	3.12 Hz	4.69 Hz	5.72 Hz	UNITS
			Deterministic Values			
a	0.500	0.313	0.234	0.172	0.125	-
b	0.500	0.688	0.766	0.828	0.875	-
m_1	2.22×10^4	2.20×10^4	2.19×10^4	2.19×10^4	2.18×10^4	$\frac{lb}{ft/sec^2}$
m_2	5.84×10^3	6.01×10^3	6.08×10^3	6.14×10^3	6.19×10^3	$\frac{lb}{ft/sec^2}$
c_2	4.37×10^2	7.20×10^2	1.90×10^3	8.68×10^2	1.48×10^3	$\frac{lb-sec}{ft}$
			Identified Values			
k_2	7.50×10^5	2.11×10^6	3.31×10^6	5.33×10^6	6.31×10^6	$\frac{lb}{ft}$
0.0-1.0 sec.						
c_1	1.18×10^6	1.28×10^6	1.56×10^6	1.46×10^6	1.22×10^6	$\frac{lb-sec}{ft}$
k_1	6.59×10^7	4.77×10^7	3.23×10^7	3.01×10^7	3.00×10^7	$\frac{lb}{ft}$
c_3	2.25×10^4	3.96×10^4	6.93×10^4	1.27×10^5	1.67×10^5	$\frac{lb-sec}{ft}$
error in fit	0.0566	0.0589	0.0716	0.0966	0.0739	
1.0-2.5 sec.						
c_1	9.64×10^5	1.91×10^6	1.87×10^6	9.64×10^5	2.36×10^6	$\frac{lb-sec}{ft}$
k_1	8.92×10^7	1.00×10^8	1.00×10^8	8.92×10^7	1.00×10^8	$\frac{lb}{ft}$
c_3	0.00	0.00	0.00	8.02×10^3	1.01×10^4	$\frac{lb-sec}{ft}$
error in fit	0.2490	0.0437	0.0729	0.1414	0.1074	
2.5-5.0 sec.						
c_1	9.64×10^5	1.65×10^6	1.32×10^6	9.64×10^5	2.41×10^6	$\frac{lb-sec}{ft}$
k_1	8.92×10^7	1.00×10^8	1.00×10^8	8.92×10^7	1.00×10^8	$\frac{lb}{ft}$
c_3	0.00	0.00	0.00	7.52×10^3	1.30×10^4	$\frac{lb-sec}{ft}$
error in fit	0.1029	0.2460	0.2172	0.2237	0.2727	
			Text Book Values			
c_1	1.79×10^6	1.79×10^6	1.79×10^6	1.79×10^6	1.79×10^6	$\frac{lb-sec}{ft}$
k_1	7.63×10^7	7.63×10^7	7.63×10^7	7.63×10^7	7.63×10^7	$\frac{lb}{ft}$
c_3	0.00	4.04×10^4	4.04×10^4	8.16×10^4	1.62×10^5	$\frac{lb-sec}{ft}$

TABLE 6.13
EQUATION PARAMETERS OF 2DOF MODEL

STRUCTURE WITH AN EMBEDDED RECTANGULAR (L/W=2) FOOTING

($M_{base} = 4.36\times10^4$ $M_{mass} = 5.37\times10^3$ $M_{stem} = 9.33\times10^2$ $\frac{lb}{ft/\sec^2}$)

PARAMETER	FREQUENCY OF SUPERSTRUCTURE (f_{str}) 1.66 Hz	2.98 Hz	4.69 Hz	UNITS
	Deterministic Values			
a	0.500	0.313	0.172	-
b	0.500	0.688	0.828	-
m_1	4.40×10^4	4.39×10^4	4.37×10^4	$\frac{lb}{ft/\sec^2}$
m_2	5.84×10^3	6.01×10^3	6.14×10^3	$\frac{lb}{ft/\sec^2}$
c_2	4.37×10^2	7.20×10^2	8.68×10^2	$\frac{lb-sec}{ft}$
	Identified Values			
k_2	7.70×10^5	2.04×10^6	5.33×10^6	$\frac{lb}{ft}$
0.0-1.0 sec.				
c_1	2.27×10^6	2.23×10^6	2.41×10^6	$\frac{lb-sec}{ft}$
k_1	1.03×10^8	7.53×10^7	7.53×10^7	$\frac{lb}{ft}$
c_3	0.00	0.00	9.33×10^4	$\frac{lb-sec}{ft}$
error in fit	0.0288	0.0437	0.0512	
1.0-2.5 sec.				
c_1	3.67×10^6	4.00×10^6	4.23×10^6	$\frac{lb-sec}{ft}$
k_1	2.04×10^8	2.08×10^8	2.00×10^8	$\frac{lb}{ft}$
c_3	0.00	1.43×10^2	6.79×10^3	$\frac{lb-sec}{ft}$
error in fit	0.0365	0.0758	0.1089	
2.5-5.0 sec.				
c_1	1.60×10^6	4.00×10^6	1.96×10^6	$\frac{lb-sec}{ft}$
k_1	2.04×10^8	2.08×10^8	2.00×10^8	$\frac{lb}{ft}$
c_3	0.00	0.00	4.24×10^3	$\frac{lb-sec}{ft}$
error in fit	0.1409	0.3583	0.2086	
	Text Book Values			
c_1	3.48×10^6	3.48×10^6	3.48×10^6	$\frac{lb-sec}{ft}$
k_1	1.30×10^8	1.30×10^8	1.30×10^8	$\frac{lb}{ft}$
c_3	0.00	6.89×10^4	4.30×10^5	$\frac{lb-sec}{ft}$

TABLE 6.14
EQUATION PARAMETERS OF 2DOF MODEL

STRUCTURE WITH AN EMBEDDED RECTANGULAR (L/W=4) FOOTING

($M_{base} = 8.68\times10^4$ $M_{mass} = 5.37\times10^3$ $M_{stem} = 9.33\times10^2$ $\frac{lb}{ft/sec^2}$)

PARAMETER	FREQUENCY OF SUPERSTRUCTURE (f_{str}) 1.66 Hz	2.98 Hz	4.69 Hz	UNITS
	Deterministic Values			
a	0.500	0.313	0.172	-
b	0.500	0.688	0.828	-
m_1	8.73×10^4	8.71×10^4	8.70×10^4	$\frac{lb}{ft/sec^2}$
m_2	5.84×10^3	6.01×10^3	6.14×10^3	$\frac{lb}{ft/sec^2}$
c_2	4.37×10^2	7.20×10^2	8.68×10^2	$\frac{lb-sec}{ft}$
	Identified Values			
k_2	8.00×10^5	2.30×10^6	5.33×10^6	$\frac{lb}{ft}$
0.0-1.0 sec.				
c_1	4.34×10^6	3.76×10^6	1.71×10^6	$\frac{lb-sec}{ft}$
k_1	2.95×10^6	2.95×10^6	2.95×10^6	$\frac{lb}{ft}$
c_3	0.00	0.00	4.89×10^4	$\frac{lb-sec}{ft}$
error in fit	0.0413	0.0175	0.2067	
1.0-2.5 sec.				
c_1	1.68×10^7	1.68×10^7	1.68×10^7	$\frac{lb-sec}{ft}$
k_1	4.09×10^8	4.12×10^8	4.23×10^8	$\frac{lb}{ft}$
c_3	0.00	8.67×10^2	1.16×10^3	$\frac{lb-sec}{ft}$
error in fit	0.1059	0.2322	0.2107	
2.5-5.0 sec.				
c_1	1.92×10^6	1.68×10^7	1.68×10^7	$\frac{lb-sec}{ft}$
k_1	4.09×10^8	4.12×10^8	4.23×10^8	$\frac{lb}{ft}$
c_3	0.00	1.03×10^2	1.16×10^3	$\frac{lb-sec}{ft}$
error in fit	0.1157	0.1535	0.3027	
	Text Book Values			
c_1	7.95×10^6	7.95×10^6	7.95×10^6	$\frac{lb-sec}{ft}$
k_1	2.59×10^8	2.59×10^8	2.59×10^8	$\frac{lb}{ft}$
c_3	0.00	4.64×10^5	4.65×10^6	$\frac{lb-sec}{ft}$

TABLE 6.15
EQUATION PARAMETERS OF 2DOF MODEL

STRUCTURE WITH AN EMBEDDED STRIP (L/W=8) FOOTING

($M_{base} = 4.36\times10^4$ $M_{mass} = 5.37\times10^3$ $M_{stem} = 9.33\times10^2$ $\frac{lb}{ft/sec^2}$)

PARAMETER	FREQUENCY OF SUPERSTRUCTURE (f_{str}) 1.66 Hz	2.98 Hz	4.69 Hz	UNITS
	Deterministic Values			
a	0.500	0.313	0.172	-
b	0.500	0.688	0.828	-
m_1	4.40×10^4	4.39×10^4	4.37×10^4	$\frac{lb}{ft/sec^2}$
m_2	5.84×10^3	6.01×10^3	6.14×10^3	$\frac{lb}{ft/sec^2}$
c_2	4.37×10^2	7.20×10^2	8.68×10^2	$\frac{lb-sec}{ft}$
	Identified Values			
k_2	7.50×10^5	2.18×10^6	5.03×10^6	$\frac{lb}{ft}$
0.0-1.0 sec.				
c_1	3.19×10^6	2.44×10^6	2.61×10^6	$\frac{lb-sec}{ft}$
k_1	2.35×10^6	2.67×10^6	2.19×10^6	$\frac{lb}{ft}$
c_3	0.00	2.75×10^4	1.14×10^5	$\frac{lb-sec}{ft}$
error in fit	0.1486	0.0840	0.0869	
1.0-2.5 sec.				
c_1	5.26×10^6	5.02×10^6	5.25×10^6	$\frac{lb-sec}{ft}$
k_1	2.14×10^8	2.08×10^8	2.13×10^8	$\frac{lb}{ft}$
c_3	0.00	6.41×10^3	1.03×10^4	$\frac{lb-sec}{ft}$
error in fit	0.0385	0.0496	0.1795	
2.5-5.0 sec.				
c_1	1.15×10^6	3.49×10^6	6.68×10^6	$\frac{lb-sec}{ft}$
k_1	2.14×10^8	2.08×10^8	2.13×10^8	$\frac{lb}{ft}$
c_3	0.00	0.00	1.52×10^4	$\frac{lb-sec}{ft}$
error in fit	0.2414	0.1871	0.2029	
	Text Book Values			
c_1	4.28×10^7	4.28×10^7	4.28×10^7	$\frac{lb-sec}{ft}$
k_1	5.41×10^7	5.41×10^7	5.41×10^7	$\frac{lb}{ft}$
c_3	0.00	4.98×10^6	8.92×10^6	$\frac{lb-sec}{ft}$

TABLE 6.16
RELATIVE ERROR BETWEEN IDENTIFIED AND TEXT BOOK VALUES
STRUCTURE WITH AN EMBEDDED SQUARE FOOTING

PARAMETER	FREQUENCY OF SUPERSTRUCTURE (f_{str})				
	1.66 Hz	2.98 Hz	3.12 Hz	4.69 Hz	5.72 Hz
0.0-1.0 sec.					
c_1	-0.341	0.285	-0.128	-0.184	-0.318
k_1	-0.136	-0.375	-0.577	-0.606	-0.607
c_3	-	-0.020	-0.715	-0.556	-0.031
1.0-2.5 sec.					
c_1	-0.461	0.067	0.045	-0.461	0.318
k_1	0.169	0.311	0.311	0.169	0.311
c_3	0.000	-1.000	-1.000	-0.902	-0.938
2.5-5.0 sec.					
c_1	-0.461	-0.078	-0.263	-0.461	0.346
k_1	0.169	0.311	0.311	0.169	0.311
c_3	0.000	-1.000	-1.000	-0.908	-0.920

TABLE 6.17
RELATIVE ERROR BETWEEN IDENTIFIED AND TEXT BOOK VALUES
STRUCTURE WITH AN EMBEDDED RECTANGULAR (L/W=2) FOOTING

PARAMETER	FREQUENCY OF SUPERSTRUCTURE (f_{str})		
	1.66 Hz	2.98 Hz	4.69 Hz
0.0-1.0 sec.			
c_1	-0.348	-0.359	-0.307
k_1	-0.209	-0.421	-0.421
c_3	0.000	-1.000	-0.783
1.0-2.5 sec.			
c_1	0.055	0.149	0.215
k_1	0.566	0.600	0.535
c_3	0.000	-0.998	-0.972
2.5-5.0 sec.			
c_1	-0.540	0.149	-0.436
k_1	0.585	0.600	0.538
c_3	0.000	-1.000	-0.971

TABLE 6.18
RELATIVE ERROR BETWEEN IDENTIFIED AND TEXT BOOK VALUES
STRUCTURE WITH AN EMBEDDED RECTANGULAR (L/W=4) FOOTING

PARAMETER	FREQUENCY OF SUPERSTRUCTURE (f_{str})		
	1.66 Hz	2.98 Hz	4.69 Hz
0.0-1.0 sec.			
c_1	-0.454	-0.527	-0.785
k_1	-0.979	-0.989	-0.989
c_3	0.000	-1.000	-0.989
1.0-2.5 sec.			
c_1	1.116	1.113	1.113
k_1	0.579	0.591	0.633
c_3	0.000	-0.998	-1.000
2.5-5.0 sec.			
c_1	-0.758	1.113	1.113
k_1	0.579	0.591	0.633
c_3	0.000	-0.999	-1.000

TABLE 6.19
RELATIVE ERROR BETWEEN IDENTIFIED AND TEXT BOOK VALUES
STRUCTURE WITH AN EMBEDDED STRIP (L/W=8) FOOTING

PARAMETER	FREQUENCY OF SUPERSTRUCTURE (f_{str})		
	1.66 Hz	2.98 Hz	4.69 Hz
0.0 0.0 sec.			
c_1	-0.926	-0.943	-0.939
k_1	-0.956	-0.951	-0.960
c_3	0.000	-0.994	-0.987
1.0-2.5 sec.			
c_1	-0.877	-0.883	-0.877
k_1	2.956	2.845	2.935
c_3	0.000	-0.999	-0.999
2.5-5.0 sec.			
c_1	-0.973	-0.918	-0.844
k_1	2.956	2.845	2.937
c_3	0.000	-1.000	-0.998

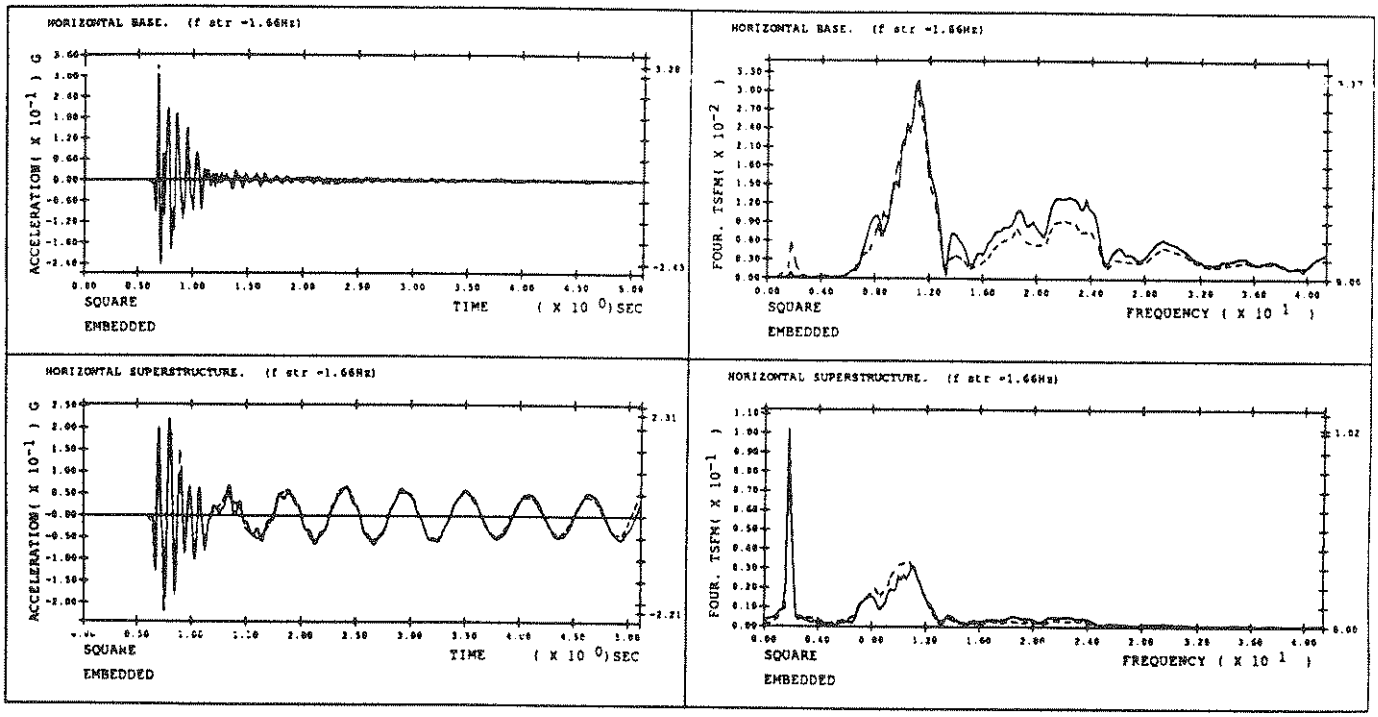

FIGURE 6.6
Square Embedded Footing, f_{str} =1.66Hz
Comparison of —Two Degree of Freedom Model and ----Centrifuge Results

6.6 Sensitivity Analysis and Stability of Parameter Estimates

In this section the subject of parameter accuracy is addressed. Even with a small error in fit (Sections 6.4.1 and 6.5.1) it is possible that the individual parameter estimates have a large amount of error but their combined effect on the measure of fit is canceled. It is, therefore, beneficial to determine a measure of the correlation between two parameters. This is done through sensitivity analysis. It is also desirable to show that the identified parameters are representative of the soil-structure system in general, and not dependent on the specific earthquake used in the data set. This is done through an investigation of the stability of the parameter estimates.

6.6.1 Sensitivity Analysis

In performing system identification it is important to assess the sensitivity of the function $S(\mathbf{q})$ (Equation 6.4) to variations in the parameters which are being identified (the elements of $\mathbf{q}$). Let the estimated parameter values be denoted by $\mathbf{q}^*$. Beck [6.11] has shown that the sensitivity of S to variations about the optimal estimates, $\mathbf{q}^*$, is governed by the hessian of S evaluated at the optimal estimates, $\mathbf{H}(\mathbf{q}^*)$. The hessian matrix, $\mathbf{H}$ is also called the sensitivity matrix. Ideally, the sensitivity matrix should be nearly diagonal, with diagonal terms that are large compared to $S(\mathbf{q}^*)$. An off diagonal term, H_{kl}, which has roughly the same order of magnitude as the diagonal terms H_{kk} or H_{ll} implies that there is more than one combination of the parameters q_k and q_l that gives the same value of $S(\mathbf{q}^*)$. Thus, both parameters may be in error, but their combined effect on S is canceled. For nearly orthogonal parameters, large values of the diagonal term implies there is only a small amount of error in the parameters. If $\mathbf{H}$ is not nearly diagonal, then the error in parameters is inversely proportional to the eigenvalues of $\mathbf{H}$. The reader is referred to Beck [6.11] for proofs of these properties.

In this study the sensitivity matrix is evaluated numerically by the program ZXMIN for each set of parameters as they are identified. The accuracy of the hessian matrix is dependent on how quickly the program converges because it is updated with each iteration. Thus, the sensitivity matrix may not be very accurate if the program converges very quickly. Because of the uncertainty in the estimation of the hessian matrix, the sensitivity analysis is used in this report to provide a qualitative assessment of the error rather than a quantitative value.

Since k_2 varies only slightly from the value determined by the fixed base free vibration experiment (see Equation 6.3a) the vector of unknown parameters is taken to be $\mathbf{q} = \{c_1, k_1, c_3\}$ in the evaluation of the hessian. For the cases where c_3 equals zero, $\mathbf{q}$ reduces to: $\mathbf{q} = \{c_1, k_1\}$. Since this process involves the calculation of over 90 matrices for all the test cases, the information gained from the sensitivity analysis is summarized below and the matrices themselves are not shown.

The sensitivity matrices show a strong correlation between the two damping terms c_1 and c_3. This means that there is more than one combination of these two parameters that gives the same error in fit. However, in the current study it is possible to check if the identified values are close to the "true" values by examining the variation in the damping of the base of the structure (c_1) with the frequency of the superstructure (f_{str}). The value of c_1 should remain constant as f_{str} is varied because the base remains the same for all values of f_{str}. If there is a substantial variation in the value of c_1, then c_1 may be compensating for error in c_3. These errors may be corrected by first computing the value of c_1 for the cases with f_{str}=1.66Hz, while c_3 is held fixed at zero (no radiation damping in the superstructure), and then fixing c_1 at the resulting value and identifying c_3 for all subsequent cases where the radiation damping in the superstructure is greater than zero. This procedure illustrates the role of sensitivity analysis and engineering judgement in system identification.

The off diagonal terms relating the stiffness, k_1, to each of the damping terms indicate that k_1 is relatively uncorrelated to both of the damping parameters. The eigenvalues of the sensitivity matrix indicate that the smallest error occurs in the the stiffness term k_1.

6.6.2 Stability of Parameter Estimates

Another topic worth investigating is the sensitivity of the estimated parameter values to the acceleration time histories that are used as input. Ideally this would be determined by identifying the parameters for the same system subjected to different earthquakes to see if the estimates vary. Since there is only one earthquake available in the current data set this is not possible. However, it is possible to identify the parameters over intervals of varying lengths of time within the same data set to ensure that the estimates are at least stable in this regard. Figure 6.36 shows the variation in the parameters k_1, c_1 and c_3 with interval length for a typical test case. All the intervals are taken from a region in which the system is responding linearly. The values shown in the figure are the relative difference between the estimated value over a particular interval and the mean value calculated by averaging the values obtained from all the intervals. Figure 6.36 indicates that the variation in k_1 is undetectable and the largest variation, which occurs for c_3, is less than 2% of the mean. This means that essentially the same parameters will be estimated over a two second interval and an eight second interval even for frequencies as low as 1.66Hz. For the strong motion response it is expected that the parameters may be accurately estimated over an even shorter interval because the frequencies are much higher and more cycles are contained in a shorter duration. This stability provides some reassurance that the estimated parameter values are not very dependent on the input time histories.

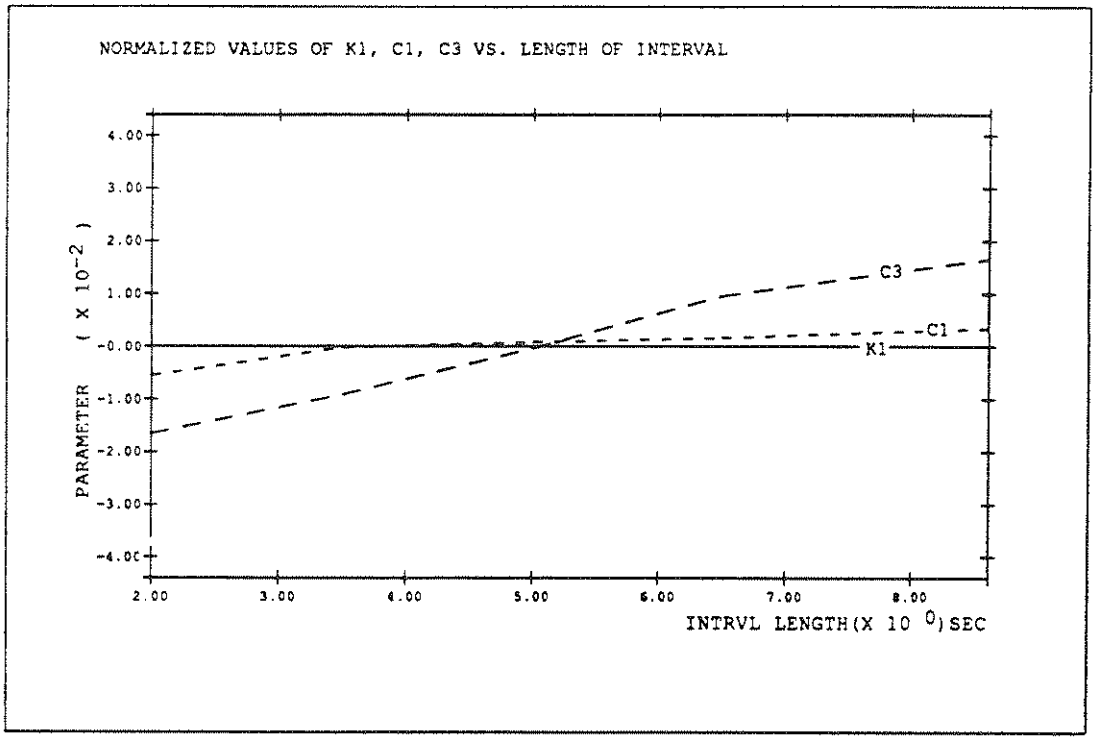

FIGURE 6.7
Stability of k_1, c_1 and c_3 With Interval Length

6.7 Conclusions

In this chapter a numerical analysis of the experimental results is performed in order to further validate the centrifuge model system. A simple, linear two degree of freedom model is introduced to represent the experimental system. The damping and stiffness coefficients of this numerical model are computed by methods of system identification from the results of the soil-structure interaction experiments performed in Chapter 5. It is found by applying this linear numerical model that there is some nonlinearity in the experimental response. To account for the nonlinearity, a piecewise linear approach is adopted in which the duration of the response is divided into three intervals, and three sets of parameters are identified. Plots comparing the structural response in the experiments to the response calculated numerically (using the identified parameter values) show that the piecewise linear model provides an improved fit to the experimental results. The error in fit between the experimental and analytical responses is typically quite small (less than 10%).

Next, a comparison is made between the identified parameter values and those computed by classical text book formulas to show that the behavior of the centrifuge model is consistent with established theory. The identified values of the damping and stiffness of the base (c_1 and k_1) are remarkably close to the text book values with few exceptions (i.e. the structures with strip footings). The identified value of the radiation damping in the superstructure (c_3) is close to the text book value when there is little or no radiation damping in the superstructure. For cases with significant radiation damping in the superstructure, the text book formulas tend to overestimate the value of c_3.

Finally, the accuracy of the system identification scheme is investigated through a sensitivity analysis and an examination of the stability of the parameter estimates. The sensitivity analysis shows a strong correlation between the two damping terms c_1 and c_3, indicating the pos-

sibility that there are large amounts of error associated with each of these identified values but that their combined effect on the error in fit is canceled. It is shown how these errors may be avoided by using the properties of the systems in this study to fix one parameter value while identifying the other. In the stability analysis the parameters are identified over intervals of varying lengths of time within the same data set to ensure that the estimates are stable and not dependent on the specific interval of the earthquake used as input. The results show that essentially the same parameter values are estimated over each of the interval lengths.

This chapter shows that the behavior of the centrifuge model is consistent with established theory for the variety of soil-structure systems examined in Chapter 5. These findings, along with the results of Chapters 4 and 5, clearly establish the centrifuge model in this thesis as a useful and realistic tool for the validation and future development of soil-structure interaction theory.

6.8 References For Chapter 6

6.1 Lin, Albert N., "Experimental Observations of the Effects of Embedment on Structural Response," Ph.D. Thesis, Cal. Inst. of Tech., Report No. EERL 82-01, May, 1982.

6.2 Gazetas, G., "Analysis of Machine Foundation Vibrations: State of the Art," *Soil Dynamics and Earthquake Engineering*, 1983, Vol. 2, No. 1.

6.3 Distefano, Nestor, Rath, Amitav, "System Identification in Nonlinear Structural Seismic Dynamics," *Computer Methods in Applied Mechanics and Engineering*, 1975, Vol. 5, pp 353-372.

6.4 Wolf, J.P., *Dynamic Soil-Structure Interaction*, Prentice Hall, Englewood Cliffs, N.J., 1985, pp 18-50, 295, 405-408.

6.5 Kausel, E., "Forced Vibrations of Circular Foundations on Layered Media," *Research Report*, R74-11, MIT, 1974.

6.6 Barkan, D.D., *Dynamics of Bases and Foundations*, McGraw Hill (translated), 1962.

6.7 Dominguez, J., Roesset, J.M., "Dynamic Stiffness of Rectangular Foundations," Research Report R78-20, MIT, 1978.

6.8 Kausel, E., Roesset, J.M., "Dynamic Stiffness of Circular Foundations," *Journal of Engineering Mechanics Division, ASCE*, 1975 , 101, EM12, 771.

6.9 Dobry, R., Gazetas, G., "Stiffness and Damping of Arbitrary-shaped Embedded Foundations," Research Report CE-82-04, RPI, 1982.

6.10 Jakub, M., and Roesset, J.M., "Dynamic Stiffness of Foundations: 2-D vs. 3-D Solutions," Research Report R77-36, MIT, 1977.

6.11 Beck, James L., "Determining Models of Structures from Earthquake Records," Ph.D. Thesis, California Institute of Technology, Report No. EERL 78-01, June, 1978.

6.12 Weissman, K., "Centrifugal Modeling of Dynamic Soil-Structure Interaction," Ph.D. Thesis, Princeton University, Princeton, NJ, 1989.

CHAPTER 7

CONCLUSIONS AND FUTURE RESEARCH

This report presents a centrifuge model that is capable of realistically representing soil-structure systems subjected to earthquake-like excitation. A simple and economical method of earthquake simulation, called the hammer-exciter plate technique, is used, and special attention is given to problem of wave reflection at the boundary of the soil sample. The model is validated by first, characterizing the model system, second, performing an in depth experimental study of radiation damping and soil-structure interaction effects, and third, performing a numerical analysis of the experimental results. In characterizing the model system it is demonstrated that the simulated earthquake and its propagational characteristics in the experimental soil deposit are representative of a realistic system. Free field experiments show that the simulated earthquake generated by the hammer-exciter plate method, is similar in amplitude and frequency content to a real earthquake (*viz.*, the October 16, 1979 earthquake in Jenkinsville, S.C., recorded at the Monticello Dam site, M=3.0). In addition to this, the simulated earthquake is repeatable, allowing for comparisons of the response of various systems to the same earthquake. The free field experiments also demonstrate that a confined soil sample can satisfactorily model a horizontal soil stratum of infinite lateral extent when the containment walls are lined with an absorptive material (such as Duxseal) to attenuate wave reflections that would otherwise occur. Measurements of the acceleration at different locations on the free soil surface indicate that the surface motion is fairly uniform over a relatively large area. This is further confirmed by a comparison made between the measured free and scattered field motions for a surface foundation. A preliminary soil-structure interaction experiment involving the response of a rigid circular footing demonstrates the potential of the centrifuge model in investigating soil-structure interaction effects.

Next, an experimental study of radiation damping and soil-structure interaction effects is performed in the centrifuge. The study shows that radiation damping and the lack thereof can be observed in the centrifuge model. The experimental results, which demonstrate the influence of (1) the frequencies of the structure (2) the foundation embedment, and (3) the foundation shape on radiation damping and soil-structure interaction effects for a structure on a layer of soil over bedrock during an earthquake, are shown to be consistent with established theories.

Finally, the experimental results are used to compute the damping and stiffness parameters of a piecewise linear, two degree of freedom numerical model of the soil-structure systems. The error in fit between the two degree of freedom model and the experimental results is shown to be typically quite small. In addition to this, the experimental parameter values are shown, to be in good agreement with those computed by classical text book formulas with few exceptions. The results of this numerical analysis demonstrate that the behavior of the centrifuge system can be modeled by established analytical procedures.

The research in this report validates the centrifuge model for use in examining soil-structure interaction effects on systems which include dry soil deposits. Researchers and engineers may now apply this model to investigate the performance of specific types of structures and foundations on (or embedded in) dry soil under earthquake type loadings. However, in order to make the model applicable to a wider range of soil conditions and earthquake loadings, the following suggestions are made for future research. First, the ability of the centrifuge model to represent saturated soil deposits needs to be investigated. Centrifugal modeling of saturated soil can be complicated because the quantity of time scales differently in dynamic terms and diffusion cases (see Table 2.1). Second, it would be beneficial to be able to vary the earthquake input to the system. This added control would obviously be useful to test the effects of different types of earthquakes on soil-structure systems, but it would also help to more thoroughly characterize the

model soil deposit. For example, harmonic input may be applied to determine the frequencies of the soil deposit. A more advanced shaker system based on the hammer-exciter plate method is currently being developed at Princeton University. This new shaker will have the added ability of producing many different types of earthquakes while still maintaining the economical features of the original hammer-exciter plate device. Lastly, the possibility of modeling multilayer soil deposits should also be investigated.

NATIONAL CENTER FOR EARTHQUAKE ENGINEERING RESEARCH
LIST OF PUBLISHED TECHNICAL REPORTS

The National Center for Earthquake Engineering Research (NCEER) publishes technical reports on a variety of subjects related to earthquake engineering written by authors funded through NCEER. These reports are available from both NCEER's Publications Department and the National Technical Information Service (NTIS). Requests for reports should be directed to the Publications Department, National Center for Earthquake Engineering Research, State University of New York at Buffalo, Red Jacket Quadrangle, Buffalo, New York 14261. Reports can also be requested through NTIS, 5285 Port Royal Road, Springfield, Virginia 22161. NTIS accession numbers are shown in parenthesis, if available.

NCEER-87-0001 "First-Year Program in Research, Education and Technology Transfer," 3/5/87, (PB88-134275/AS).

NCEER-87-0002 "Experimental Evaluation of Instantaneous Optimal Algorithms for Structural Control," by R.C. Lin, T.T. Soong and A.M. Reinhorn, 4/20/87, (PB88-134341/AS).

NCEER-87-0003 "Experimentation Using the Earthquake Simulation Facilities at University at Buffalo," by A.M. Reinhorn and R.L. Ketter, to be published.

NCEER-87-0004 "The System Characteristics and Performance of a Shaking Table," by J.S. Hwang, K.C. Chang and G.C. Lee, 6/1/87, (PB88-134259/AS). This report is available only through NTIS (see address given above).

NCEER-87-0005 "A Finite Element Formulation for Nonlinear Viscoplastic Material Using a Q Model," by O. Gyebi and G. Dasgupta, 11/2/87, (PB88-213764/AS).

NCEER-87-0006 "Symbolic Manipulation Program (SMP) - Algebraic Codes for Two and Three Dimensional Finite Element Formulations," by X. Lee and G. Dasgupta, 11/9/87, (PB88-219522/AS).

NCEER-87-0007 "Instantaneous Optimal Control Laws for Tall Buildings Under Seismic Excitations," by J.N. Yang, A. Akbarpour and P. Ghaemmaghami, 6/10/87, (PB88-134333/AS).

NCEER-87-0008 "IDARC: Inelastic Damage Analysis of Reinforced Concrete Frame - Shear-Wall Structures," by Y.J. Park, A.M. Reinhorn and S.K. Kunnath, 7/20/87, (PB88-134325/AS).

NCEER-87-0009 "Liquefaction Potential for New York State: A Preliminary Report on Sites in Manhattan and Buffalo," by M. Budhu, V. Vijayakumar, R.F. Giese and L. Baumgras, 8/31/87, (PB88-163704/AS). This report is available only through NTIS (see address given above).

NCEER-87-0010 "Vertical and Torsional Vibration of Foundations in Inhomogeneous Media," by A.S. Veletsos and K.W. Dotson, 6/1/87, (PB88-134291/AS).

NCEER-87-0011 "Seismic Probabilistic Risk Assessment and Seismic Margins Studies for Nuclear Power Plants," by Howard H.M. Hwang, 6/15/87, (PB88-134267/AS). This report is available only through NTIS (see address given above).

NCEER-87-0012 "Parametric Studies of Frequency Response of Secondary Systems Under Ground-Acceleration Excitations," by Y. Yong and Y.K. Lin, 6/10/87, (PB88-134309/AS).

NCEER-87-0013 "Frequency Response of Secondary Systems Under Seismic Excitation," by J.A. HoLung, J. Cai and Y.K. Lin, 7/31/87, (PB88-134317/AS).

NCEER-87-0014 "Modelling Earthquake Ground Motions in Seismically Active Regions Using Parametric Time Series Methods," by G.W. Ellis and A.S. Cakmak, 8/25/87, (PB88-134283/AS).

NCEER-87-0015 "Detection and Assessment of Seismic Structural Damage," by E. DiPasquale and A.S. Cakmak, 8/25/87, (PB88-163712/AS).

NCEER-87-0016 "Pipeline Experiment at Parkfield, California," by J. Isenberg and E. Richardson, 9/15/87, (PB88-163720/AS).

NCEER-87-0017 "Digital Simulation of Seismic Ground Motion," by M. Shinozuka, G. Deodatis and T. Harada, 8/31/87, (PB88-155197/AS). This report is available only through NTIS (see address given above).

NCEER-87-0018 "Practical Considerations for Structural Control: System Uncertainty, System Time Delay and Truncation of Small Control Forces," J.N. Yang and A. Akbarpour, 8/10/87, (PB88-163738/AS).

NCEER-87-0019 "Modal Analysis of Nonclassically Damped Structural Systems Using Canonical Transformation," by J.N. Yang, S. Sarkani and F.X. Long, 9/27/87, (PB88-187851/AS).

NCEER-87-0020 "A Nonstationary Solution in Random Vibration Theory," by J.R. Red-Horse and P.D. Spanos, 11/3/87, (PB88-163746/AS).

NCEER-87-0021 "Horizontal Impedances for Radially Inhomogeneous Viscoelastic Soil Layers," by A.S. Veletsos and K.W. Dotson, 10/15/87, (PB88-150859/AS).

NCEER-87-0022 "Seismic Damage Assessment of Reinforced Concrete Members," by Y.S. Chung, C. Meyer and M. Shinozuka, 10/9/87, (PB88-150867/AS). This report is available only through NTIS (see address given above).

NCEER-87-0023 "Active Structural Control in Civil Engineering," by T.T. Soong, 11/11/87, (PB88-187778/AS).

NCEER-87-0024 Vertical and Torsional Impedances for Radially Inhomogeneous Viscoelastic Soil Layers," by K.W. Dotson and A.S. Veletsos, 12/87, (PB88-187786/AS).

NCEER-87-0025 "Proceedings from the Symposium on Seismic Hazards, Ground Motions, Soil-Liquefaction and Engineering Practice in Eastern North America," October 20-22, 1987, edited by K.H. Jacob, 12/87, (PB88-188115/AS).

NCEER-87-0026 "Report on the Whittier-Narrows, California, Earthquake of October 1, 1987," by J. Pantelic and A. Reinhorn, 11/87, (PB88-187752/AS). This report is available only through NTIS (see address given above).

NCEER-87-0027 "Design of a Modular Program for Transient Nonlinear Analysis of Large 3-D Building Structures," by S. Srivastav and J.F. Abel, 12/30/87, (PB88-187950/AS).

NCEER-87-0028 "Second-Year Program in Research, Education and Technology Transfer," 3/8/88, (PB88-219480/AS).

NCEER-88-0001 "Workshop on Seismic Computer Analysis and Design of Buildings With Interactive Graphics," by W. McGuire, J.F. Abel and C.H. Conley, 1/18/88, (PB88-187760/AS).

NCEER-88-0002 "Optimal Control of Nonlinear Flexible Structures," by J.N. Yang, F.X. Long and D. Wong, 1/22/88, (PB88-213772/AS).

NCEER-88-0003 "Substructuring Techniques in the Time Domain for Primary-Secondary Structural Systems," by G.D. Manolis and G. Juhn, 2/10/88, (PB88-213780/AS).

NCEER-88-0004 "Iterative Seismic Analysis of Primary-Secondary Systems," by A. Singhal, L.D. Lutes and P.D. Spanos, 2/23/88, (PB88-213798/AS).

NCEER-88-0005 "Stochastic Finite Element Expansion for Random Media," by P.D. Spanos and R. Ghanem, 3/14/88, (PB88-213806/AS).

NCEER-88-0006 "Combining Structural Optimization and Structural Control," by F.Y. Cheng and C.P. Pantelides, 1/10/88, (PB88-213814/AS).

NCEER-88-0007 "Seismic Performance Assessment of Code-Designed Structures," by H.H-M. Hwang, J-W. Jaw and H-J. Shau, 3/20/88, (PB88-219423/AS).

NCEER-88-0008 "Reliability Analysis of Code-Designed Structures Under Natural Hazards," by H.H-M. Hwang, H. Ushiba and M. Shinozuka, 2/29/88, (PB88-229471/AS).

NCEER-88-0009 "Seismic Fragility Analysis of Shear Wall Structures," by J-W Jaw and H.H-M. Hwang, 4/30/88, (PB89-102867/AS).

NCEER-88-0010 "Base Isolation of a Multi-Story Building Under a Harmonic Ground Motion - A Comparison of Performances of Various Systems," by F-G Fan, G. Ahmadi and I.G. Tadjbakhsh, 5/18/88, (PB89-122238/AS).

NCEER-88-0011 "Seismic Floor Response Spectra for a Combined System by Green's Functions," by F.M. Lavelle, L.A. Bergman and P.D. Spanos, 5/1/88, (PB89-102875/AS).

NCEER-88-0012 "A New Solution Technique for Randomly Excited Hysteretic Structures," by G.Q. Cai and Y.K. Lin, 5/16/88, (PB89-102883/AS).

NCEER-88-0013 "A Study of Radiation Damping and Soil-Structure Interaction Effects in the Centrifuge," by K. Weissman, supervised by J.H. Prevost, 5/24/88, (PB89-144703/AS).

NCEER-88-0014 "Parameter Identification and Implementation of a Kinematic Plasticity Model for Frictional Soils," by J.H. Prevost and D.V. Griffiths, to be published.

NCEER-88-0015 "Two- and Three- Dimensional Dynamic Finite Element Analyses of the Long Valley Dam," by D.V. Griffiths and J.H. Prevost, 6/17/88, (PB89-144711/AS).

NCEER-88-0016 "Damage Assessment of Reinforced Concrete Structures in Eastern United States," by A.M. Reinhorn, M.J. Seidel, S.K. Kunnath and Y.J. Park, 6/15/88, (PB89-122220/AS).

NCEER-88-0017 "Dynamic Compliance of Vertically Loaded Strip Foundations in Multilayered Viscoelastic Soils," by S. Ahmad and A.S.M. Israil, 6/17/88, (PB89-102891/AS).

NCEER-88-0018 "An Experimental Study of Seismic Structural Response With Added Viscoelastic Dampers," by R.C. Lin, Z. Liang, T.T. Soong and R.H. Zhang, 6/30/88, (PB89-122212/AS).

NCEER-88-0019 "Experimental Investigation of Primary - Secondary System Interaction," by G.D. Manolis, G. Juhn and A.M. Reinhorn, 5/27/88, (PB89-122204/AS).

NCEER-88-0020 "A Response Spectrum Approach For Analysis of Nonclassically Damped Structures," by J.N. Yang, S. Sarkani and F.X. Long, 4/22/88, (PB89-102909/AS).

NCEER-88-0021 "Seismic Interaction of Structures and Soils: Stochastic Approach," by A.S. Veletsos and A.M. Prasad, 7/21/88, (PB89-122196/AS).

NCEER-88-0022 "Identification of the Serviceability Limit State and Detection of Seismic Structural Damage," by E. DiPasquale and A.S. Cakmak, 6/15/88, (PB89-122188/AS).

NCEER-88-0023 "Multi-Hazard Risk Analysis: Case of a Simple Offshore Structure," by B.K. Bhartia and E.H. Vanmarcke, 7/21/88, (PB89-145213/AS).

NCEER-88-0024 "Automated Seismic Design of Reinforced Concrete Buildings," by Y.S. Chung, C. Meyer and M. Shinozuka, 7/5/88, (PB89-122170/AS).

NCEER-88-0025 "Experimental Study of Active Control of MDOF Structures Under Seismic Excitations," by L.L. Chung, R.C. Lin, T.T. Soong and A.M. Reinhorn, 7/10/88, (PB89-122600/AS).

NCEER-88-0026 "Earthquake Simulation Tests of a Low-Rise Metal Structure," by J.S. Hwang, K.C. Chang, G.C. Lee and R.L. Ketter, 8/1/88, (PB89-102917/AS).

NCEER-88-0027 "Systems Study of Urban Response and Reconstruction Due to Catastrophic Earthquakes," by F. Kozin and H.K. Zhou, 9/22/88.

NCEER-88-0028 "Seismic Fragility Analysis of Plane Frame Structures," by H.H-M. Hwang and Y.K. Low, 7/31/88, (PB89-131445/AS).

NCEER-88-0029 "Response Analysis of Stochastic Structures," by A. Kardara, C. Bucher and M. Shinozuka, 9/22/88, (PB89-174429/AS).

NCEER-88-0030 "Nonnormal Accelerations Due to Yielding in a Primary Structure," by D.C.K. Chen and L.D. Lutes, 9/19/88, (PB89-131437/AS).

NCEER-88-0031 "Design Approaches for Soil-Structure Interaction," by A.S. Veletsos, A.M. Prasad and Y. Tang, 12/30/88, (PB89-174437/AS).

NCEER-88-0032 "A Re-evaluation of Design Spectra for Seismic Damage Control," by C.J. Turkstra and A.G. Tallin, 11/7/88, (PB89-145221/AS).

NCEER-88-0033 "The Behavior and Design of Noncontact Lap Splices Subjected to Repeated Inelastic Tensile Loading," by V.E. Sagan, P. Gergely and R.N. White, 12/8/88, (PB89-163737/AS).

NCEER-88-0034 "Seismic Response of Pile Foundations," by S.M. Mamoon, P.K. Banerjee and S. Ahmad, 11/1/88, (PB89-145239/AS).

NCEER-88-0035 "Modeling of R/C Building Structures With Flexible Floor Diaphragms (IDARC2)," by A.M. Reinhorn, S.K. Kunnath and N. Panahshahi, 9/7/88, (PB89-207153/AS).

NCEER-88-0036 "Solution of the Dam-Reservoir Interaction Problem Using a Combination of FEM, BEM with Particular Integrals, Modal Analysis, and Substructuring," by C-S. Tsai, G.C. Lee and R.L. Ketter, 12/31/88, (PB89-207146/AS).

NCEER-88-0037 "Optimal Placement of Actuators for Structural Control," by F.Y. Cheng and C.P. Pantelides, 8/15/88, (PB89-162846/AS).

NCEER-88-0038 "Teflon Bearings in Aseismic Base Isolation: Experimental Studies and Mathematical Modeling," by A. Mokha, M.C. Constantinou and A.M. Reinhorn, 12/5/88, (PB89-218457/AS).

NCEER-88-0039 "Seismic Behavior of Flat Slab High-Rise Buildings in the New York City Area," by P. Weidlinger and M. Ettouney, 10/15/88.

NCEER-88-0040 "Evaluation of the Earthquake Resistance of Existing Buildings in New York City," by P. Weidlinger and M. Ettouney, 10/15/88, to be published.

NCEER-88-0041 "Small-Scale Modeling Techniques for Reinforced Concrete Structures Subjected to Seismic Loads," by W. Kim, A. El-Attar and R.N. White, 11/22/88, (PB89-189625/AS).

NCEER-88-0042 "Modeling Strong Ground Motion from Multiple Event Earthquakes," by G.W. Ellis and A.S. Cakmak, 10/15/88, (PB89-174445/AS).

NCEER-88-0043 "Nonstationary Models of Seismic Ground Acceleration," by M. Grigoriu, S.E. Ruiz and E. Rosenblueth, 7/15/88, (PB89-189617/AS).

NCEER-88-0044 "SARCF User's Guide: Seismic Analysis of Reinforced Concrete Frames," by Y.S. Chung, C. Meyer and M. Shinozuka, 11/9/88, (PB89-174452/AS).

NCEER-88-0045 "First Expert Panel Meeting on Disaster Research and Planning," edited by J. Pantelic and J. Stoyle, 9/15/88, (PB89-174460/AS).

NCEER-88-0046 "Preliminary Studies of the Effect of Degrading Infill Walls on the Nonlinear Seismic Response of Steel Frames," by C.Z. Chrysostomou, P. Gergely and J.F. Abel, 12/19/88, (PB89-208383/AS).

NCEER-88-0047 "Reinforced Concrete Frame Component Testing Facility - Design, Construction, Instrumentation and Operation," by S.P. Pessiki, C. Conley, T. Bond, P. Gergely and R.N. White, 12/16/88, (PB89-174478/AS).

NCEER-89-0001 "Effects of Protective Cushion and Soil Compliancy on the Response of Equipment Within a Seismically Excited Building," by J.A. HoLung, 2/16/89, (PB89-207179/AS).

NCEER-89-0002 "Statistical Evaluation of Response Modification Factors for Reinforced Concrete Structures," by H.H-M. Hwang and J-W. Jaw, 2/17/89, (PB89-207187/AS).

NCEER-89-0003 "Hysteretic Columns Under Random Excitation," by G-Q. Cai and Y.K. Lin, 1/9/89, (PB89-196513/AS).

NCEER-89-0004 "Experimental Study of 'Elephant Foot Bulge' Instability of Thin-Walled Metal Tanks," by Z-H. Jia and R.L. Ketter, 2/22/89, (PB89-207195/AS).

NCEER-89-0005 "Experiment on Performance of Buried Pipelines Across San Andreas Fault," by J. Isenberg, E. Richardson and T.D. O'Rourke, 3/10/89, (PB89-218440/AS).

NCEER-89-0006 "A Knowledge-Based Approach to Structural Design of Earthquake-Resistant Buildings," by M. Subramani, P. Gergely, C.H. Conley, J.F. Abel and A.H. Zaghw, 1/15/89, (PB89-218465/AS).

NCEER-89-0007 "Liquefaction Hazards and Their Effects on Buried Pipelines," by T.D. O'Rourke and P.A. Lane, 2/1/89, (PB89-218481).

NCEER-89-0008 "Fundamentals of System Identification in Structural Dynamics," by H. Imai, C-B. Yun, O. Maruyama and M. Shinozuka, 1/26/89, (PB89-207211/AS).

NCEER-89-0009 "Effects of the 1985 Michoacan Earthquake on Water Systems and Other Buried Lifelines in Mexico," by A.G. Ayala and M.J. O'Rourke, 3/8/89, (PB89-207229/AS).

NCEER-89-R010 "NCEER Bibliography of Earthquake Education Materials," by K.E.K. Ross, Second Revision, 9/1/89, (PB90-125352/AS).

NCEER-89-0011 "Inelastic Three-Dimensional Response Analysis of Reinforced Concrete Building Structures (IDARC-3D), Part I - Modeling," by S.K. Kunnath and A.M. Reinhorn, 4/17/89, (PB90-114612/AS).

NCEER-89-0012 "Recommended Modifications to ATC-14," by C.D. Poland and J.O. Malley, 4/12/89.

NCEER-89-0013 "Repair and Strengthening of Beam-to-Column Connections Subjected to Earthquake Loading," by M. Corazao and A.J. Durrani, 2/28/89, (PB90-109885/AS).

NCEER-89-0014 "Program EXKAL2 for Identification of Structural Dynamic Systems," by O. Maruyama, C-B. Yun, M. Hoshiya and M. Shinozuka, 5/19/89, (PB90-109877/AS).

NCEER-89-0015 "Response of Frames With Bolted Semi-Rigid Connections, Part I - Experimental Study and Analytical Predictions," by P.J. DiCorso, A.M. Reinhorn, J.R. Dickerson, J.B. Radziminski and W.L. Harper, 6/1/89, to be published.

NCEER-89-0016 "ARMA Monte Carlo Simulation in Probabilistic Structural Analysis," by P.D. Spanos and M.P. Mignolet, 7/10/89, (PB90-109893/AS).

NCEER-89-0017 "Preliminary Proceedings of the Conference on Disaster Preparedness - The Place of Earthquake Education in Our Schools, July 9-11, 1989," 6/23/89, (PB90-108606/AS).

NCEER-89-0018 "Multidimensional Models of Hysteretic Material Behavior for Vibration Analysis of Shape Memory Energy Absorbing Devices, by E.J. Graesser and F.A. Cozzarelli, 6/7/89.

NCEER-89-0019 "Nonlinear Dynamic Analysis of Three-Dimensional Base Isolated Structures (3D-BASIS)," by S. Nagarajaiah, A.M. Reinhorn and M.C. Constantinou, 8/3/89.

NCEER-89-0020 "Structural Control Considering Time-Rate of Control Forces and Control Rate Constraints," by F.Y. Cheng and C.P. Pantelides, 8/3/89, (PB90-120445/AS).

NCEER-89-0021 "Subsurface Conditions of Memphis and Shelby County," by K.W. Ng, T-S. Chang and H-H.M. Hwang, 7/26/89, (PB90-120437/AS).

NCEER-89-0022 "Seismic Wave Propagation Effects on Straight Jointed Buried Pipelines," by K. Elhmadi and M.J. O'Rourke, 8/24/89.

NCEER-89-0023 "Workshop on Serviceability Analysis of Water Delivery Systems," edited by M. Grigoriu, 3/6/89, (PB90-127424/AS).

NCEER-89-0024 "Shaking Table Study of a 1/5 Scale Steel Frame Composed of Tapered Members," by K.C. Chang, J.S. Hwang and G.C. Lee, 9/18/89.

NCEER-89-0025 "DYNA1D: A Computer Program for Nonlinear Seismic Site Response Analysis - Technical Documentation," by Jean H. Prevost, 9/14/89.

NCEER-89-0026 "1:4 Scale Model Studies of Active Tendon Systems and Active Mass Dampers for Aseismic Protection," by A.M. Reinhorn, T.T. Soong, R.C. Lin, Y.P. Yang, Y. Fukao, H. Abe and M. Nakai, 9/15/89.

NCEER-89-0027 "Scattering of Waves by Inclusions in a Nonhomogeneous Elastic Half Space Solved by Boundary Element Methods," by P.K. Hadley, A. Askar and A.S. Cakmak, 6/15/89, (PB90-145699/AS).

NCEER-89-0028 "Statistical Evaluation of Deflection Amplification Factors for Reinforced Concrete Structures," by H.H.M. Hwang, J-W. Jaw and A.L. Ch'ng, 8/31/89.

NCEER-89-0029 "Bedrock Accelerations in Memphis Area Due to Large New Madrid Earthquakes," by H.H.M. Hawng, C.H.S. Chen and G. Yu, 11/7/89.

NCEER-89-0030 "Seismic Behavior and Response Sensitivity of Secondary Structural Systems," by Y.Q. Chen and T.T. Soong, 10/23/89.

NCEER-89-0031 "Random Vibration and Reliability Analysis of Primary-Secondary Structural Systems," by Y. Ibrahim, M. Grigoriu and T.T. Soong, 11/10/89.

NCEER-89-0032 "Proceedings from the Second U.S. - Japan Workshop on Liquefaction, Large Ground Deformation and Their Effects on Lifelines, September 26-29, 1989," Edited by T.D. O'Rourke and M. Hamada, 12/1/89.

NCEER-89-0033 "Deterministic Model for Seismic Damage Evaluation of Reinforced Concrete Structures," by J.M. Bracci, A.M. Reinhorn, J.B. Mander and S.K. Kunnath, 9/27/89, to be published.

NCEER-89-0034 "On the Relation Between Local and Global Damage Indices," by E. DiPasquale and A.S. Cakmak, 8/15/89.

NCEER-89-0035 "Cyclic Undrained Behavior of Nonplastic and Low Plasticity Silts," by A.J. Walker and H.E. Stewart, 7/26/89.

NCEER-89-0036 "Liquefaction Potential of Surficial Deposits in the City of Buffalo, New York," by M. Budhu, R. Giese and C. Baumgrass, 1/17/89, to be published.

NCEER-89-0037 "A Determinstic Assessment of Effects of Ground Motion Incoherence," by A.S. Veletsos and Y. Tang, 7/15/89.

NCEER-89-0038 "Workshop on Ground Motion Parameters for Seismic Hazard Mapping," July 17-18, 1989, edited by R.V. Whitman, 12/1/89.